DISSERTATION

BIOANALYTICAL APPLICATIONS OF CAPILLARY ELECTROPHORESIS AND MICROFLUIDICS: FROM METABOLOMICS TO BIOFUELS

Submitted by

Ryan E. Holcomb

Department of Chemistry

In partial fulfillment of the requirements

For the Degree of Doctor of Philosophy

Colorado State University

Fort Collins, Colorado

Fall 2010

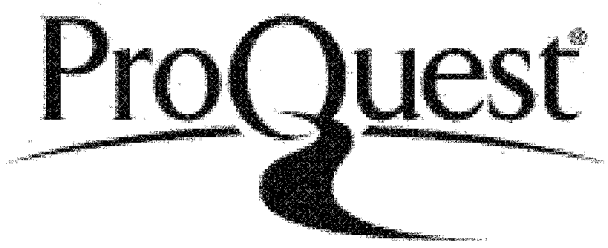

ProQuest LLC
789 East Eisenhower Parkway
P.O. Box 1346
Ann Arbor, MI 48106-1346

COLORADO STATE UNIVERSITY

September 13, 2010

WE HEREBY RECOMMEND THAT THE DISSERTATION PREPARED UNDER OUR SUPERVISION BY RYAN E. HOLCOMB ENTITLED "BIOANALYTICAL APPLICATIONS OF CAPILLARY ELECTROPHORESIS AND MICROFLUIDICS: FROM METABOLOMICS TO BIOFUELS" BE ACCEPTED AS FULFILLING IN PART REQUIREMENTS FOR THE DEGREE OF DOCTOR OF PHILOSOPHY.

Committee on Graduate Work

B. George Barisas

William H. Hanneman

Steven H. Strauss

Alan K. Van Orden

Advisor: Charles S. Henry

Chair: Ellen R. Fisher

ABSTRACT OF DISSERTATION

BIOANALYTICAL APPLICATIONS OF CAPILLARY ELECTROPHORESIS AND MICROFLUIDICS: FROM METABOLOMICS TO BIOFUELS

Capillary electrophoresis (CE) and related microfluidic technologies are increasingly being utilized as state of the art analysis tools in the field of bioanalytical chemistry. The following dissertation highlights selected applications of CE and microfluidics for metabolomics and microalgal-based biofuels research. Metabolomics research focused on targeted metabolic profiling and fingerprinting of biofluids using both conventional and microchip CE. Metabolite analysis in biofluids was of interest as this can be a useful clinical tool for monitoring disease states and treatment efficacy. Initial work in this area focused on targeted metabolic analysis of the cardiovascular disease biomarker homocysteine (Hcys). In this work, serum Hcys was analyzed using microchip CE (MCE) coupled with pulsed amperometric detection. Using this system, Hcys could be resolved from other electrochemically active serum components in under a minute by employing appropriate separation conditions. Following this targeted metabolic analysis, research shifted to a more comprehensive metabolic fingerprinting study of dogs undergoing chemotherapy for diffuse large B cell lymphoma. Urine samples from diseased and non-diseased dogs were obtained at various clinical time points and analyzed using CE with UV detection. The resulting fingerprints were compared for

differences in metabolite make-up using multivariate statistical techniques. In an attempt to conduct this type of research at the microscale, a MCE device was developed with an integrated electrode array detector for resolving the multiple components present in biological samples. Selective detection and electrochemical resolution of co-migrating analytes could be facilitated with this device via judicious choice of detection potential at the multiple working electrodes. Improvement in detection capability of this system compared to single electrode MCE systems should allow for its use in rapid metabolic fingerprinting and profiling analyses. The final area of research presented in this dissertation involved use of microfluidics for culturing and screening cellular lipid accumulation in microalgae exposed to various environmental stressors. A microfluidic device was developed which contained integrated valves for facilitating cell culture and conducting imaging assays on-chip. Lipid accumulation in stressed microalgae was determined using fluorescence microscopy techniques. Additional experiments were conducted using gas chromatography to determine the types of lipids being accumulated in these stressed microalgae.

Ryan E. Holcomb
Department of Chemistry
Colorado State University
Fort Collins, CO 80523
Fall 2010

ACKNOWLEDGEMENTS

On a personal note, I would like to acknowledge my grandfather Dr. Rolf S. Bruenner for fostering in me a genuine love of the natural world and interest in the sciences in general. He was the primary inspiration for my scholastic endeavors and the catalyst for my career in chemistry. I would also like to acknowledge my parents Raymond and Doris Holcomb for all their love and support and for pushing me to realize my potential. Acknowledgements are in order for the rest of my wonderful family as well, nuclear and extended, for all their love and encouragement. I would be remiss not to acknowledge new friends I have met along the way and old friends I have reconnected with for rekindling inspiration and for making this journey so enjoyable.

Personally and professionally, I would like to acknowledge Dr. Corey J. Bloom and my former colleagues at Bend Research, Inc. for helping develop me as a scientist and for imparting in me the confidence to pursue an advanced degree in chemistry. I am also indebted to Dr. Bloom for pointing me in the direction of Colorado State University; it was a great backdrop in which to play out this phase of my life. I would like to acknowledge the Henry group post doctoral fellows Dr. James R. Kraly and Dr. Carlos F. Gonzalez for all their invaluable assistance and mentorship. I would also like to acknowledge members of the Henry research group, past and present, for helping me when it was needed and for generating a light hearted atmosphere in the lab. Finally, I would like to acknowledge my advisor Dr. Charles S. Henry for his guidance and role in developing me into an independent, critically thinking scientist.

This work is dedicated to

my Opa Dr. Rolf S. Bruenner

and my parents Raymond and Doris Holcomb

TABLE OF CONTENTS

Page

CHAPTER 1. *Introduction*

1.1 Dissertation Overview

Capillary electrophoresis and related microfluidic technologies have been utilized with great success for a variety of bioanalytical applications. Material presented in the following dissertation focuses on the use of these technologies for metabolomics and biofuels related research. Since these are seemingly two disparate topics, they will be addressed in a separate and sequential manner in this dissertation. First, the use of conventional and microchip capillary electrophoresis for metabolomics based research will be discussed. Following this, the feasibility of using microfluidics as a means to rapidly screen microalgal lipid accumulation for biofuels applications is examined. A discussion of targeted lipid profiling as it relates to microalgae will also be included. In a similar manner, the first part of this chapter will serve to familiarize the reader with the field of metabolomics and the use of conventional and microchip capillary electrophoresis as a tool for metabolic analysis. As an addendum, a general description of capillary electrophoresis is given. In the last part of this chapter, the reader will be introduced to the rapidly expanding field of microalgal biofuels research and applications of microfluidics for microalgal culturing and lipid analysis. Additionally, a brief discussion of microalgal lipid profiling will be included. This chapter will serve as a cursory introduction to these topics as well as the impetus behind research presented in this dissertation. More in depth discussions of specific topics and techniques are given in the following research chapters.

1.2 Metabolomics

1.2.1 Background

Metabolomics is an emerging research field focused on the analysis of small molecules (i.e., metabolites) in biological systems. Despite formally existing for little over a decade, the amount of research conducted in this field has been substantial and diverse.[1-5] Metabolomics studies are multifaceted, but generally fall into five distinct categories: metabolomics, metabonomics, metabolic profiling, metabolic fingerprinting, and targeted metabolic analysis. Metabolomics is the broadest based of these techniques and is generally defined as the comprehensive identification and quantification of metabolites within a biological system at any given point in time.[1] Since this technique measures the entire metabolome, it is often times used to identify disease biomarkers and/or help elucidate biochemical pathways.[4,6] Metabonomics is a more focused approach involving the quantification of the metabolic response of a living system to either physiological or genetic stimuli. Pharmacological studies often employ metabonomics as a way to determine how a specific drug is affecting metabolite expression within an organism.[7-8] Metabolic profiling is an even more focused discipline which attempts to identify and quantify chemically similar metabolites (e.g., carbohydrates, lipids, etc.), or metabolites related through specific metabolic pathways. An example of this is lipidomics, which aims to identify all lipid components present in a sample. In contrast to the previous techniques, metabolic fingerprinting is a relatively non-specific approach in which data sets (e.g., peaks in a chromatogram) are globally compared to evaluate differences existing in metabolite make-up (fingerprint).[9] Typically this is done using peak picking software or various mathematical approaches to prevent bias.[9] The final, and most well

established technique, is targeted metabolic analysis which focuses on the analysis one or more metabolites in a sample. Many times these target metabolites are disease biomarkers, whose measurement can be used for diagnosing disease and evaluating treatment efficacy.[5,10]

Metabolite measurements are conducted in a variety of biomatrices including blood, urine, cell extracts, and tissue homogenates.[1,3] As a result, metabolomics studies pose a challenging analytical problem due to the large number of metabolites and non-metabolites (e.g., proteins) present in these matrices. Therefore, analytical methodologies used for these studies must be capable of not only resolving, but also simultaneously detecting metabolites of interest among multiple other matrix components. Techniques such as NMR[1,5] and MS[1-3] are most often employed as they provide powerful qualitative and quantitative information regarding the metabolites being studied. Additionally, vibrational spectroscopy techniques such as FT-IR and Raman are also commonly employed towards this end.[1] Many times, techniques such as MS are preceded by a high performance separation step to improve resolution and selectivity of the analysis.[1-4] Typically, liquid chromatography (LC) and gas chromatography (GC) are employed,[1-4] with LC being the most common as it is not limited by analyte volatility or thermal stability.

Capillary electrophoresis (CE) is an alternative to the aforementioned separation techniques that is increasingly being utilized in the field of metabolomics.[1,9,11-12] This is largely due the high separation efficiencies and resolving power afforded by this technique. These attributes make it well suited for the analysis of the complex, multi-

component biological samples encountered in most metabolomic studies. To date, CE has been used primarily for metabolic fingerprinting applications[9,13-15] and targeted metabolic analysis.[1,11-12] The most commonly used detection technique for these analyses is MS,[1,11-12] although UV-detection has been used for some metabolic fingerprinting studies.[9,13-15]

Although relatively new to the metabolomics arena, microchip capillary electrophoresis (MCE) is a technique which is also increasingly being utilized for metabolomics studies.[6] As with conventional CE, most applications involve targeted metabolic analysis;[6] however, MCE has the additional advantage of being portable which makes its use attractive for point-of-care (POC) medical applications.[16-20] Since its inception in the early 1990s,[21-22] MCE has gained increasing attention due to the portability, low sample consumption, and rapid measurement capabilities afforded by this technique. To date, MCE has been routinely used in fully integrated (sample preparation and analysis) micro-total analysis systems (μTAS)[23-24] for fluid manipulation, mixing, and separation of multi-component mixtures.[23-24]

Systems such as these are ideal for POC applications as their portability allows them to be used in a variety of different settings outside of a clinical diagnostics laboratory. Furthermore, the integrated nature of these systems should allow them to be used in a rapid, straightforward manner by a variety of medical personnel. Analysis of metabolic disease biomarkers using a POC device would be a powerful way in which to directly diagnose and monitor disease. It is envisioned these systems would not only be used by physicians for bedside diagnosis, but also by patients outside of the clinical setting for monitoring and managing disease. This would be particularly useful for medicine in the

developing world, as diagnostic testing (laboratory) is not readily available in many of these regions.

Research presented in Chapters 2-4 of this dissertation describe the use of CE and MCE for metabolic fingerprinting and targeted metabolic analyses. These analyses have applications for both medical diagnostics and disease monitoring. Furthermore, MCE systems were implemented for selected analyses as a first step in developing relevant POC technologies based around the measurement of metabolic disease biomarkers.

1.2.2 CE Theory

Since Chapters 2-4 of this dissertation are focused on the use of CE and MCE for metabolic analysis, it is worthwhile to introduce the fundamentals of this separation technique and associated terminology here. The modern form of CE was introduced by Mikkers et al.[25-26] and Jorgensson et al.[27] in the late 1970s and early 1980s using polytetrafluoroethylene and silica based capillary systems, respectively. Today, silica capillaries are used almost exclusively for the majority of CE applications. The high separation performance afforded by CE systems arises from the mechanism of the electrophoretic separation itself. Unlike chromatography, there is no packing material or stationary phase associated with this technique, which eliminates band (i.e., peak) broadening due to multiple flow paths (packing material) or mass transfer with a stationary phase. Additionally, the lack of hydrodynamic flow (parabolic flow) in CE eliminates the band broadening which accompanies this flow type.[28] Theoretically, the only source of band broadening in CE arises from longitudinal diffusion of the analyte

during separation, although in practice other factors contribute to band broadening, such as resistive heating (Joule heating) and analyte/capillary interactions.[29]

Although multiple forms of CE exist,[29] by far the most common is normal polarity capillary zone electrophoresis (CZE). All CE separations described in this dissertation were conducted using normal polarity CZE, unless stated otherwise (i.e., Chapter 3). In normal polarity CZE, the capillary is filled with a background electrolyte (BGE) and charged analytes are separated in the BGE based upon their differential migration velocities in an applied electrical field. This field is established between anodic (positive) and cathodic (negative) electrodes positioned in buffer reservoirs at opposite ends of the capillary. The resulting analyte velocities in this field are described by Equation 1.1 in which velocity (v_{ep}) is equal to the intrinsic electrophoretic mobility of an analyte (μ_{ep}) multiplied by the field strength (E).

$$v_{ep} = \frac{q}{f}E \equiv \mu_{ep}E \tag{1.1}$$

Electrophoretic mobility (μ_{ep}) is governed by the analyte's charge (q) and frictional coefficient (f) as defined by the Stokes Equation (1.2).

$$f = 6\pi\eta r \tag{1.2}$$

This equation describes the frictional coefficient (f) for a spherical particle having a hydrodynamic radius r in a solution of viscosity η. Since analytes are injected at the anodic end of the capillary, positively charged analytes will migrate down the capillary towards the cathode (positive mobility), negatively charged analytes will migrate towards the anode (negative mobility), and neutral analytes will remain stationary at the injection site (no net mobility).

In practice, most analytes in CZE have net movement towards the cathode as the result of electroosmotic flow (EOF) which exists in silica capillaries above pH ~ 2. At this pH, the surface of the capillary becomes charged due to deprotonation of surface silanol groups, which results in formation of an electrical double layer at the capillary wall. This double layer contains counter-ions from the BGE as well as their associated waters of hydration which migrate down the capillary towards the cathode upon application of an electric field. The resulting migration results in bulk solution flow (EOF) inside the capillary. As a result, a new apparent velocity (v_{app}) for an analyte is observed which is dependent upon the mobility of the EOF (μ_{eo}). Equation 1.3 describes this new, apparent velocity (v_{app}) which is proportional to the sum of both the electrophoretic (μ_{ep}) and electroosmotic mobilities (μ_{eo}).

$$v_{app} = \mu_{app}E \equiv (\mu_{ep} + \mu_{eo})E \tag{1.3}$$

Since electroosmotic mobility (μ_{eo}) is generally larger than electrophoretic mobility (μ_{ep}), most analytes (positive, negative, and neutral) will have a net positive mobility (μ_{app}), and thus migrate down the capillary towards the cathode. These analytes are detected by measuring an associated physical property (e.g., absorbance, fluorescence, etc.) on-capillary or at the immediate exit of the capillary.

1.3 Microalgal Biofuels

1.3.1 Background

Recently, there has been a great deal of interest in developing renewable alternatives to petroleum based transportation fuels. Biofuels are seen as the most promising alternative liquid fuels, with biodiesel and "green" diesel receiving the most attention.[30-31] Currently,

biofuels are produced mainly using cellulosic and lipid feedstocks derived from terrestrial plants.[31-33] However, this production method requires vast tracts of land for crop cultivation, and is potentially unsustainable given current and projected fuel demands.[31-33] Because of this, attention has shifted towards use of microalgae as a potential lipid source for biofuels production.[30-31] Producing biofuels from microalgae shows promise due to the high lipid yields and small cultivation footprint which may be attainable using this resource.[30-31] Additional interest in microalgae stems from their higher growth rate, higher productivity per unit land area, and lower requirement for fresh water compared to terrestrial plants.[34] Furthermore, microalgae can be cultivated in environments not suited for food or biofuels crops, making them more practical from a production standpoint.[30-31] Microalgal lipids used for producing biofuels consist primarily of triacylglycerols (TAGs) which are accumulated and stored in the cytosol of microalgal cells.[30] Biofuels are produced from these TAGs by extracting them from the cells and transesterifying to fatty acid methyl esters (FAMEs) or decarboxylating to alkanes to form biodiesel and green diesel, respectively.[30-31]

Utilization of microalgae for biofuels production is not a new idea and was pursued by the US Department of Energy under the Aquatic Species Program (ASP) from 1978 to 1996.[30,34] The purpose of this program was to determine the feasibility of generating renewable fuels from a variety of aquatic organisms including microalgae. From this research endeavor, a variety of useful advances regarding microalgal physiology and biochemistry were made as well as strain isolation and characterization of species capable of lipid accumulation.[34] Most often, lipid accumulation in microalgae is the result of environmental stress conditions which alter lipid metabolism within the cell.[30]

Environmental stressors known to cause lipid accumulation include changes in temperature, light, salinity, pH, and the nutrient (e.g., nitrates, phosphorus, silicon, etc.) composition of the culturing medium.[30,35-36] Of these, it has been shown that the highest levels of lipid accumulation generally result from nutrient deprivation during culturing.[34] Knowledge of these stress conditions is useful from a biofuels standpoint, as it allows for optimization of culturing conditions to obtain maximum lipid yields for a given species of microalgae.

Since there are multiple microalgal species capable of lipid accumulation[30,37-40] and multiple environmental stress conditions, there exists a need for rapid screening tools to determine optimum combinations. Increasing the screening throughput would be beneficial as it would reduce development cost and time to commercial production. As alluded to in the previous section (1.1), microfluidic devices are uniquely suited to these types of applications due to the ability to integrate sample preparation and analysis onto a single platform.[23-24] It is envisioned integrated microfluidic systems operating in parallel could be used to simultaneously screen multiple microalgal species and stress conditions. Initial progress towards this goal is presented in Chapter 5.

In addition to determining stress conditions leading to lipid accumulation in microalgae, determining the types of lipids (TAGs) being produced is also of interest. Knowledge of these lipids and their associated biosynthetic intermediates could help in elucidating biosynthetic pathways. An understanding of these pathways would allow for factors responsible for lipid accumulation to be controlled, and could aid in the development of genetically engineered species capable of producing specific types of TAGs.[41]

Methods for profiling TAG composition in microalgae are well established.[42-47] Typically, these consist of GC techniques where non-volatile TAGs are chemically converted to volatile fatty acid methyl esters (FAMEs) for analysis.[43-47] Similarly, charged species and other lipid intermediates can be profiled using MS and LC-MS techniques.[48] While TAG composition for multiple microalgal species[42-47] have been ascertained, complete knowledge of their biosynthesis has yet to be determined.[30] Current knowledge suggests TAG biosynthesis in microalgae proceeds via fatty acid biosynthesis in which acetyl-CoA is first converted to malonyl-CoA and then malonyl-ACP.[30] Following this, butyryl-ACP is formed, with subsequent additions of malonyl-ACP yielding fatty acids of increasing chain length (C16 and C18 are most common).[30] TAGs are likely formed from these fatty acids by chain transfer to glycerol-3-phosphate.[49] While some of this is known, much is assumed and additional questions need to be answered to gain a full understanding of these pathways. Conceivably this can be achieved using a bioinformatics approach where information gleaned from lipidomic and proteomic studies are analyzed in a synergistic manner for pathway determination. Lipidomic studies would involve determine of TAGs and intermediate fatty acid CoA and ACP species while proteomics studies would focus on determining the enzymes involved in lipid biosynthesis. Chapter 6 of this dissertation presents initial progress towards this end in developing GC methods for TAG determination in stressed and non-stressed microalgae.

1.4 References

(1) Dunn, W. B.; Bailey, N. J. C.; Johnson, H. E. *Analyst* **2005**, *130*, 606-625.

(2) Weckwerth, W.; Morgenthal, K. *Drug Discov. Today* **2005**, *10*, 1551-1558.

(3) Dettmer, K.; Aronov, P. A.; Hammock, B. D. *Mass Spectrom. Rev.* **2007**, *26*, 51-78.

(4) Oldiges, M.; Lutz, S.; Pflug, S.; Schroer, K.; Stein, N.; Wiendahl, C. *Appl. Microbiol. Biot.* **2007**, *76*, 495-511.

(5) Gowda, G. A.; Zhang, S.; Gu, H.; Asiago, V.; Shanaiah, N.; Raftery, D. *Expert Rev. Mol. Diagn.* **2008**, *8*, 617-633.

(6) Kraly, J. R.; Holcomb, R. E.; Guan, Q.; Henry, C. S. *Anal. Chim. Acta* **2009**, *653*, 23-35.

(7) Staack, R. F.; Hopfgartner, G. *Anal. Bioanal. Chem.* **2007**, *388*, 1365-1380.

(8) Lu, X.; Zhao, X. J.; Bai, C. M.; Zhao, C. X.; Lu, G.; Xu, G. M. *J. Chromatogr., B* **2008**, *866*, 64-76.

(9) Garcia-Perez, I.; Vallejo, M.; Garcia, A.; Legido-Quigley, C.; Barbas, C. *J. Chromatogr., A* **2008**, *1204*, 130-139.

(10) I. Matsumoto, T. K. *Mass Spectrom. Rev.* **1996**, *15*, 43-57.

(11) Monton, M. R. N.; Soga, T. *J. Chromatogr., A* **2007**, *1168*, 237-246.

(12) Ramautar, R.; Somsen, G. W.; de Jong, G. J. *Electrophoresis* **2009**, *30*, 276-291.

(13) Barbas, C.; Vallejo, M.; Garcia, A.; Barlow, D.; Hanna-Brown, A. *J. Pharm. Biomed. Anal.* **2008**, *47*, 388-398.

(14) Garcia-Perez, I.; Whitfield, P.; Bartlett, A.; Angulo, S.; Legido-Quigley, C.; Hanna-Brown, M.; Barbas, C. *Electrophoresis* **2008**, *29*, 3201-3206.

(15) Vallejo, M.; Angulo, S.; Garcia-Martinez, D.; Garcia, A.; Barbas, C. *J. Chromatogr., A* **2008**, *1187*, 267-274.

(16) Sia, S. K.; Kricka, L. J. *Lab Chip* **2008**, *8*, 1982-1983.

(17) Ouellette, A. L.; Li, J. J.; Cooper, D. E.; Ricco, A. J.; Kovacs, G. T. A. *Anal. Chem.* **2009**, *81*, 3216-3221.

(18) Warsinke, A. *Anal. Bioanal. Chem.* **2009**, *393*, 1393-1405.

(19) Jokerst, J. V.; Jacobson, J. W.; Bhagwandin, B. D.; Floriano, P. N.; Christodoulides, N.; McDevitt, J. T. *Anal. Chem.* **2010**, *82*, 1571-1579.

(20) Mark, D.; Haeberle, S.; Roth, G.; von Stetten, F.; Zengerle, R. *Chem. Soc. Rev.* **2010**, *39*, 1153-1182.

(21) Manz, A.; Harrison, D. J.; Verpoorte, E. M. J.; Fettinger, J. C.; Paulus, A.; Ludi, H.; Widmer, H. M. *J. Chromatogr.* **1992**, *593*, 253-258.

(22) Harrison, D. J.; Manz, A.; Fan, Z. H.; Ludi, H.; Widmer, H. M. *Anal. Chem.* **1992**, *64*, 1926-1932.

(23) West, J.; Becker, M.; Tombrink, S.; Manz, A. *Anal. Chem.* **2008**, *80*, 4403-4419.

(24) Dittrich, P. S.; Tachikawa, K.; Manz, A. *Anal. Chem.* **2006**, *78*, 3887-3907.

(25) Mikkers, F. E. P.; Everaerts, F. M.; Verheggen, T. *J. Chromatogr.* **1979**, *169*, 11-20.

(26) Mikkers, F. E. P.; Everaerts, F. M.; Verheggen, T. *J. Chromatogr.* **1979**, *169*, 1-10.

(27) Jorgenson, J. W.; Lukacs, K. D. *Anal. Chem.* **1981**, *53*, 1298-1302.

(28) Harris, D. C. *Quantitative chemical analysis*; 5th ed. ed.; W.H. Freeman: New York, 1999.

(29) Landers, J. P. *Handbook of capillary and microchip electrophoresis and associated microtechniques*; 3rd ed.; CRC Press: Boca Raton, 2008.

(30) Hu, Q.; Sommerfeld, M.; Jarvis, E.; Ghirardi, M.; Posewitz, M.; Seibert, M.; Darzins, A. *Plant J.* **2008**, *54*, 621-639.

(31) Greenwell, H. C.; Laurens, L. M.; Shields, R. J.; Lovitt, R. W.; Flynn, K. J. *J. R. Soc. Interface* **2010**, *7*, 703-726.

(32) Chisti, Y. *Biotechnol. Adv.* **2007**, *25*, 294-306.

(33) Chisti, Y. *Trends Biotechnol.* **2008**, *26*, 126-131.

(34) Pienkos, P. T.; Darzins, A. *Biofuels Bioprod. Bioref.* **2009**, *3*, 431-440.

(35) Guschina, I. A.; Harwood, J. L. *Prog. Lipid Res.* **2006**, *45*, 160-186.

(36) Arts, M. T.; Brett, M. T.; Kainz, M. J. *Lipids in aquatic ecosystems*; Springer: Dordrecht, 2009.

(37) Roessler, P. G. *J. Phycol.* **1990**, *26*, 393-399.

(38) Banerjee, A.; Sharma, R.; Chisti, Y.; Banerjee, U. C. *Crit. Rev. Biotechnol.* **2002**, *22*, 245-279.

(39) Gouveia, L.; Marques, A. E.; da Silva, T. L.; Reis, A. *J. Ind. Microbiol. Biotechnol.* **2009**, *36*, 821-826.

(40) Rodolfi, L.; Zittelli, G. C.; Bassi, N.; Padovani, G.; Biondi, N.; Bonini, G.; Tredici, M. R. *Biotechnol. Bioeng.* **2009**, *102*, 100-112.

(41) Courchesne, N. M. D.; Parisien, A.; Wang, B.; Lan, C. Q. *J. Biotechnol.* **2009**, *141*, 31-41.

(42) Volkman, J. K.; Dunstan, G. A.; Jeffrey, S. W.; Kearney, P. S. *Phytochemistry* **1991**, *30*, 1855-1859.

(43) Berge, J. P.; Gouygou, J. P.; Dubacq, J. P.; Durand, P. *Phytochemistry* **1995**, *39*, 1017-1021.

(44) Brown, M. R.; Dunstan, G. A.; Norwood, S. J.; Miller, K. A. *J. Phycol.* **1996**, *32*, 64-73.

(45) Budge, S. M.; Parrish, C. C. *Lipids* **2003**, *38*, 781-791.

(46) Guiheneuf, F.; Mimouni, V.; Ulmann, L.; Tremblin, G. *J. Exp. Mar. Biol. Ecol.* **2009**, *369*, 136-143.

(47) Paik, M. J.; Kim, H.; Lee, J.; Brand, J.; Kim, K. R. *J. Chromatogr., A* **2009**, *1216*, 5917-5923.

(48) Roberts, L. D.; McCombie, G.; Titman, C. M.; Griffin, J. L. *J. Chromatogr., B* **2008**, *871*, 174-181.

(49) Ratledge, C.; Wilkinson, S. G. *Microbial lipids*; Academic Press: London, 1988.

CHAPTER 2. *Targeted Metabolic Analysis of Serum Homocysteine Using Microchip Capillary Electrophoresis and Pulsed Electrochemical Detection*

2.1 Introduction

This chapter describes a targeted metabolic analysis of the thiol-containing amino acid homocysteine (Hcys). As mentioned in the previous chapter, targeted metabolic analysis is the measurement of one or more selected metabolites in a biological sample. Interest in Hcys as a target metabolite stems from its diagnostic value in assessing cardiovascular disease (CVD) risk.[1-3] Hcys has been linked to the onset of premature CVD when present at elevated levels in blood plasma or serum, and therefore is considered a clinically relevant biomarker of CVD.[1-3] Concentrations of total Hcys (tHcys) in blood plasma or serum typically range from 5-15 μM for healthy individuals to more than 100 μM for individuals suffering from severe hyperhomocysteinemia.[4] tHcys comprises both the oxidized (disulfide) and reduced (thiol) form of the molecule and is typically the quantity measured for clinical analysis.[1-3] Oxidized forms of Hcys in blood plasma include both the free and protein-bound disulfide.

Many analytical methodologies have been used to measure tHcys in serum or plasma samples including hyphenated liquid and gas chromatography techniques, mass spectrometry, and immunoassays.[5-6] While these methodologies are not without merit, the majority are time consuming and require use of expensive and/or complex instrumentation. Thus, the aim of this work was to reduce the time and cost of the

analysis through miniaturization. As discussed in Chapter 1, miniaturized point-of-care (POC) technologies are increasingly being developed for these types of assays due to their simplicity, low operating costs, and the ability to obtain real time results in a clinical setting.[7] Here, initial steps towards realizing a POC technology for measuring tHcys in blood serum were taken utilizing a miniaturized analysis system.

Microchip capillary electrophoresis (MCE)[8-9] integrated with electrochemical detection (ECD) was employed towards this end to isolate and detect the target metabolite. MCE was used as it is a highly efficient separation technique capable of resolving multiple components such as those found in blood serum or plasma. Additionally, ECD was utilized because it can be easily miniaturized without loss of performance,[10] and allows for direct detection of the target metabolite without the need for derivitization. The effectiveness of this detection mode has been demonstrated previously for multiple separation systems including conventional CE[11] and MCE.[12-13]

Two types of ECD are typically employed in the detection of Hcys (or thiols in general): dc amperometric detection with chemically modified electrodes (CME),[14-19] and pulsed electrochemical detection (PED) with noble metal electrodes.[20-27] The most popular CMEs used for detecting thiols are Au-Hg amalgam[14-15] and cobalt phthalocyanine doped carbon paste[16-18] or carbon ink electrodes.[19] While these CMEs are effective in selectively detecting thiol containing species, electrode lifetimes are limited due to consumption of electrode material (mercury electrodes) or irreversible fouling of the working electrode. An attractive alternative to CMEs is PED as this technique requires no electrode modification steps or physical regeneration of the electrode surface. With PED the

electrode surface is regenerated in situ via an electrochemical cleaning pulse employed prior to the detection step.[28] It is used commonly for biological samples like blood plasma or serum which tend to foul the working electrode, and thus limit its effective lifetime.[23] Our lab has demonstrated the utility of PED coupled with MCE for the analysis of a broad range of analytes including thiols, amines, and carbohydrates.[29] The robust nature of PED along with its functionality in MCE systems thus makes it an ideal candidate for tHcys analysis.

Material presented in the following chapter explores the utility of PED coupled with MCE for the targeted metabolic analysis of serum tHcys. This work was conducted using a poly(dimethylsiloxane) (PDMS) MCE device integrated with a gold microelectrode for Hcys detection. Initial separation and detection conditions for Hcys were developed using a biologically relevant mixture of thiol containing compounds commonly found in blood plasma or serum. Performance of two different PED waveforms were then compared to determine which would be best suited for Hcys detection. Following this, tHcys was analyzed in a human serum sample using the MCE-ECD device. Finally, work was conducted to improve detection limits of this device using increased surface area electrodes.

2.2 Materials and Methods

2.2.1 Chemicals and Materials

DL-homocysteine, L-cysteine (free base), glutathione, γ-glutamyl-cysteine, cysteinyl-glycine, *N*-acetyl-L-cysteine, and propylene glycol monomethyl ether acetate were purchased from Sigma-Aldrich (St. Louis, MO). Boric acid and sodium hydroxide were

purchased from Fisher Scientific (Pittsburgh, PA). Tris(2-carboxyethyl)phosphine (TCEP) solution (5.0 M, buffered at pH 7.5) was purchased from Pierce Biotechnology, Inc. (Rockford, IL). Molecular weight cut off micro-centrifuge filters (3 kDa) were purchased from Pall Corp. (Ann Arbor, MI). Silicon wafers (4 in) were purchased from University Wafer (South Boston, MA). SU-8 2035 negative photoresist was purchased from MicroChem Corp. (Newton, MA). Sylgard 184 elastomer and curing agent (PDMS) were purchased from Dow Corning (Midland, MI). Gold and palladium wire (0.025 mm dia., 99.99% purity) were purchased from Goodfellow Corp. (Huntingdon, England). Glass slides (75 mm × 50 mm) were purchased from Corning Glass Works (Corning, NY). Insulated copper wire (1 mm dia.) was purchased from Radioshack (Fort Collins, CO). High purity silver paint was purchased from Structure Probe, Inc. (West Chester, PA). Instant adhesive was purchased from Loctite Corp. (Rocky Hill, CT). Clear room temperature vulcanizing (RTV) silicone adhesive was purchased from Permatex, Inc. (Solon, OH). All chemicals were used as received without further purification.

2.2.2 Solution Preparation

Stock solutions of 10 mM DL-homocysteine, L-cysteine, glutathione, γ-glutamyl-cysteine, cysteinyl-glycine, and *N*-acetyl-L-cysteine were prepared weekly in 10 mM HCl. Stock solutions were stored at 4 °C when not in use. A 20 mM boric acid buffer was adjusted to pH 9.2 with 30% (w/w) NaOH and used as background electrolyte (BGE) for MCE. All solutions were prepared using ultra-pure 18.2 MΩ water (Milli-Q, Millipore Corp.; Billerica, MA).

2.2.3 Device Fabrication

Microchips employed in this study were of a standard cross design commonly used in our laboratory.[29-31] These microchips utilize electrode alignment channels orthogonal to the separation channel for reproducible electrode alignment.[30-31] The general design used for the following fabrication is shown in Figure 1. All separation and injection channels in the microchip were 50 μm in width and depth except the microwire alignment channels which were 25 μm in width. The separation channel had a total length of 50 mm and an effective length of 49.3 mm while the injection channels were 10 mm in length. All reservoirs were 5 mm in diameter. The working electrode was positioned 250 μm downstream from a current decoupler at the end of the separation channel, as is seen in the bright-field image in Figure 1. Previous work found that this electrode spacing gives the best compromise between increased signal-to-noise (S/N) and decreased separation efficiency as the distance from the decoupler increases.[31-32] The purpose of the decoupler in this system was to isolate the working electrode from the high voltage used for electrophoretic separations.[33-34] In the present case the decoupler acts as the CE cathode. The decoupler consisted of palladium microwire as this metal absorbs H_2 (g) generated at the decoupler during electrophoresis.[31,34] Solution leakage around the decoupler was prevented by employing discontinuous electrode alignment channels which terminated 50 μm short of the separation channel (PDMS bridges).[31]

Microchips were fabricated from PDMS using standard soft lithographic techniques.[35-36] Initially, a master mold was prepared by photo-polymerizing SU-8 2035 negative photoresist on a 100 mm silicon wafer. To fabricate the master mold, a 50 μm thick layer

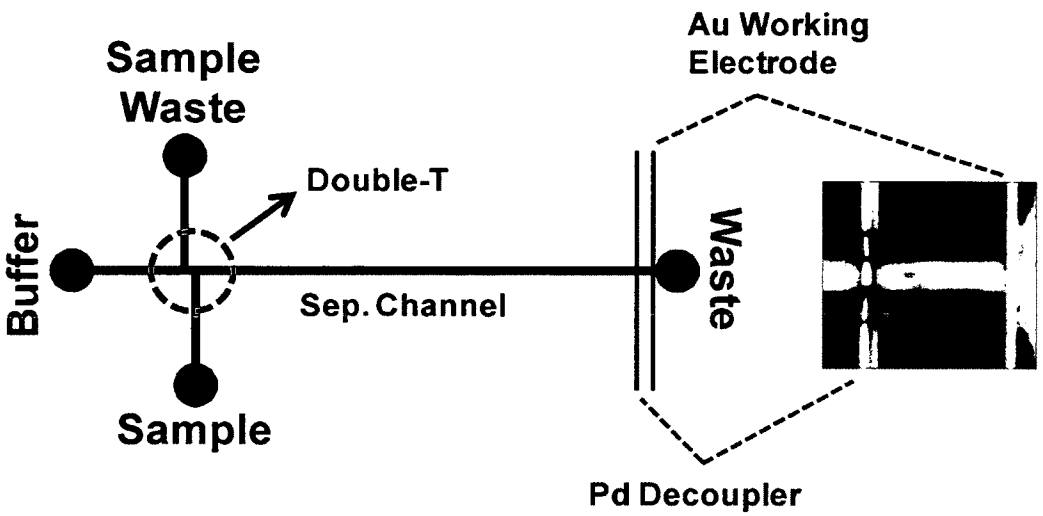

Figure 1. Schematic of MCE-ECD device showing the position of solution reservoirs, double-T injector, decoupler, and working electrode. The bright-field image shows the detection region of the microchip. In this image a palladium decoupler is positioned upstream of a gold working electrode inside the separation channel of the microchip. PDMS bridges which prevent solution flow down the decoupler alignment channels are seen in this image formed around the electrode.

of photoresist was first spun onto the wafer using a spin coater (Laurell Technologies Corp.; North Wales, PA) operating at 2,250 rpm for 30 s. The wafer with photoresist was then baked on a hotplate at 65 °C for 3 min followed by 95 °C for 5 min. After baking, device features were defined by placing a digitally produced photomask (Printing Services, Colorado State University) on the photoresist and exposing under an Intelli-Ray 400 flood UV source (Uvitron International; West Springfield, MA) at 100 W for 7 s. The photomask was removed and the wafer baked again at 65 °C for 2 min and 95 °C for 6 min. The unexposed photoresist was then developed from the wafer using propylene glycol monomethyl ether acetate, and the resulting master mold baked in an oven at 95 °C for 24 hrs before use.

Molded PDMS was prepared by curing a 10:1 mixture of degassed PDMS elastomer and curing agent on the master mold in a 60 °C oven for at least three hours. The cured PDMS was cut from the master mold using a scalpel and reservoirs formed at the end of the microfluidic channels using a 6 mm diameter biopsy punch (Robbins Instruments, Chatham, NJ). Palladium and gold microwire electrodes were then incorporated at the end of the separation channel of the PDMS microchip by inserting the microwires into the alignment channels of the molded PDMS by hand under a stereo-microscope (Meiji Techno Co., LTD; Tokyo, Japan). The microwires were held in place with transparent tape during the fabrication process. Following this, the molded PDMS with microwires was oxidized alongside a blank piece of PDMS in an air plasma (Harrick Plasma Cleaner/Sterilizer PDC-32G) at 18 W for 45 s. The microchip was assembled in an irreversible fashion by bringing the molded and blank PDMS pieces into conformal contact, and placing on a 75 mm × 50 mm glass microscope slide. Slight pressure was

applied to the electrode region of the microchip, and the microchip then placed in a 60 °C oven for 30 min to ensure sealing of the PDMS bridges around the decoupler. Following this, the microwire electrodes were trimmed to size with a scalpel at the ends of the electrode alignment channels, and these channels then sealed using quick curing epoxy. Electrode leads consisting of insulated 1 mm diameter copper wire were cut to size and glued to the assembled device using quick curing epoxy. Electrical contact between the electrode leads and microwire electrodes was made using high purity silver paint. The exposed electrical contacts were then insulated with clear RTV silicone adhesive and allowed to cure 24 hrs before use.

2.2.4 Microchip CE

Microfluidic channels were conditioned with 1 M NaOH for 30 minutes prior to conducting separations. NaOH was rinsed from the channels with ultra-pure water before filling with BGE. All solutions were introduced into the microfluidic channels by applying pressure to a reservoir containing the solution with a 5 mL disposable syringe (Becton-Dickinson; Franklin Lakes, NJ). The buffer, sample waste, and waste reservoirs were filled with 80 μL of BGE and the sample reservoir with 80 μL of sample solution prior to running analyses.

Applied voltages for sample injection and electrophoretic separation were facilitated by a programmable high voltage power supply built in-house.[37] Sample introduction was achieved using a 15 s pinched injection[38] through a 250 μm double-T injector.[39-40] For pinched injections, the sample and buffer reservoirs were held at +450 V while the sample waste reservoir was held at -160 V and the decoupler at ground. Separations were

conducted by applying +1,000-1,500 V to the buffer reservoir while holding the palladium decoupler at ground. A pushback voltage of +450 V was applied to the sample and sample waste reservoirs during separation to prevent sample leakage into the separation channel.[38,41] Use of pushback voltages resulted in junction potentials of +594-750 V for the separation voltages given above. This translated to field strengths of 119-150 V/cm in the separation channel of the microchip calculated using Kirchhoff's rules.

2.2.5 Electrochemical Detection

A commercially available potentiostat (CHI 660B Electrochemical Analyzer; CH Instruments, Austin, TX) was used for electrochemical measurements. All experiments were conducted using a two-electrode cell in which a 1.0 mm diameter platinum wire in the waste reservoir of the microchip acted as a counter electrode. All detection potentials were applied versus this platinum counter electrode, as is commonly done in MCE-ECD.[31] To condition the gold working electrode, 75 cyclic voltammetric scans were conducted from -1.0 V to +2.0 V at a scan rate of 500 mV/s while BGE was electrokinetically pumped over the electrodes. Two different PED waveforms were compared for detection of Hcys: pulsed amperometric detection (PAD)[20,28] and integrated pulsed amperometric detection (iPAD).[21,28] Parameters for these waveforms were optimized using hydrodynamic voltammetry at the gold working electrode of the MCE-ECD device. PAD was used for the final tHcys analysis, employing the following detection parameters: E_{ox} = +1.7 V for 50 ms, E_{red} = -0.4 V for 100 ms, and E_{det} = +1.6 V for 150 ms.

2.2.6 tHcys Preparation

tHcys was measured from serum immediately after being obtained from a healthy human volunteer. The disulfide reducing reagent TCEP (5.0 M) was added at 10 mM effective concentration to the serum and allowed to react for 20 min to reduce the oxidized forms of Hcys (free and protein-bound disulfide). Following the reduction step, protein was removed from the serum sample by filtering with a 3 kDa microcentrifuge filter. For centrifugation, the sample was spun at 14,500 rpm for 20 min. The resulting filtrate containing the tHcys fraction was removed, diluted 10× with BGE, and analyzed using the MCE-ECD device.

2.3 Results and Discussion

2.3.1 Separation Conditions

In order to analyze tHcys in serum, separation conditions needed to be developed which were capable of resolving Hcys from potential interferants in the sample. Initially, separation conditions were developed for a mixture of biologically relevant metabolites commonly found in blood plasma or serum. This mixture consisted of the thiol containing metabolites *N*-acetyl-cysteine, cysteine, cysteinyl-glycine, glutamyl-cysteine, glutathione, and Hcys. Using this mixture, multiple separation conditions were screened examining the effects of pH, ionic strength, and BGE additives on the separation. From these studies it was found BGE additives such as surfactants and organic modifiers had negligible benefits for the present analysis, and therefore their use was not pursued further.

The condition having the most marked effect on analyte resolution was the pH of the BGE. This was expected as all metabolites in the mixture had multiple functional groups

with differing pKa values. Because of this, the pH of the BGE could be manipulated to change the charge-to-mass ratio of Hcys and thus effect separation of this analyte from the remaining components in the mixture. It was found Hcys could be resolved from these components at pH conditions above ~pH 8.0 and below ~pH 3.0. However, separations below pH 3.0 were problematic due to bubble formation at the palladium decoupler. Increased solution conductivity at low pH (increased concentration of hydronium ion) is speculated to increase the electrolytic rate of H_2 (g) generation at the palladium decoupler, thus causing bubble formation. As a result, separations were conducted under mildly alkaline pH conditions as these problems were largely absent in this pH regime.

Baseline resolution (Resolution = 1.5) between Hcys and the remaining mixture components could be achieved using a 20 mM borate buffer at pH 9.2. As a result this buffer was used as the BGE for all subsequent experiments. An example separation obtained using this BGE is shown in Figure 2. Resolution between Hcys and the closest adjacent peak (cysteine) was calculated to be 3.3 ± 0.1 (n = 3) using the standard chromatographic definition of resolution. This definition is shown below as Equation 2.1 where t_m denotes analyte migration time and $w_{1/2av}$ the average peak width at half height for two adjacent peaks.

$$Resolution = \frac{0.589\Delta t_m}{w_{1/2av}} \tag{2.1}$$

Additionally, separation efficiency, or number of theoretical plates (N), for Hcys was calculated to be 3,400 ± 800 N (n = 3) using the chromatographic definition given below

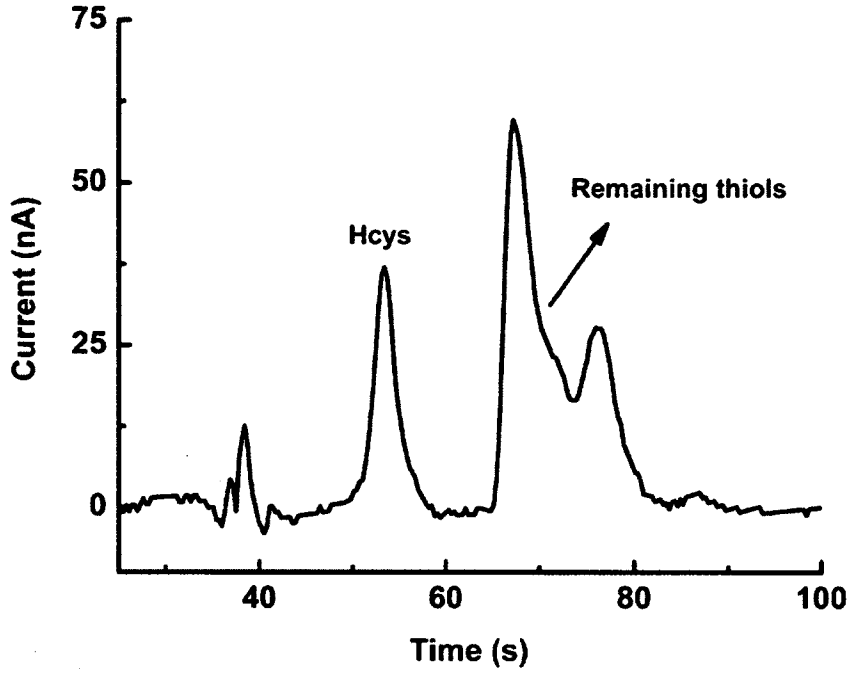

Figure 2. Electropherogram showing baseline separation of Hcys (1 mM) from Cys, *N*-acetyl-Cys, Cys-Gly, Glu-Cys, and Gsh (1 mM each). BGE was 20 mM borate, pH 9.2. Field strength was 150 V/cm. Analytes were oxidized using PAD at a detection potential of +1.4 V applied vs. a platinum counter electrode. Baseline was fit and subtracted using the baseline function in Origin Pro 8.

as Equation 2.2. In this equation t_m again denotes migration time and $w_{1/2}$ peak width at half height for the analyte of interest.

$$N = \frac{5.5t_m^2}{w_{1/2}^2} \tag{2.2}$$

While this efficiency is lower than those reported for other MCE systems,[38-39] it is typical of those obtained with MCE-ECD systems constructed from PDMS.[31,42] These lower efficiencies result from a need to use reduced field strengths with MCE-ECD to prevent bubble formation and field induced interference at the decoupler and working electrode, respectively.

2.3.2 Comparison of PED Techniques

Two different PED waveforms were compared to determine which was the most suitable for tHcys analysis. These waveforms consisted of pulsed amperometric detection (PAD) and integrated pulsed amperometric detection (iPAD). Schematics of the waveforms and optimized detection parameters are shown in Figure 3(a) and Figure 3(b), respectively. Both waveforms consist of an anodic cleaning and cathodic regeneration step that precede the detection step. In the anodic cleaning step, a high positive potential is applied to the working electrode and adsorbed materials displaced as a monolayer of oxide forms on the surface of the noble metal electrode. The cathodic regeneration step reduces this inert surface oxide layer leaving a bare metal electrode surface at which electrolysis reactions can occur. Oxidation of Hcys at this electrode proceeds via a surface oxide catalyzed mechanism in which labile surface oxide intermediates facilitate the transfer of oxygen to the thiol group, ultimately oxidizing it to a sulfate.[20]

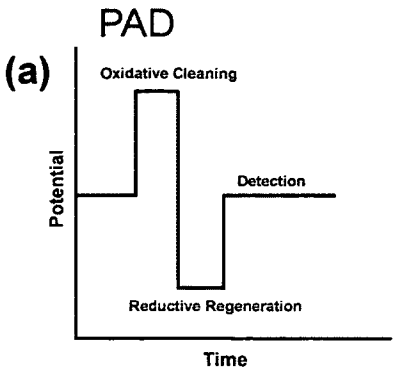

Typical PAD Parameters

Parameter	Potential (V)	Time (ms)
E_{ox}	+2.0	100
E_{red}	-0.4	100
E_{det}	+1.4-1.6	150

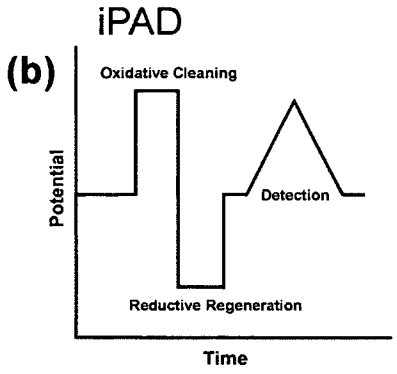

Typical iPAD Parameters

Parameter	Potential (V)	Time (ms)
E_{ox}	+1.8	50
E_{red}	-0.4	100
E_{det}	+1.4-1.6	300
$^{*}E_{hold}$	-0.4	150

*Holding potential preceding and following the detection step

Figure 3. (a) Schematic showing typical PAD waveform and corresponding detection parameters. (b) Schematic showing typical iPAD waveform and corresponding detection parameters.

Because Hcys oxidation occurs concomitantly with surface oxide formation, a large portion of the analytical signal is dominated by oxide formation currents. It has been shown experimentally in both HPLC and conventional CE that iPAD results in increased sensitivity and more stable baselines than PAD.[21-22,24-25] This is due to cancellation of the surface oxide background current as the result of using a triangular detection waveform. Using this waveform, oxide formation current generated in the anodic sweep is negated by oxide reduction current in the cathodic sweep, thus decreasing background current caused by surface oxide formation.

To determine whether this would be the case for our MCE-ECD system both PAD and iPAD of a Hcys standard were compared. Lower background currents were seen with iPAD; however, improvement in sensitivity was not observed. These results are consistent with those of a previously published report in which PAD and iPAD were compared in a MCE system.[43] The lack of improved sensitivity using iPAD in MCE systems is speculated to be due to the slower cycling time of this waveform compared to PAD. The faster cycling times attainable with PAD results in more oxidation events being integrated or captured at the working electrode, thus yielding better peak shapes and lower limits of detection (LOD) than iPAD.

Since better detection performance was obtained using PAD, this waveform was used for the following tHcys analysis. It was determined current response for Hcys using PAD was linear from the limit of quantitation to concentrations above 100 μM, thus allowing for quantification over the clinically relevant range. The limit of detection (LOD) of Hcys was calculated to be 4.0 ± 1.2 μM (n = 3) using S/N = 3. This corresponded to a mass

limit of 14.0 ± 4.3 fmol which is comparable to those given for PED of thiols in conventional capillary electrophoresis systems.[26] Mass limits were calculated for an injection plug length of 3.4 ± 0.3 nL (n = 3), as measured using fluorescence microscopy. The injected plug length was larger than that defined by the double-T injector of the microchip due to sample leakage into the separation channel during injection. This leakage arose from the need to hold the decoupler at ground during injection to prevent damage to the potentiostat.[31] It should be noted alternate injection schemes have now been developed which confine the plug to the volume defined by the double-T; however, these injection conditions were determined after the conclusion of the present studies.

2.3.3 Serum tHcys Analysis

After developing suitable separation and detection conditions, serum tHcys was analyzed using the MCE-ECD device. To keep the analysis as direct as possible sample preparation was kept to a minimum. In the present case minimal sample preparation was desired as it makes the analysis easier to perform, which is one of the major goals of POC technologies. Here, a true, direct analysis of the serum sample could not be conducted as most Hcys was sequestered in disulfide bonds with proteins and other thiol containing species in solution. As a result, a disulfide reduction step was required to recover the tHcys fraction (oxidized and reduced forms). For this step, TCEP was used as reactions using this reducing reagent typically proceed to 100% conversion and do not result in mixed thiol formation.[44] Additionally, a microcentrifuge filtration step was employed to remove proteins from the tHcys fraction.[15] Removal of protein was necessary as proteins adsorb to the PDMS and adversely affect electroosmotic flow (EOF) and thus fluid manipulation on-chip.

Following these initial sample preparation steps the tHcys fraction was diluted and analyzed on-chip. An example electropherogram (black trace) showing the metabolite profile of a tHcys fraction analyzed in this manner is shown Figure 4; however, as is evident from this electropherogram no signal was seen for tHcys. This is readily apparent when comparing to a serum sample in which Hcys has been spiked (red trace). The lack of a discernable tHcys peak in this case is most likely the result of a low basal level of tHcys in the serum sample itself. Since serum was obtained from a healthy individual, it is assumed the concentration of tHcys was at or below ~15 μM. Upon 10× dilution with BGE tHcys in this sample was below the detection limit of the device (~5 μM). A 10× sample dilution was required for the present analysis as it ensured reproducible sample injection. Direct injection of undiluted filtrate and dilutions below 10× were tested, but resulted in irreproducible results. This irreproducibility stemmed from the high ionic strength of the sample solution relative to the BGE. Ionic strength mismatches such as this have been shown to cause sample destacking and other electroosmotic flow effects which disrupt electrokinetic injections in MCE devices.[41]

Despite the inability to measure tHcys in this sample, the ability to resolve and detect spiked Hcys in serum is promising. It is evident when comparing this electropherogram (red trace) to the unspiked serum sample in Figure 4 (black trace) that Hcys is well resolved from interferants and could potentially be quantified if the LOD was lowered. At the present time this system could be used to analyze tHcys in individuals suffering from hyper-homocysteinemia at tHcys concentrations above ~50 μM. However, improvements in detection limits are needed if this technology is to be used in measuring tHcys concentrations across the clinically relevant range (~5 μM-100 μM).

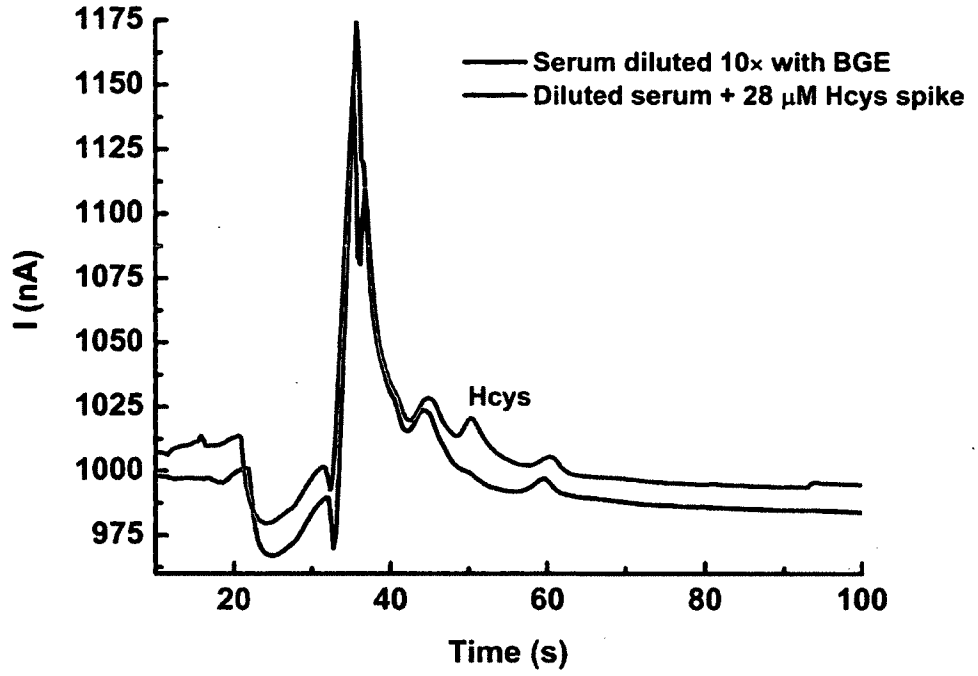

Figure 4. Electropherogram of a serum tHcys fraction (black trace) and the same fraction spiked with 28 μM Hcys (red trace). BGE was 20 mM borate, pH 9.2. Field strength was 131 V/cm. Analytes were oxidized using PAD at a detection potential of +1.6 V applied vs. a platinum counter electrode. The red trace has been shifted in the vertical direction to aid in visualization.

2.3.4 Electrode Surface Area Studies

One approach explored to lower detection limits for this system was increasing the size of the working electrode. Since ECD is a surface derived phenomenon, increasing electrode surface area should increase collection efficiency and thus signal for the analyte of interest. In the present case, electrode surface area was increased in our MCE-ECD system by placing two gold microwires adjacent to each other at the end of the separation channel. These microwires were connected to a common electrode lead to make them function as a single working electrode. A bright-field image of this electrode setup is shown in Figure 5(a). Electrochemical response between a one microwire ECD system and the increased surface area, two microwire ECD system was compared using a Hcys standard, with the resulting electropherograms shown in Figure 5(b). As seen in these electropherograms, response for the two microwire system is approximately double that of the one microwire system; however, improvements in detection limits were not observed for this electrode system as noise increased by approximately two times as well. Thus, this system was ineffective in lowering the detection limit for the MCE-ECD device.

Recently, our lab has demonstrated improved S/N levels for larger surface area electrodes contained within bubble cell detection regions of MCE devices.[45] This improvement in S/N is the result of decreased resistance and hence a decreased voltage drop in the bubble cell region of the microchip.[45] The use of bubble cells has improved detection limits, although at this time these limits are not adequate enough to detect tHcys at the lower end of the clinically relevant range. Potentially, bubble cell detectors could be integrated with

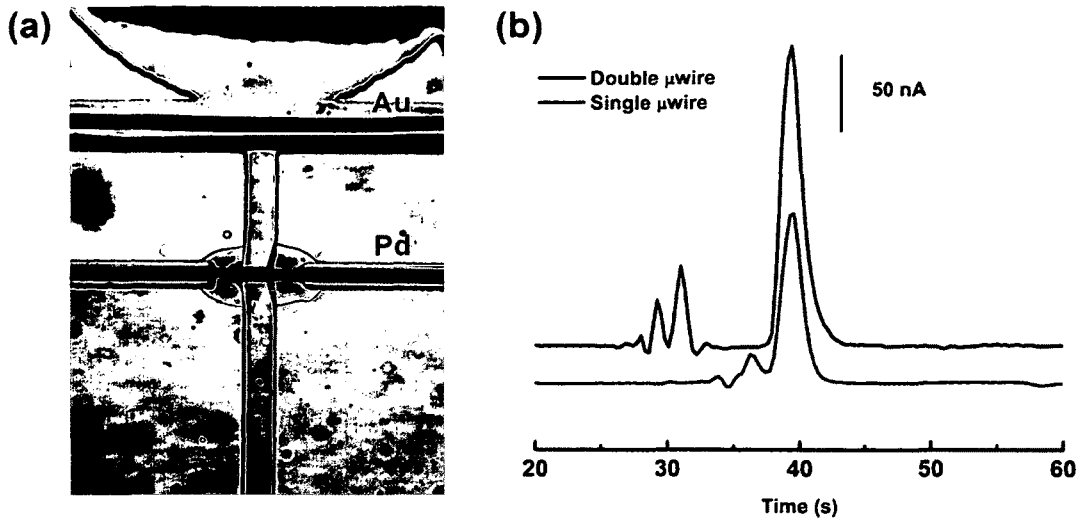

Figure 5. (a) Bright-field image showing detection region of a MCE device with a larger surface area working electrode. As seen in this image the working electrode consists of two gold microwires placed side by side in the electrode alignment channel. (b) Electropherograms comparing electrochemical response of 200 μM Hcys at a single microwire (μwire) electrode (red trace) and the increased surface area, double microwire electrode (black trace). BGE was 20 mM borate, pH 9.2. Field strength was 150 V/cm. Analytes were oxidized using PAD at a detection potential of +1.6 V applied vs. a platinum counter electrode. Baselines were fit and subtracted using the baseline function in Origin Pro 8. Electropherograms were offset in the vertical direction to aid in visualization.

coulametric electrodes to improve collection efficiency, and thus detection limits for these systems.

2.4 Conclusions

Targeted metabolic analysis is a useful clinical tool for diagnosing and monitoring disease states. This chapter discussed an initial approach towards developing a POC system for target analysis of Hcys using MCE coupled with ECD. Methodology was developed that allowed for spiked Hcys to be successfully resolved from interfering components in a serum sample; however, detection limits were not low enough to detect tHcys in this sample. Increased surface area electrodes show promise for lowering limits of detection, but at this time these detection limits are not sufficiently low enough to detect tHcys at the lower end of the clinically relevant range. Further sample preparation steps such as solid phase extraction could be employed to pre-concentrate tHcys for MCE-ECD analysis; however, these steps are time consuming and negate the initial motivations for using a miniaturized analysis platform (i.e. speed and simplicity). Nonetheless, integration of these sample preprocessing steps onto a single microfluidic platform could prove to be beneficial if the analysis is faster, simpler, and more cost effective than traditional methods.

2.5 References

(1) Jacobsen, D. W. *Clin. Chem.* **1998**, *44*, 1833-1843.

(2) Nappo, F.; De Rosa, N.; Marfella, R.; De Lucia, D.; Ingrosso, D.; Perna, A. F.; Farzati, B.; Giugliano, D. *JAMA* **1999**, *281*, 2113-2118.

(3) Anderson, J. L.; Muhlestein, J. B.; Horne, B. D.; Carlquist, J. F.; Bair, T. L.; Madsen, T. E.; Pearson, R. R. *Circulation* **2000**, *102*, 1227-1232.

(4) Kang, S. S.; Wong, P. W.; Cook, H. Y.; Norusis, M.; Messer, J. V. *J. Clin. Invest.* **1986**, *77*, 1482-1486.

(5) Ueland, P. M.; Refsum, H.; Stabler, S. P.; Malinow, M. R.; Andersson, A.; Allen, R. H. *Clin. Chem.* **1993**, *39*, 1764-1779.

(6) Powers, H. J.; Moat, S. J. *Curr. Opin. Clin. Nutr. Metab. Care* **2000**, *3*, 391-397.

(7) Ouellette, A. L.; Li, J. J.; Cooper, D. E.; Ricco, A. J.; Kovacs, G. T. A. *Anal. Chem.* **2009**, *81*, 3216-3221.

(8) Manz, A.; Harrison, D. J.; Verpoorte, E. M. J.; Fettinger, J. C.; Paulus, A.; Ludi, H.; Widmer, H. M. *J. Chromatogr.* **1992**, *593*, 253-258.

(9) Harrison, D. J.; Manz, A.; Fan, Z. H.; Ludi, H.; Widmer, H. M. *Anal. Chem.* **1992**, *64*, 1926-1932.

(10) Nyholm, L. *Analyst* **2005**, *130*, 599-605.

(11) Chen, R. S.; Cheng, H.; Wu, W. Z.; Ai, X. O.; Huang, W. H.; Wang, Z. L.; Cheng, J. K. *Electrophoresis* **2007**, *28*, 3347-3361.

(12) Vandaveer, W. R.; Pasas-Farmer, S. A.; Fischer, D. J.; Frankenfeld, C. N.; Lunte, S. M. *Electrophoresis* **2004**, *25*, 3528-3549.

(13) Wang, J. *Electroanalysis* **2005**, *17*, 1133-1140.

(14) Oshea, T. J.; Lunte, S. M. *Anal. Chem.* **1993**, *65*, 247-250.

(15) Pasas, S. A.; Lacher, N. A.; Davies, M. I.; Lunte, S. M. *Electrophoresis* **2002**, *23*, 759-766.

(16) Halbert, M. K.; Baldwin, R. P. *Anal. Chem.* **1985**, *57*, 591-595.

(17) Oshea, T. J.; Lunte, S. M. *Anal. Chem.* **1994**, *66*, 307-311.

(18) Huang, X. J.; Kok, W. T. *J. Chromatogr., A* **1995**, *716*, 347-353.

(19) Kuhnline, C. D.; Gangel, M. G.; Hulvey, M. K.; Martin, R. S. *Analyst* **2006**, *131*, 202-207.

(20) Vandeberg, P. J.; Kowagoe, J. L.; Johnson, D. C. *Anal. Chim. Acta* **1992**, *260*, 1-11.

(21) Vandeberg, P. J.; Johnson, D. C. *Anal. Chem.* **1993**, *65*, 2713-2718.

(22) Vandeberg, P. J.; Johnson, D. C. *Anal. Chim. Acta* **1994**, *290*, 317-327.

(23) Evrovski, J.; Callaghan, M.; Cole, D. E. C. *Clin. Chem.* **1995**, *41*, 757-758.

(24) Lacourse, W. R.; Owens, G. S. *Anal. Chim. Acta* **1995**, *307*, 301-319.

(25) LaCourse, W. R.; Owens, G. S. *Electrophoresis* **1996**, *17*, 310-318.

(26) Owens, G. S.; LaCourse, W. R. *J. Chromatogr., B* **1997**, *695*, 15-25.

(27) LaCourse, W. R.; Modi, S. J. *Electroanalysis* **2005**, *17*, 1141-1152.

(28) LaCourse, W. R. *Pulsed Electrochemical Detection in High-Performance Liquid Chromatography*; John Wiley & Sons, Inc.: New York, 1997.

(29) Garcia, C. D.; Henry, C. S. *Anal. Chem.* **2003**, *75*, 4778-4783.

(30) Liu, Y.; Vickers, J. A.; Henry, C. S. *Anal. Chem.* **2004**, *76*, 1513-1517.

(31) Vickers, J. A.; Henry, C. S. *Electrophoresis* **2005**, *26*, 4641-4647.

(32) Lacher, N. A.; Lunte, S. M.; Martin, R. S. *Anal. Chem.* **2004**, *76*, 2482-2491.

(33) Wallingford, R. A.; Ewing, A. G. *Anal. Chem.* **1987**, *59*, 1762-1766.

(34) Kok, W. T.; Sahin, Y. *Anal. Chem.* **1993**, *65*, 2497-2501.

(35) Duffy, D. C.; McDonald, J. C.; Schueller, O. J. A.; Whitesides, G. M. *Anal. Chem.* **1998**, *70*, 4974-4984.

(36) McDonald, J. C.; Duffy, D. C.; Anderson, J. R.; Chiu, D. T.; Wu, H. K.; Schueller, O. J. A.; Whitesides, G. M. *Electrophoresis* **2000**, *21*, 27-40.

(37) Garcia, C. D.; Liu, Y.; Anderson, P.; Henry, C. S. *Lab Chip* **2003**, *3*, 324-328.

(38) Jacobson, S. C.; Hergenroder, R.; Koutny, L. B.; Warmack, R. J.; Ramsey, J. M. *Anal. Chem.* **1994**, *66*, 1107-1113.

(39) Effenhauser, C. S.; Manz, A.; Widmer, H. M. *Anal. Chem.* **1993**, *65*, 2637-2642.

(40) Koutny, L. B.; Schmalzing, D.; Taylor, T. A.; Fuchs, M. *Anal. Chem.* **1996**, *68*, 18-22.

(41) Shultz-Lockyear, L. L.; Colyer, C. L.; Fan, Z. H.; Roy, K. I.; Harrison, D. J. *Electrophoresis* **1999**, *20*, 529-538.

(42) Martin, R. S.; Gawron, A. J.; Lunte, S. M.; Henry, C. S. *Anal. Chem.* **2000**, *72*, 3196-3202.

(43) Garcia, C. D.; Henry, C. S. *Electroanalysis* **2005**, *17*, 223-230.

(44) Burns, J. A.; Butler, J. C.; Moran, J.; Whitesides, G. M. *J. Org. Chem.* **1991**, *56*, 2648-2650.

(45) Guan, Q.; Henry, C. S. *Electrophoresis* **2009**, *30*, 3339-3346.

CHAPTER 3. *Metabolic Fingerprinting of Canine Chemotherapy Using Capillary Electrophoresis*

3.1 Introduction

As mentioned in Chapter 1, the field of metabolomics has expanded to include a variety of different analysis approaches ranging from the global determination of all metabolites (metabolomics) to only one or a few metabolites (metabolite target analysis).[1] Data acquired from these studies are analyzed using a variety of different techniques which can highlight certain aspects of the biochemistry occurring within the cell or organism. This makes the field relevant to a multitude of bioanalytical applications, especially those concerned with disease diagnosis and monitoring.

The majority of metabolomic studies require instrumental techniques which provide high spatial resolution as well as qualitative and quantitative information on the metabolites being analyzed. For these reasons, NMR,[2] MS,[2-3] and hyphenated techniques such as GC-MS[2,4] and LC-MS[2,5] are typically employed. In recent years capillary electrophoresis (CE) has increasingly been utilized as a separation technique for metabolomics applications.[1,6-7] This trend is due in large part to the excellent resolving power and the high throughput capability of CE systems. In certain respects, CE is better suited for the analysis of biological samples like blood plasma and urine as it requires less sample preparation than GC and LC. With CE, analytes can be directly sampled from these biomatrices and analyzed without any prior sample preparation or derivitization (i.e., unlike GC). The downside to direct sample analysis using CE is limited capillary

lifetimes resulting from capillary plugging and/or protein adsorption.[1] However, these problems are limited when analyzing samples like urine as this biofluid typically has low viscosity, limited or no particulate matter, and low protein content.

Recently, the applicability of CE for the direct analysis of urine has been shown for metabolic fingerprinting analyses.[1,8-10] Metabolic fingerprinting is a technique in which data sets (e.g., peaks in an electropherogram) are globally compared to evaluate whether differences exist in their metabolite make-up (i.e., fingerprint). Data sets are usually compared using multivariate techniques such as partial least squares, parallel factor, or principle component analysis (PCA) to discern what differences, if any, exist in the data.[1,11] One benefit of using this approach is the ability to distinguish a disease state without having to target and analyze specific disease biomarkers. Since identification of specific metabolites is not necessary, the detection step does not need to provide qualitative information on the metabolites being analyzed. Thus, fingerprinting analyses can be conducted using non-specific detection techniques like UV absorbance.[8-10] This detection mode helps to increase the throughput of the analysis, but is also the major limitation of the technique as absolute identities of metabolites and potential biomarkers cannot be determined.

The following chapter explores upon these themes, examining the effectiveness of CE-UV as a tool for monitoring chemotherapy in dogs. For these studies, we examined metabolite fingerprints in urine obtained at multiple clinical time points for dogs diagnosed with cancer as well as fingerprints for a control population of healthy dogs. Urine was used for fingerprinting studies as collection methods are relatively non-

invasive compared to other biofluids (i.e., serum or plasma) and to date its utility has not been extensively explored for cancer related research.[11] In order to generate fingerprints, a rapid separation method was developed which resolved a maximum number of urine metabolites in a relatively short amount of time. The resulting data was analyzed using PCA to determine whether the metabolite make-up differed between time points and study groups (i.e., disease versus control). Additionally, z-scores were calculated for individual metabolites in the fingerprints of the diseased dogs to determine which metabolites, if any, were up-regulated or down-regulated versus controls.

3.2 Materials and Methods

3.2.1 Chemicals and Materials

Reagent grade acetonitrile (ACN), reagent grade 1-butanol (BuOH), reagent grade 1-propanol (PrOH), sodium benzoate, sodium borate, sodium hydroxide, and urea were purchased from Fisher Scientific (Pittsburgh, PA). Absolute ethanol (EtOH) and reagent grade methanol (MeOH) were purchased from Pharmco-Aaper (Brookfield, CT) and Mallinckrodt Baker, Inc. (Phillipsburg, NJ), respectively. Allantoin, creatinine, 3-hydroxybutyric acid, phenylalanine, phenylacetic acid, sodium dodecyl sulfate (SDS), sulfated β-cyclodextrin sodium salt, uracil, and uric acid were purchased from Sigma-Aldrich (St. Louis, MO). Polyimide coated, fused silica capillary (50 μm i.d., 360 μm o.d.) was purchased from Polymicro Technologies (Phoenix, AZ).

3.2.2 Solution Preparation

Stock solutions of the following compounds were prepared at 500 μM to 5 mM total concentration in 100 mM NaOH: allantoin, 3-hydroxybutyric acid, sodium benzoate,

creatinine, phenylalanine, phenylacetic acid, uracil, urea, and uric acid. Background electrolyte (BGE) for electrophoretic separations consisted of 25 mM borate, 75 mM SDS, 6.25 mM sulfated β-cyclodextrin, and 10% ACN adjusted to pH 9.5 with 1 M NaOH. All solutions were prepared using ultra-pure 18.2 MΩ water (Milli-Q, Millipore Corp.; Billerica, MA).

3.2.3 Urine Collection and Preparation

Fingerprinting studies were conducted using urine samples collected from a control population of healthy dogs (i.e., no cancer) and a population of diseased dogs diagnosed with diffuse large B cell lymphoma. The control population consisted of 14 dogs between the ages of 7 and 11 while the diseased population consisted of 9 dogs (ages unknown). A single urine sample was obtained from the control while four different samples were obtained from the diseased dogs at distinct time points during treatment. These time points were as follows: (1) prior to any treatment when disease was clinically detectable, (2) week 9 of treatment when all dogs were in remission and had received their last chemotherapy treatment, (3) prior to or out of remission (PTOR) when disease progression was not clinically detectable, and (4) out of remission (OR) when the disease was again clinically detectable (enlarged lymph nodes). All cancer patients received a 9 week multiple drug, CHOP based[12] chemotherapy protocol. Throughout the duration of their first remission dogs were randomized to receive a daily supplement of *n*-3 fatty acid (docosahexaenoic acid and eicosapentaenoic acid) or placebo. Urine samples obtained from these dogs were stored at -80 °C until analysis by CE, at which time they were allowed to thaw at room temperature and loaded into the CE autosampler.

3.2.4 Capillary Electrophoresis

All CE experiments were conducted using a Beckman Coulter P/ACE MDQ system (Beckman Coulter, Inc.; Brea, CA). Capillaries were prepared at 50 cm total length (40 cm effective) by cutting from bulk capillary using a ceramic knife. New capillaries were "prepped" by sequentially rinsing (pneumatically, 20 psi) with 1 M NaOH for 30 min, 0.1 M NaOH for 20 min, and ultra-pure water for 10 min. Prior to electrophoretic separation of standards and urine samples, the capillary was pneumatically (20 psi) rinsed with 0.1 M NaOH for 2 min, followed by ultra pure water for 0.5 min, and unelectrophoresed BGE for 4 min. Following this, BGE was electrophoresed through the capillary at 20 kV for 3 min, sample injected pneumatically at 0.5 psi for 5 sec, and the sample electrophoresed at 20 kV for 20 min. Detection was conducted using single wavelength UV absorbance at 200 nm with a data collection rate of 4 Hz. All electrophoretic separations were carried out at room temperature (non-thermostatted).

3.2.5 Data Pretreatment and Analysis

Migration times and peak areas were obtained using the data analysis tools available with the Beckman-Coulter 32 Karat software (Version 7.0). Integration events were defined using peak width and threshold values of 0.2 and 350, respectively. Some peaks were integrated manually as their response was below these set integration conditions. Migration times were normalized to an endogenous internal standard to correct for fluctuations in electroosmotic flow (EOF) using the method described by Yang et al.[13] All peak areas for a given electropherogram were normalized to that of creatinine to account for the differing hydration states between dogs.[14] PCA of the various data sets

was conducted using Partek Discovery Suite analysis software, version 6.0 (Partek, Inc.; St Louis, MO).

3.3 Results and Discussion

3.3.1 CE Method Development

In order to generate a comprehensive metabolite fingerprint, separation conditions were developed to resolve a maximum number of urine components. Initial electrophoresis conditions were adapted from previously published methods[8,15-16] which utilized micellar electrokinetic chromatography (MEKC) with sulfated β-cyclodextrin (BCD) additives to resolve urine metabolites. MEKC was used as it allows for the separation of components, including both charged and neutral compounds, which cannot be separated using standard capillary zone electrophoresis (CZE). The operational features of this separation technique are shown in Figure 1. In MEKC, surfactant is added to the BGE above its critical micelle concentration (CMC) to form a pseudostationary phase (i.e., the micelles) in which analytes can be retained. Since MEKC employs this pseudostationary phase, it is generally thought to be a form of chromatography, and thus chromatographic terms are used in lieu of electrophoretic terms in the following text to reflect this association. With MEKC, neutral compounds are separated based upon their differential partitioning with the micelle while charged species can also be retained via partitioning or electrostatic interactions. Since a negatively charged surfactant (SDS) was used in the present experiments, analyte retention times were longer than their corresponding migration times in normal polarity CZE. The decreased migration velocities (increased retention time) of these analytes stem from the negative electrophoretic mobility (μ_{ep}) of the SDS

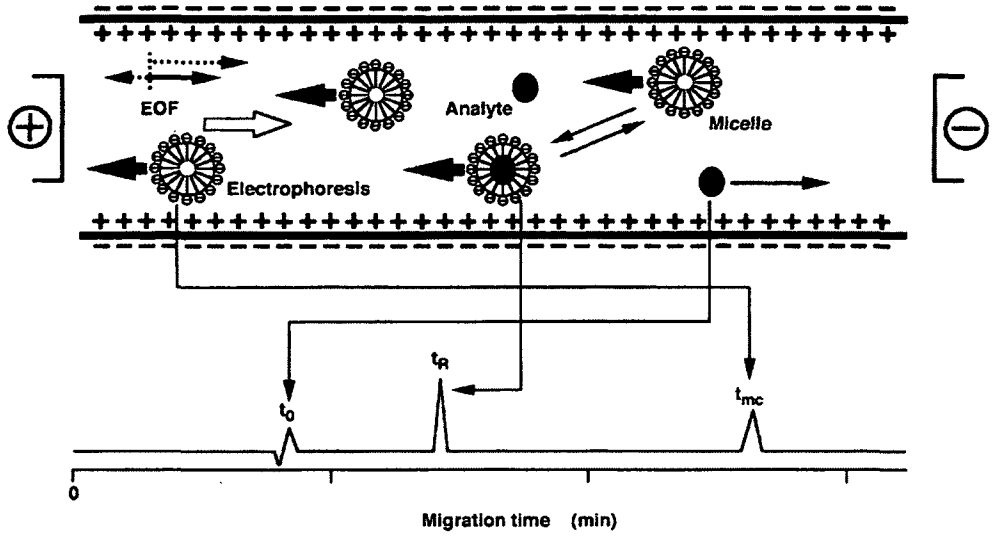

Figure 1. Schematic showing operational principle of MEKC. t_o = migration time of a neutral 'unretained' analyte in CZE; t_r = retention time of the same analyte in MEKC; t_m = migration time of micellar aggregate. Figure was obtained from Watanabe et al.[17]

micelles (negative charge), which acts to slow the velocity of interacting compounds relative to CZE.

In addition to surfactant, sulfated BCDs were added to the BGE to increase peak capacity beyond that provided by MEKC. Because the core or cavity region of cyclodextrins (CDs) are optically active, they are frequently used in CE[15,18] and other separation systems[19] to resolve optical isomers. For the present experiments, CDs acted to increase the total number of resolved metabolites via hydrogen bonding of certain metabolites with the core region of the CD.[15] Previous reports have shown sulfated BCDs to be the most desirable for urine analyses as they are able to resolve a larger number of components than other CD species,[15] and thus were used here for this specific purpose.

Utilizing these conditions as an initial starting point, we further developed our methods to stabilize the electroosmotic flow (EOF) and improve retention time reproducibility. This was accomplished by adding organic solvents to the BGE. Addition of organic solvents acts to decrease and stabilize EOF by disrupting double layer formation and consequently bulk fluid movement down the capillary.[20] Since organic modifiers stabilize EOF, the reproducibility in migration (or retention) time improves as well. Additionally, resolution improves due to longer on-capillary residence times, decreased thermal diffusion (as a consequence of reduced solution conductivity), and increased solubility for certain compounds.[20] Here, we analyzed the effect of some commonly used organic modifiers including ACN, MeOH, EtOH, PrOH, and BuOH on the separation of a standard mixture of urine metabolites.

Modifiers were added at 10% (v/v) to the BGE, as previous studies have shown this to be an appropriate compromise between analyte resolution and speed of analysis. The resulting separation profiles obtained using the modified BGEs are shown in Figure 2(a). As evident in this figure, the alcohol modifiers slowed analyte velocities relative to the ACN modifier. This phenomenon is thought to be the result of increased double layer disruption due to hydrogen bonding of the alcohols with water. RSDs of analyte retention times (n = 6) were calculated for the different modifier systems and are shown in Figure 2(b). From these, it is evident that addition of modifiers improved reproducibility relative to the BGE. The most notable improvement in reproducibility was obtained with ACN, MeOH, and BuOH modifiers. Separation efficiencies (n = 6) for the modifier systems were calculated as described in Chapter 2 (Equation 2.2), and are shown in Figure 2(c). Efficiencies obtained using the modified BGEs were largely equivalent to those of the BGE without modifier, with the exception of a few analytes (e.g., creatinine for PrOH and BuOH). Those of urea and creatinine were not included for the PrOH and BuOH modifiers, as these analytes did not give a signal response in these systems.

Following initial characterization with standard analytes, the utility of ACN and MeOH modifiers for the analysis of actual urine samples was investigated. The number of resolved peaks in chromatograms obtained using these modified buffer systems were equivalent to those obtained using the unmodified BGE, suggesting these modifiers to be suitable for urine analyses. ACN was chosen for the subsequent fingerprinting experiments as this modifier gave the best compromise between speed of analysis and separation performance.

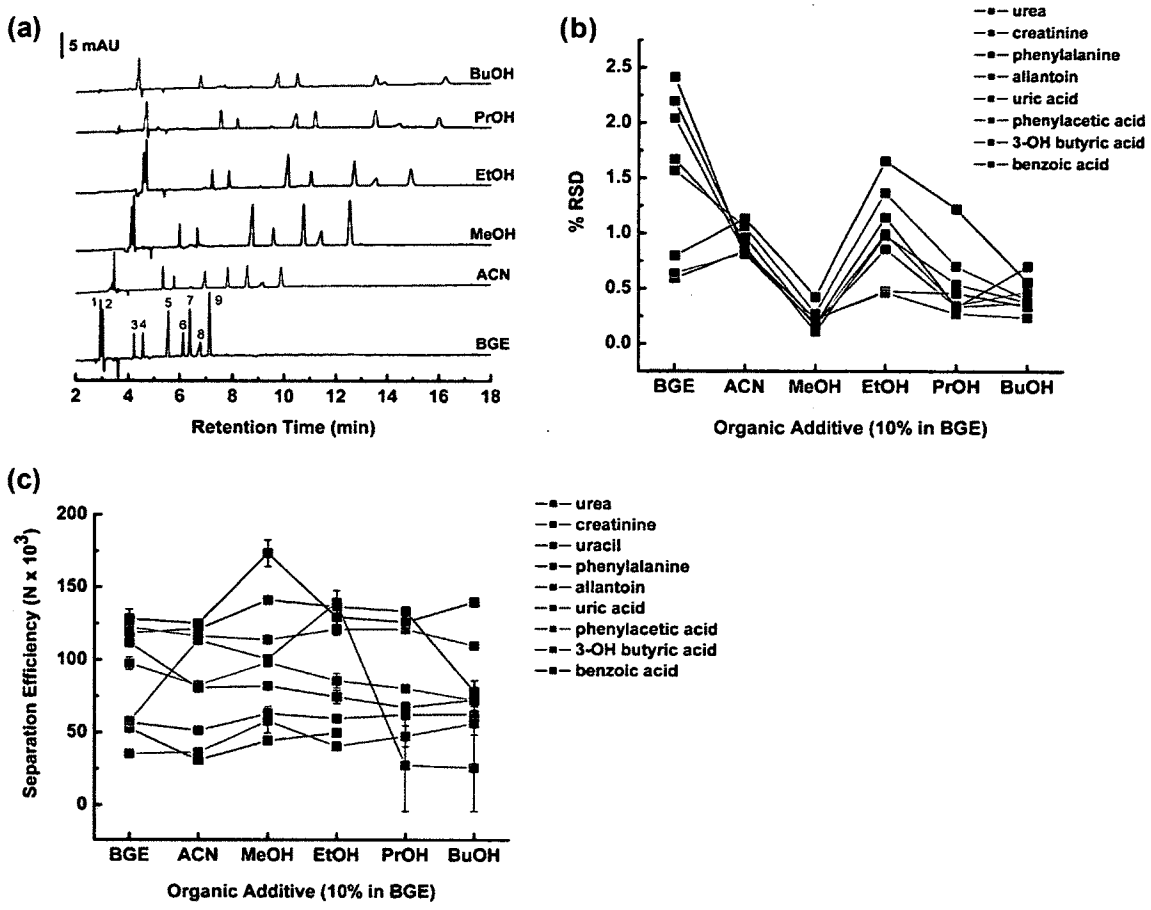

Figure 2. (a) Separation of standard analytes in BGE with and without organic modifiers. Labeled analytes included the following: (1) urea, (2) creatinine, (3) uracil, (4) phenylalanine, (5) allantoin, (6) uric acid, (7) phenylacetic acid, (8) 3-hydroxybutyric acid, and (9) benzoic acid. (b) Comparison of percent RSD (n= 6) in retention time for standard analytes separated in BGE with and without organic modifiers. (c) Separation efficiency (n = 6) of standard analytes separated in BGE with and without organic modifiers. The BGE used for all separations consisted of 25 mM borate, 75 mM SDS, and 6.25 mM sulfated β-cyclodextrin (pH 9.5) with and without 10% (v/v) organic modifier. The field strength employed was 400 V/cm, and analytes were detected using UV absorbance at a wavelength of 200 nm.

3.3.2 Retention Time and Peak Area Normalization

While addition of ACN helped to stabilize EOF, it did not altogether eliminate fluctuations in analyte retention times. This was problematic for the present analyses as the use of a non-selective detection technique (UV absorbance) required use of migration times for metabolite identification. As a result, it was necessary to correct for variations in migration time before assigning peak identities in chromatograms. Multiple methods have been reported for aligning peaks including warping[1,21] and normalization techniques.[13] Here, a normalization technique was utilized in which retention time ratios[13] were used to align peaks. With this technique, retention times are normalized to an internal standard which is present in the sample. A mathematical description of the retention time ratio is given below in Equation 3.1 where t_{Peak} is the retention time of the metabolite and t_{Std} the retention time of the internal standard.

$$T_{R\,Normal} = \frac{t_{Peak}}{t_{Std}} \tag{3.1}$$

The effectiveness of this technique for aligning peaks can be seen by comparing the chromatograms shown in Figure 3. These chromatograms were obtained from treatment time point (T1-T4) samples of a diseased dog (Bryant) as well as a sample from a control dog (Jessi). Figure 3(a) shows the chromatograms prior to alignment while Figure 3(b) shows the chromatograms after normalization to the internal standard (marked as 1). The internal standard was an endogenous metabolite present in all urine samples, and was employed for normalization purposes as it gave a strong signal in all chromatograms. Spiking experiments suggested this metabolite to be allantoin, a uric acid oxidation product, as both had identical migration times. The location of the internal standard in the middle of the metabolite profile was ideal as it improved the relative standard deviation

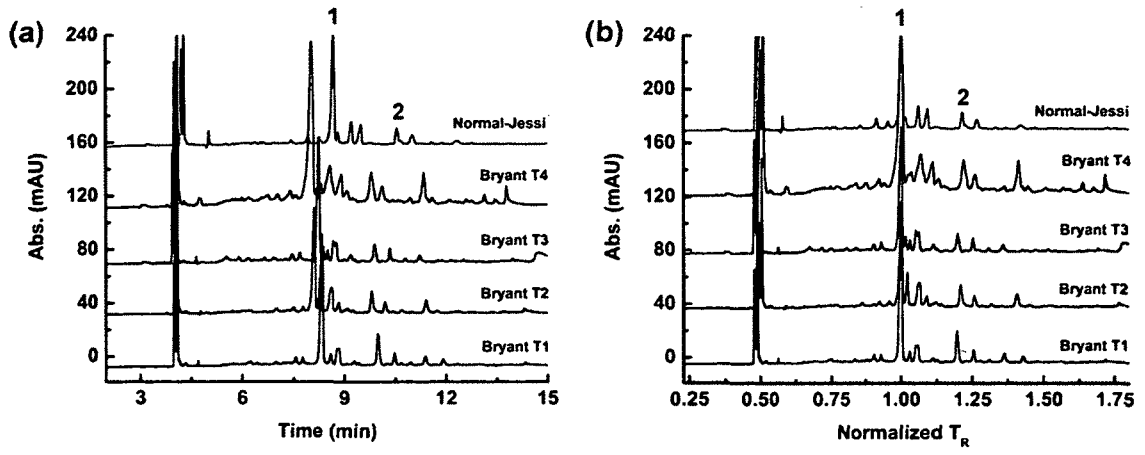

Figure 3. (a) Chromatograms showing urine profiles at four treatment time points (Bryant T1-T4) and for a control (Jessi) prior to peak alignment. The peak marked (1) is the endogenous metabolite used for aligning peaks, and that marked (2) a metabolite used for calculating percent RSD in retention time between samples. (b) Chromatograms showing the same urine profiles in Figure 3(a) after normalizing retention times to that of peak (1). Visual inspection shows an improvement in peak alignment relative to Figure 3(a), with the percent RSD in migration for peak (2) improving from 3.2% to 0.9% before and after alignment, respectively. Separation and detection conditions for Figures 3(a) and (b) were the same as those given in Figure 2; the BGE contained 10% (v/v) ACN.

(RSD) of normalized retention times compared to internal standards having retention times at the temporal extremes. The improvement in retention time RSDs obtained with normalization to this internal standard is highlighted for the peak marked with the number 2 in Figure 3, where the RSD in retention time improved from 3.2% before normalization (Figure 3(a)) to 0.9% after normalization (Figure 3(b)).

In addition to correcting for variations in migration time, peak areas were also normalized to that of creatinine to account for variations in metabolite concentration arising from animal hydration state. Creatinine normalization is commonly used for quantifying urinary metabolites as it is endogenously produced and released into body fluids at a constant rate, regardless of disease state.[14,22] Thus, this normalization strategy allows for direct mass comparison of metabolites between samples by eliminating the effect of urine volume on metabolite concentration. Separation conditions were developed to ensure baseline resolution (R = 1.5) of creatinine from urea, as seen in the inset of Figure 4(a). Both creatinine and urea were identified with spiking experiments. Following normalization, all measurable peaks in chromatograms were used to construct the metabolite fingerprints. The metabolites labeled 1-9 in Figure 4(a) were chosen as the representative fingerprint for all samples (i.e., diseased and control) as they were reproducibly measured throughout. The remaining, smaller peaks seen in this and other electropherograms were not used as they lacked sufficient signal for quantification, or could not be identified based on migration times. Additionally, many of these peaks were system peaks or baseline artifacts which gave irreproducible signal response with replicate analyses.

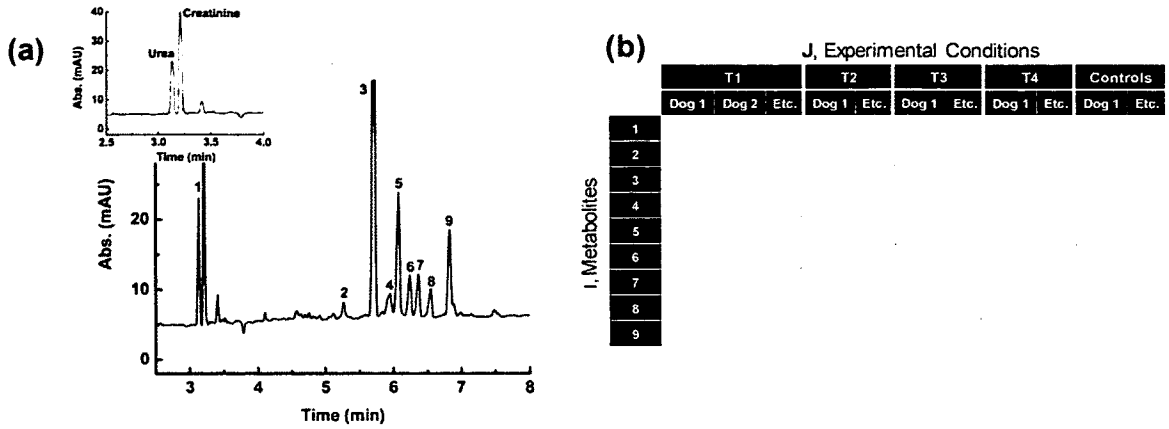

Figure 4. (a) Chromatogram showing metabolites (1-9) used to construct fingerprints. The inset shows baseline resolution of urea and creatinine, a necessary requirement for conducting creatinine normalization. Separation and detection conditions were the same as those given in Figure 2; the BGE contained 10% (v/v) ACN. (b) Data matrix into which peak areas for the metabolites (1-9) were entered for PCA analysis. Rows (I) correspond to the individual metabolites (i.e., 1-9) and the columns (J) the experimental conditions. These conditions consisted of both the treatment time points (diseased dogs) and controls (healthy dogs), with respective peak areas being entered for nine diseased dogs (T1-T4) and fourteen control dogs.

Normalized peak areas were entered into a data matrix or table such as that shown in Figure 4(b) for subsequent analysis by PCA. The rows (I) of this matrix consisted of the individual metabolites (1-9) while the columns (J) were comprised of the experimental conditions or variables. These conditions included the four treatment time points (T1-T4) for the diseased dogs as well as the control. Each treatment time point in the matrix contained nine columns, one for each of the nine diseased dogs, while the control contained fourteen columns corresponding to the fourteen control dogs. Entering data into a matrix such as this was necessary for conducting data pretreatment prior to PCA, which is discussed in detail in the following section.

3.3.3 PCA of Fingerprints

Following data normalization, PCA was used to assess whether statistical differences existed in the metabolite make-up between sample populations (i.e., control and disease groups) and time point data. Since we were dealing with a complex, multivariate data set, PCA was an ideal starting point for data analysis as this technique allows for visualization of trends in the data by how the variables group in a score plot. PCA was conducted using the creatinine normalized peak areas which were entered into the data matrix shown in Figure 4(b). The resulting score plot for the PCA of this data is shown in Figure 5(a), and consists of data points for each of the nine diseased dogs (time points 1-4) as well as the fourteen control dogs. If significant differences existed in the metabolite make-up between sample populations (i.e., the time points and control), their respective data points (i.e., dogs) would be separated into distinct groups in the score plot. As seen in this figure, no significant separation of the control and diseased groups occurred. Additionally, no significant separation or clustering of the time point data was seen,

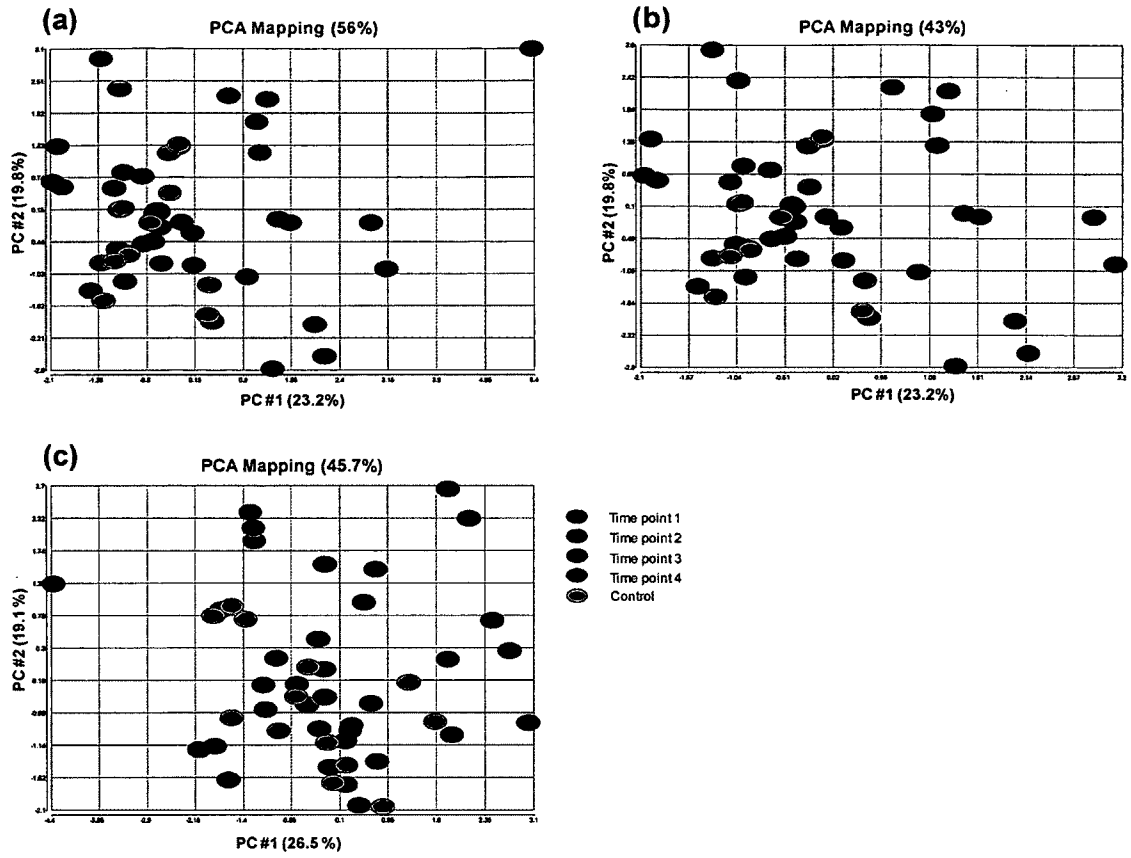

Figure 5. (a) PCA score plot of fingerprint data for diseased dogs (time points 1-4) and control dogs. Each data point corresponds to the fingerprint of a single dog; thus, there are nine data points (nine dogs) for each treatment time point and fourteen data points (fourteen dogs) for the control. Percentage of variability explained by each principle component is denoted on the respective axes with PC #1 being principle component 1 and PC #2 principle component 2. (b) PCA score plot for centered fingerprint data. (c) PCA score plot for autoscaled fingerprint data.

suggesting limited difference in the metabolite concentration (mass) between these samples.

In many cases, the interpretability of biological data in PCA can be obscured by large differences in concentration between metabolites.[23] While these differences may not be proportional to the biological relevance of the metabolites, the same distinction cannot be made by the PCA.[23] Therefore, data pretreatment methods are often employed to eliminate these effects and to ensure that the variability within the variables themselves (i.e., time points and control) is the quantity being assessed in the PCA.[23] Here, we employed two different data pretreatment methods to improve separation of variables with PCA. The first pretreatment method involved a technique termed "centering" which adjusts for differences in the offset between high and low abundance metabolites. With this technique, all concentrations were converted to fluctuations around a zero point instead of mean metabolite concentrations, thus leaving only the variation between samples to be analyzed.[23] A mathematical description of this technique is given below as Equation 3.2 where data is centered ($\tilde{x}_{ij}$) by subtracting the mean peak area ($\bar{x}_i$) for metabolites in row i of the data matrix (shown in Figure 4(b)) from the individual metabolite peak areas contained within the columns (j) of that same row.

$$\tilde{x}_{ij} = x_{ij} - \bar{x}_i \tag{3.2}$$

The resulting score plot from the mean centered PCA is shown in Figure 5(a), and from this it is evident that little separation of population and time point data is occurring. This suggests minimal variation in metabolite concentrations (mass) between sample populations or treatment time points.

Previous fingerprinting studies of urine have shown autoscaling to be an effective pretreatment method prior to PCA.[10] The mathematical description of this technique is given below as Equation 3.3. The technique is similar to centering, but contains an additional scaling factor (s_i) which corresponds to the standard deviation of metabolite areas across the matrix row (i).

$$\tilde{x}_{ij} = \frac{x_{ij} - \bar{x}_i}{s_i} \tag{3.3}$$

Following an autoscaling pretreatment, all metabolites have a standard deviation of one which allows data to be analyzed on the basis of correlations instead of covariances.[23] The resulting score plot from the PCA of the autoscaled data is shown in Figure 5(c), and again little separation is seen between the population or treatment time points. These results, along with those discussed previously (Figures 5(a-c)), imply that the metabolite fingerprints in this study did not differ significantly enough to discriminate between disease states. Furthermore, the similarity of the time point data suggests limited up- or down-regulation of metabolites during the treatment interval (time points 1-4), which limits the effectiveness of using this approach as a tool for monitoring treatment efficacy.

3.3.4 Z-Scores

Since global differences in the data set could not be distinguished using PCA, an alternate approach was taken to discern whether individual metabolites were up-regulated or down-regulated in the diseased population versus the control. Z-scores are sometimes used for these purposes as they describe how much a value deviates from a normal "Gaussian" distribution. In the present context, this translated to the deviation of metabolite concentration in the diseased population from that of the control. The

mathematical description of a z-score is given below in Equation 3.4 where x_{Metab} represents the peak area of a single metabolite (average from replicate measurements) obtained from the fingerprint of a single dog, $\bar{x}_{Ctrl}$ the average peak area of that metabolite for the whole control population, and s_{Ctrl} the standard deviation of this peak area for the control population.

$$z = \frac{x_{Metab} - \bar{x}_{Ctrl}}{s_{Ctrl}} \tag{3.4}$$

In most cases, a large control population (n > 40) is used to calculate the normal distribution. Unfortunately, this was not possible in this case due to a population size of only 14 dogs. Regardless, z-scores calculated in this manner should be sufficient to garner an indication of the degree of up- or down-regulation of metabolites in the diseased population. A standard deviation of two or more indicates up- (positive deviation) or down-regulation (negative deviation) versus the control. Z-scores for the control dogs are shown in Figure 6(a), and as expected, metabolite concentrations are within two standard deviations of the mean. The same is seen for z-scores of the diseased dogs in treatment time points 1-4 shown in Figures 6(b)-(e). Disregarding outliers (e.g., time point 1, metabolite 6), metabolite concentrations for the majority of diseased dogs lie within two standard deviations of the mean, indicating a lack of up- or down-regulation of metabolites in these fingerprints. These results help explain why little separation of the population or treatment time point data was occurring in the PCA score plots. Nevertheless, biomarkers indicative of disease state and treatment efficacy most likely exist in these urine samples; however, a more sensitive and selective detection technique is needed to measure them. Use of a mass selective detector would be

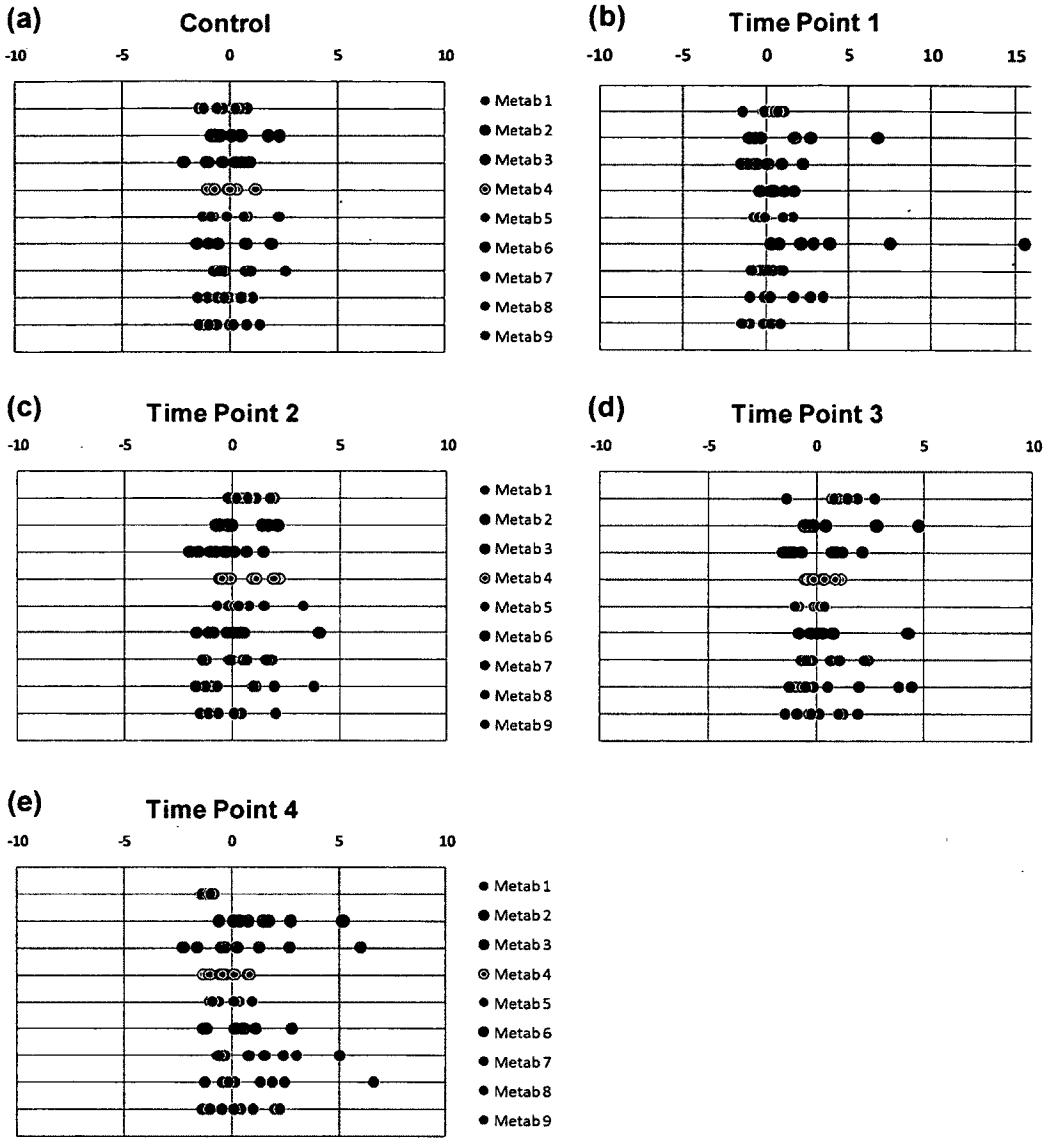

Figure 6. (a) Z-scores for metabolites 1-9 with data points given for each dog (14 dogs) in the control population. The horizontal axis denotes the number of standard deviations from the normal, mean concentration of a metabolite. (b) Z-scores for the diseased population (9 dogs) at time point 1. (c) Z-scores for the diseased population at time point 2. (d) Z-scores for the diseased population at time point 3. (d) Z-scores for the diseased population at time point 4.

beneficial as it would allow for identification of the smaller, less intense components in chromatograms which were excluded from the present fingerprints (irreproducible migration times).

3.4 Conclusions

This chapter explores the utility of CE-UV as a tool for analyzing efficacy of chemotherapy through metabolic fingerprinting of urine samples. Fingerprinting studies were conducted using MEKC with sulfated BCD additives to allow for resolution of a maximum number of urine components. Additionally, organic modifiers were added to improve migration time reproducibility for MEKC. It was found ACN worked well for these purposes as it improved reproducibility in migration times relative to the BGE, and still allowed for separation of urine components in under 12 min. Chromatograms obtained with the finalized BGE conditions were aligned using retention time ratios to obtain peak identities, and the resulting fingerprints analyzed using PCA. Population (e.g., disease and control) and time point data did not separate in the PCA score plots, indicating similarity in metabolite concentrations (mass) within all samples. This was confirmed with a subsequent determination of z-scores for individual metabolites, which showed concentrations did not deviate substantially from control values. Together, these results indicate the fingerprints obtained using CE-UV contained insufficient information to discriminate disease state and treatment efficacy. The use of a qualitative detection technique such as mass spectrometry could help to increase the number of analytes detected as well as identify potential disease and treatment biomarkers. Furthermore, a

more selective technique such as electrochemical detection could be used to target and fingerprint specific classes of electrochemically active analytes in these samples.

3.5 Acknowledgements

First, I would like to thank Dr. James R. Kraly for his collaboration and equal involvement in this work; data for Figure 2 and 3 was obtained courtesy of Dr. Kraly. Also, I would like to thank Roy A. Miller for all his assistance in preparing and conducting experiments. Additionally, I would like to acknowledge our collaborator Dr. Susan E. Lana at the Animal Cancer Center (Colorado State University) for providing us with dog urine samples. Finally, I would like to thank Dr. Meghan M. Mensack for her assistance in conducting PCA of the urine data.

3.6 References

(1) Garcia-Perez, I.; Vallejo, M.; Garcia, A.; Legido-Quigley, C.; Barbas, C. *J. Chromatogr., A* **2008**, *1204*, 130-139.

(2) Dunn, W. B.; Bailey, N. J. C.; Johnson, H. E. *Analyst* **2005**, *130*, 606-625.

(3) Dettmer, K.; Aronov, P. A.; Hammock, B. D. *Mass Spectrom. Rev.* **2007**, *26*, 51-78.

(4) Pasikanti, K. K.; Ho, P. C.; Chan, E. C. Y. *J. Chromatogr., B* **2008**, *871*, 202-211.

(5) Lu, X.; Zhao, X. J.; Bai, C. M.; Zhao, C. X.; Lu, G.; Xu, G. M. *J. Chromatogr., B* **2008**, *866*, 64-76.

(6) Monton, M. R. N.; Soga, T. *J. Chromatogr., A* **2007**, *1168*, 237-246.

(7) Ramautar, R.; Somsen, G. W.; de Jong, G. J. *Electrophoresis* **2009**, *30*, 276-291.

(8) Barbas, C.; Vallejo, M.; Garcia, A.; Barlow, D.; Hanna-Brown, A. *J. Pharm. Biomed. Anal.* **2008**, *47*, 388-398.

(9) Garcia-Perez, I.; Whitfield, P.; Bartlett, A.; Angulo, S.; Legido-Quigley, C.; Hanna-Brown, M.; Barbas, C. *Electrophoresis* **2008**, *29*, 3201-3206.

(10) Vallejo, M.; Angulo, S.; Garcia-Martinez, D.; Garcia, A.; Barbas, C. *J. Chromatogr., A* **2008**, *1187*, 267-274.

(11) Szymanska, E.; Markuszewski, M. J.; Capron, X.; van Nederkassel, A. M.; Vander Heyden, Y.; Markuszewski, M.; Krajka, K.; Kaliszan, R. *J. Pharm. Biomed. Anal.* **2007**, *43*, 413-420.

(12) Chun, R. *Top. Companion Anim. M.* **2009**, *24*, 157-162.

(13) Yang, J.; Rose, S.; Hage, D. S. *J. Chromatogr., A* **1996**, *735*, 209-220.

(14) Burtis, C. A.; Ashwood, E. R.; Border, B. P.; Tietz, N. W. *Fundamentals of clinical chemistry*; 5th ed.; W.B. Saunders: Philadelphia, 2001.

(15) Alfazema, L. N.; Howells, S.; Perrett, D. *Electrophoresis* **2000**, *21*, 2503-2508.

(16) Guillo, C.; Perrett, D.; Hanna-Brown, M. *Chromatographia* **2004**, *59*, S157-S164.

(17) Watanabe, T.; Terabe, S. *J. Chromatogr., A* **2000**, *880*, 311-322.

(18) Poole, S. K.; Poole, C. F. *J. Chromatogr., A* **1996**, *749*, 247-255.

(19) Poole, C. F. In *The Essence of Chromatography*; Elsevier Science: Amsterdam, 2003.

(20) Landers, J. P. *Handbook of capillary and microchip electrophoresis and associated microtechniques*; 3rd ed.; CRC Press: Boca Raton, 2008.

(21) Guillo, C.; Barlow, D.; Perrett, D.; Hanna-Brown, M. *J. Chromatogr., A* **2004**, *1027*, 203-212.

(22) Warrack, B. M.; Hnatyshyn, S.; Ott, K. H.; Reily, M. D.; Sanders, M.; Zhang, H.; Drexler, D. M. *J. Chromatogr., B* **2009**, *877*, 547-552.

(23) van den Berg, R. A.; Hoefsloot, H. C.; Westerhuis, J. A.; Smilde, A. K.; van der Werf, M. J. *BMC Genomics* **2006**, *7*, 142.

CHAPTER 4. *Electrode Array Detector for Microchip Capillary Electrophoresis*

4.1 Introduction

This chapter is an adaptation of a research article previously published by this author in the *Analyst* which describes the development of a microchip capillary electrophoresis (MCE) system containing an integrated electrode array detector for improving detection selectivity.[1] Conceivably, a system like this would have applications for conducting rapid metabolic fingerprinting or profiling analyses like those described in Chapter 3. One of the major obstacles of using MCE for these types of analyses is the lack of resolution and selectivity in many of these systems. Typically, selectivity in MCE is gained through the separation step; however, resolution (and hence selectivity) is usually compromised due to the short separation channels employed in the majority of these systems. One way to improve resolution and selectivity is to increase the total number of individually addressable detection elements in the device. While this concept has successfully been applied to macro-scale separation systems in the forms of electrode[2-7] and photodiode arrays,[8] application to micro-scale separation systems has been limited.

Many detection modes have been used with MCE including optical and electrochemical detection (ECD).[9] Laser induced fluorescence (LIF) is the most frequently used detection technique due to its high sensitivity, low limits of detection (LOD), and relative ease of implementation with MCE systems.[10] However, as many compounds are non-fluorescent LIF usually requires a labeling step which increases the time and complexity of the

analysis. ECD is an attractive alternative to optical detection in MCE devices as it can be easily miniaturized without loss of performance and as a result has seen a resurgence in use for microfluidic and lab-on-a-chip applications.[11] Most modes of ECD are based on the electroactivity of the target analyte removing the need to derivatize prior to analysis. Additionally, differences in electroactivity can be exploited to increase selectivity by proper choice of detection potential.[2-3] Selectivity is improved further by increasing the total number of working electrodes in the system and thus the total number of detection potentials which can be applied during an analysis.[2-7] This concept has been successfully implemented with metabolic profiling analyses using liquid chromatography,[2-7] and should be transferrable to analyses on the microscale as well.

Currently, ECD in microfluidic systems is typically conducted using dc amperometry[12] or pulsed electrochemical detection (PED),[13] with dc amperometry being the most common due its simplicity and sensitivity.[12] There are numerous reports of one[12,14-15] and two working electrode[12,16-20] MCE systems in the literature using these ECD techniques; however, use of electrode array systems with multiple working electrodes is less prevalent. The first report detailing inclusion of multiple working electrodes in a MCE device was given by Keynton et al.. In this work the authors incorporated eight, diametrically opposed platinum working electrodes in series at the end of the CE separation channel.[21] Each electrode was operated sequentially as the working electrode to detect millimolar concentrations of dopamine with dc amperometry. Use of this device as an ECD array where each electrode was independently controlled and operated in a simultaneous, concerted fashion was not explored. Lee et al. described the incorporation of thin film, gold arrays into poly(dimethylsiloxane) (PDMS) devices. ECD in this

system was conducted using dc amperometry at only a single working electrode to demonstrate the viability of the patterned electrodes for ECD applications.[22] More recently Ordeig et al. demonstrated field induced detection at gold microband electrodes inside the channel of a hybrid PDMS/glass microchip.[23] Amperometric detection of electrochemically active compounds could be conducted between any two electrodes in a 20-electrode array based upon the potential difference which exists between the electrodes in the presence of a CE separation field. Potential step detection was carried out by increasing the distance between active electrodes. However, use of the array for improving detection selectivity with simultaneous, multi-potential detection was not explored.

The following chapter discusses the use of electrode arrays for improving resolution and detection selectivity in microfluidic devices. Unlike the previous reports of electrode arrays in MCE systems, this device contained an integrated electrode array which could be operated in a simultaneous, multi-potential fashion. The MCE-ECD array device was fabricated from PDMS, and included eight individually addressable gold microwire working electrodes aligned serially after a palladium current decoupler.[24-26] Selective detection of biologically relevant metabolites and xenobiotics was demonstrated using potential step detection with dc amperometry. Using this detection scheme, co-migrating analytes were resolved based upon differences in their redox potentials. The applicability of this device for complex sample analysis was subsequently demonstrated using a human urine sample. It is envisioned a device such as this will find applications in the field of metabolomics as a useful tool for conducting rapid profiling and fingerprinting analyses.

4.2 Materials and Methods

4.2.1 Chemicals and Materials

(±)-Arterenol ((±)-norepinephrine (+)-bitartrate salt), 4-aminophenol, acetaminophen, 3,4-dihydroxy-L-phenylalanine, uric acid, 3,4-dihyroxyphenylacetic acid, dopamine hydrochloride, and sodium dodecyl sulfate (SDS) were purchased from Sigma-Aldrich (St. Louis, MO). 2-(4-Morpholino)ethansulfonic acid (MES) was purchased from Fisher Scientific (Pittsburgh, PA). Silicon wafers (4 in) were purchased from University Wafer (South Boston, MA). SU-8 2035 negative photoresist was purchased from MicroChem Corp. (Newton, MA). Sylgard 184 elastomer and curing agent (PDMS) were purchased from Dow Corning (Midland, MI). Gold and palladium wire (0.025 mm dia., 99.99% purity) were purchased from Goodfellow Corp. (Huntingdon, England). Glass slides (75 mm × 50 mm) were purchased from Corning Glass Works (Corning, NY). Insulated copper wire (1 mm dia.) was purchased from Radioshack (Fort Collins, CO). High purity silver paint was purchased from Structure Probe, Inc. (West Chester, PA). Clear room temperature vulcanizing (RTV) silicone adhesive was purchased from Permatex, Inc. (Solon, OH). All chemicals were used as received without further purification.

4.2.2 Solution Preparation

Stock solutions (10 mM) of norepinephrine, 4-aminophenol, acetaminophen, 3,4-dihydroxy-L-phenylalanine, 3,4-dihydroxyphenylacetic acid, and dopamine were prepared daily in 10 mM HCl while a 10 mM stock solution of uric acid was prepared in 20 mM NaOH. A 20 mM MES buffer with 20 μM SDS was adjusted to pH 6.0 with 30% (w/w) NaOH and used as background electrolyte (BGE). SDS was added to the BGE to

stabilize electroosmotic flow (EOF). All solutions were prepared using ultra-pure 18.2 MΩ water (Milli-Q, Millipore Corp.; Billerica, MA).

4.2.3 MCE-ECD Array Fabrication

PDMS capillary electrophoresis microchips were fabricated using standard soft lithographic techniques.[27-28] Briefly a master mold was prepared by photo-polymerizing SU-8 2035 negative photoresist on a 4 in silicon wafer. The device features were defined using a digitally produced photomask (Printing Services, Colorado State University) placed on a 50 μm thick layer of photoresist (as measured by profilometry) spun onto the wafer. A more detailed description of this process is given in Chapter 2, section 2.2.4. Molded PDMS was prepared by curing a 10:1 mixture of degassed PDMS elastomer and curing agent on the resulting master. The molded PDMS was extracted of unreacted oligomer according to previously published reports[29-30] to improve separation performance.[30]

Array microchips used in the present study were adapted from a standard cross-microchip design commonly used in our laboratory which employs electrode alignment channels orthogonal to the separation channel for reproducible electrode alignment.[27,31] The general design used in the following fabrication is shown in Figure 1(a). Channel width and depth was 50 μm for all channels except the microwire alignment channels which were 25 μm in width; channel dimensions were confirmed with profilometry (data not shown). The separation channel had a total length of 51 mm and an effective length of 50 mm while the injection channels were 10 mm in length. Reservoirs were defined using a 4 mm diameter biopsy punch (Robbins Instruments; Chatham, NJ).

Nine microwire electrodes were integrated into the end of the separation channel of the PDMS microchip by inserting the microwires into the alignment channels of the molded PDMS by hand under a stereo-microscope (Meiji Techno Co., LTD; Tokyo, Japan). The microwires were held in place with transparent tape during the fabrication process. A bright-field image of the array region of the microchip is shown in Figure 1(b). A palladium current decoupler was placed 250 μm upstream from eight gold working electrodes, each spaced 100 μm apart. A 250 μm spacing between the decoupler and first working electrode was used as it was determined from previous work to provide the best compromise between improved signal-to-noise and decreased separation efficiency as the distance from the decoupler increased.[26-27] The last working electrode in the array was 100 μm upstream from the waste reservoir of the microchip. The gold working electrodes were each spaced 100 μm apart to facilitate connection of the electrodes to external leads without grounding the electrodes to each other. To prevent solution leakage into the microwire alignment channels, 61 μm PDMS bridges were left between the alignment channels and separation channel.[27] The surface areas of the working electrodes were defined by the exposed electrode area in the microfluidic channel.

After the microwires were inserted into the alignment channels, both the molded and a blank piece of PDMS were oxidized in an air plasma (Harrick Plasma Cleaner/Sterilizer PDC-32G) at 18 W for 45 s. The microchip was assembled with irreversible sealing by bringing the molded and blank PDMS pieces into conformal contact and placing on a 75 mm × 50 mm glass microscope slide. Light pressure was applied to the electrodes for several hours after plasma oxidation to ensure sealing of the PDMS bridges around the

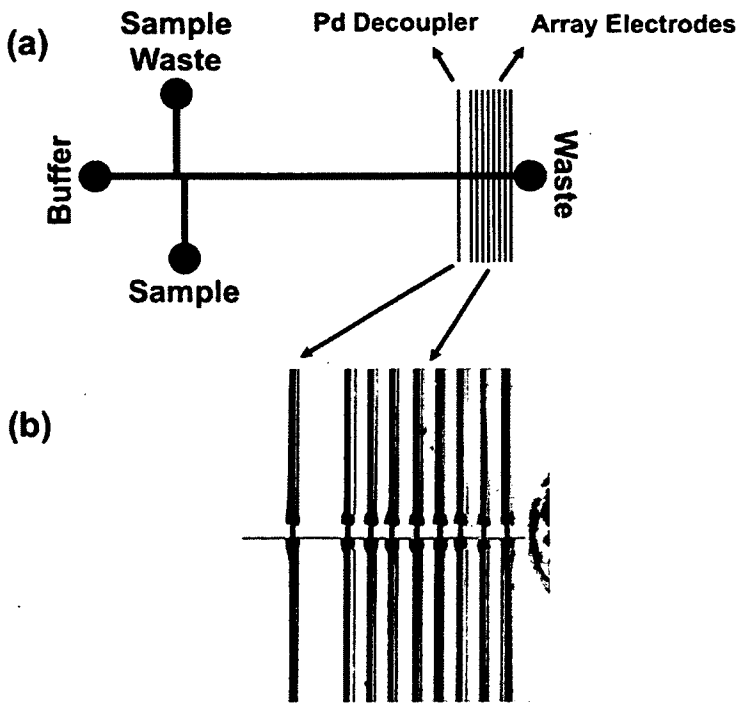

Figure 1. (a) Schematic of the MCE-ECD array. (b) Bright-field image of array electrodes showing the palladium decoupler and eight gold working electrodes. All electrodes are 25 μm in diameter while the separation channel is 50 μm in height. Color and contrast have been modified to aid in visualization.

electrodes. Microwire electrodes were trimmed to size with a scalpel at the ends of the electrode alignment channels and sealed with a 10:1 mixture of PDMS elastomer and curing agent by rapidly polymerizing on a 95 °C hotplate. Insulated, braided copper wires (1 mm dia.) were used as electrode leads. The microwires were wrapped around the copper leads using fine tipped tweezers and conductive silver paint was applied to ensure a complete electrical connection. The exposed wires were insulated with a 10:1 mixture of PDMS elastomer and curing agent which was cured at 35 °C. Additional RTV silicone adhesive was added after the PDMS had cured to ensure rigidity of the copper leads.

4.2.4 Microchip CE

A protocol similar to that given in Chapter 2 was again used here. Briefly, channels were conditioned with 1 M NaOH for 30 minutes prior to running analyses. NaOH was rinsed from the channels with ultra-pure water before filling with BGE. All solutions were introduced into the microfluidic channels by applying pressure to a reservoir containing the solution with a 5 mL disposable syringe (Becton-Dickinson; Franklin Lakes, NJ). The buffer, sample waste, and waste reservoirs were filled with 35 μL of BGE and the sample reservoir with 35 μL of sample solution prior to running analyses.

Applied voltages were facilitated by a programmable high voltage power supply built in-house.[32] Sample introduction was achieved using a 15 s pinched injection[33] through a 250 μm double-T injector.[34-35] For pinched injections, the sample and buffer reservoirs were held at +450 V while the sample waste reservoir was held at -160 V and the decoupler at ground. Separations were achieved by applying +1,000 V to the buffer reservoir while holding the palladium decoupler at ground. A pushback voltage of +450

V was applied to the sample and sample waste reservoirs during separation to prevent sample leakage into the separation channel.[33,36] Use of pushback voltages resulted in a junction potential of +594 V, or equivalently a field strength in the separation channel of 119 V/cm calculated using Kirchhoff's rules.

4.2.5 Electrochemical Detection

A commercially available multi-channel potentiostat (CHI 1010A Electrochemical Analyzer; CH Instruments, Austin, TX) with eight individually addressable electrode channels was used for electrochemical measurements. All experiments were conducted using a two electrode cell in which a 1.0 mm diameter platinum wire in the waste reservoir of the microchip acted as a counter electrode.[27] All detection potentials were applied versus this platinum counter electrode as is commonly done in MCE-ECD.[27] To condition the eight gold working electrodes, 75 cyclic voltammetric scans were conducted from -1.0 V to +2.0 V at a scan rate of 500 mV/s while BGE was electrokinetically pumped over the electrodes. DC amperometry was used for all detection schemes employed at the array electrodes. The sampling rate for all analyses was 10 Hz.

4.2.6 Urine Preparation

A urine sample was obtained from a healthy volunteer and filtered using a 0.2 μm cellulose-acetate membrane syringe filter (Nalgene, Fisher Scientific; Pittsburgh, PA). The resulting filtrate was subsequently filtered with a 3 kDa cutoff micro-centrifuge filter (Pall Corp.; Ann Arbor, MI) to remove proteins or peptides present in the urine. This step was necessary to prevent sample injection problems resulting from protein or peptide

adsorption to the PDMS capillaries. Filtrate from the micro-centrifuge step was then diluted 20× with BGE and analyzed immediately without further preparation.

4.3 Results and Discussion

4.3.1 Device Fabrication

PDMS soft lithography used in conjunction with microwire electrodes allowed for relatively fast fabrication of MCE-ECD array devices. Total fabrication time including curing of the PDMS and RTV silicone took less than 24 hours. Use of microwires and electrode alignment channels enabled rapid and reproducible integration of the array into the microchip device. Because the electrodes were integrated directly into the separation channel of the MCE device, it was necessary to include a current decoupler as the first electrode in the array. This was done to prevent grounding of the CE current through the potentiostat as well as to isolate the working electrodes from the CE separation field. Palladium was used as a decoupler material as it absorbed the hydrogen gas evolved at the CE cathode which would otherwise interfere with separation and detection. In the present case the decoupler and CE cathode are synonymous.

The primary source of ECD array failure resulted from breakage of the microwires at the connection points with the external copper leads. Breakage would occur when the external leads were connected to the potentiostat leads. This problem was solved by insulating and securing the electrode connections with PDMS. Curing of the PDMS was conducted at 35 °C to prevent bending of the microwires which was observed to occur at higher curing temperatures from the thermal expansion of PDMS. Securing of the

electrode leads with PDMS eliminated electrode failure due to breakage and resulted in fully functional arrays with subsequent device fabrications.

In order to prevent solution leakage around the array electrodes, it was necessary to apply pressure to the array region of the microchip for several hours after the plasma oxidation step. This ensured the PDMS bridges sealed completely around the microwires. Delamination of the PDMS bridges tended to occur after prolonged use of the device and with application of high solution pressure. Resultant leakage around the array electrodes from this delamination was evident when imaged with fluorescence microscopy.

4.3.2 MCE-ECD Array Characterization

A mixture of biologically relevant metabolites and xenobiotics was used to characterize the separation and detection performance of the MCE-ECD array device. Figure 2 shows the separation and detection of norepinephrine (NE), acetaminophen (APAP), 4-aminophenol (PAP), uric acid (UA), and 3,4-dihydroxyphenylacetic acid (DOPAC). All five compounds were baseline resolved (R>1.5) in under 2 minutes using 20 mM MES with 20 μM SDS, pH 6.0 as the BGE at a separation field strength of 119 V/cm. The analytes were oxidized at a single array electrode biased to a detection potential of +0.8 V. SDS was added to the BGE as it helped to stabilize the EOF and ensure a reproducible injection and separation.[37-38] In the present case SDS acted as a dynamic coating and increased the negative charge density on the surface of the PDMS, thus increasing EOF.[37] Average peak heights of 200 μM NE, PAP, APAP, UA, and DOPAC for three replicate injections using SDS in the BGE were 1.97 ± 0.20 nA, 1.03 ± 0.05 nA, 1.19 ± 0.19 nA, 0.48 ± 0.11 nA, and 0.33 ± 0.06 nA, respectively.

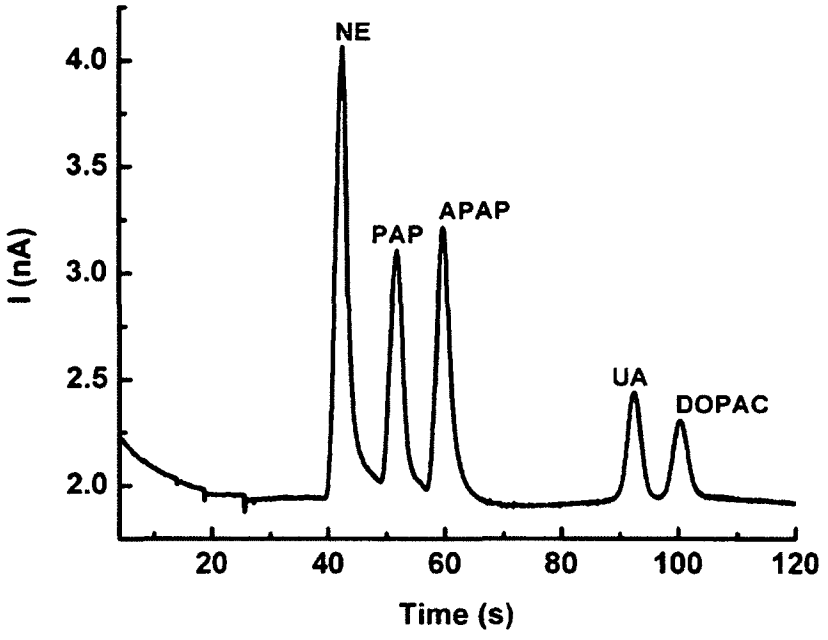

Figure 2. Electropherogram showing separation and ECD of 200 μM NE, PAP, APAP, UA, and DOPAC. BGE was 20 mM MES with 20 μM SDS, pH 6.0. Field strength was 119 V/cm. Analytes were oxidized at a single array electrode with E_{det} = +0.8 V versus a platinum counter electrode.

Separation efficiencies for three replicate injections of 200 μM NE, PAP, APAP, UA, and DOPAC detected at the most downstream electrode (farthest from the decoupler) in the array were calculated to be 1,900 ± 100 plates (N), 2,800 ± 300 N, 3,300 ± 200 N, 8,000 ± 1,000 N, and 9,000 ± 1,000 N, respectively. These efficiencies were calculated using the same plate equation (Equation 2.2) given in Chapter 2. While these efficiencies are relatively low, they are not out of line in comparison to other reports of MCE-ECD.[20,27] Comparison of these efficiencies against those obtained at the most upstream electrode in the array showed no statistical difference at 95% confidence. Analyte velocities were statistically equivalent across all electrodes at 95% confidence as well, explaining why minimal band broadening was occurring between the upstream and downstream working electrodes.

Resolution between UA and DOPAC, the two slowest migrating analytes in the mixture, was calculated to be 1.81 ± 0.06, 1.81 ± 0.04, 1.78 ± 0.09, 1.80 ± 0.08, 1.50 ± 0.28, 1.82 ± 0.03, 1.60 ± 0.37, and 1.85 ± 0.06 (n = 3) going from the most upstream to downstream working electrodes, respectively. Again, resolution was calculated using the resolution equation (Equation 2.1) given in Chapter 2. Similarity in resolution across the array indicates minimal band broadening is occurring from parabolic flow after the decoupler.[26,39] These results are in contrast to previous reports which showed decreased separation efficiency farther from the decoupler.[26] The exact nature of this difference is currently under investigation.

Calculated LODs (signal-to-noise = 3) of 2.6 ± 1.2 μM, 4.9 ± 2.2 μM, 4.3 ± 2.1 μM, 10.9 ± 5.5 μM, and 15.8 ± 7.5 μM (n = 3) were obtained for NE, PAP, APAP, UA, and

DOPAC, respectively, at the most downstream working electrode in the array; analytes were oxidized at a detection potential of +0.8 V. These correspond to mass LODs of 8.8 ± 4.2 fmol, 16.7 ± 7.6 fmol, 14.6 ± 7.3 fmol, 37.1 ± 19.0 fmol, and 53.7 ± 25.9 fmol for NE, PAP, APAP, UA, and DOPAC, respectively. Mass LODs were calculated for an average injection volume of 3.4 ± 0.3 nL (n = 3) measured using fluorescence imaging. Injection volumes were larger than the volume defined by the double-T injector due to sample leakage into the separation channel during injection. This leakage arises from the need to apply a ground potential at the decoupler during injection to prevent damage to the potentiostat [27,30] (Note: alternate potential schemes have now been developed which confine the sample plug to the volume defined by the double-T). While these detection limits are not as low as single electrode schemes, they are sufficient to achieve the detection of many important compounds. Additional gains in LODs can be achieved with sample stacking.

Collection efficiency of individual array electrodes was determined to be 26.7 ± 0.4% (n = 3) using the generation collection method[20,40] with 200 μM dopamine. The equation used for calculating collection efficiency is given below as Equation 4.1. In this equation C_{red} is the charge in coulombs (or equivalently peak area) resulting from the reduction of a reversible redox species at a downstream, cathodic working electrode. C_{oxd} is the charge in coulombs from oxidation of this analyte at a corresponding upstream, anodic working electrode.

$$Efficiency = \frac{C_{red}}{C_{oxd}} \qquad 4.1$$

Collection efficiency for our system was comparable to other values given in the literature for multiple electrode MCE systems.[20] Given the collection efficiency and the number of array electrodes, analyte depletion will be of concern for certain analyses such as hydrodynamic voltammetry where maxima in current versus potential curves could be shifted to lower potentials as the result of depletion effects. However, depletion is not a major concern for the potential step analyses described here as improvements in detection selectivity and resolution from these analyses are not necessarily dependent on depletion effects. Further discussion of these effects as related to array analyses is given in the following text.

4.3.3 Potential Step Detection

Use of array detection is advantageous for analysis of complex mixtures containing multiple redox active species as detection selectivity and resolution can be improved by varying the detection potential at the individual array electrodes. Response of electrochemically active species is dependent on the applied detection potential, so specific analytes or classes of analytes can be detected in the presence of interfering species with differing redox chemistries by judicious choice of detection potential. Increasing the number of electrodes in the array improves selectivity by increasing the total number of potentials that can be simultaneously applied for detection. This concept is demonstrated in the electropherograms shown in Figure 3. In this figure electropherograms for each individually addressable array electrode have been offset for clarity. Figure 3(a) shows detection of NE, PAP, APAP, UA, and DOPAC at eight array electrodes individually biased to a common detection potential of +0.8 V. Use of a common detection potential should result in similar responses at the individual array

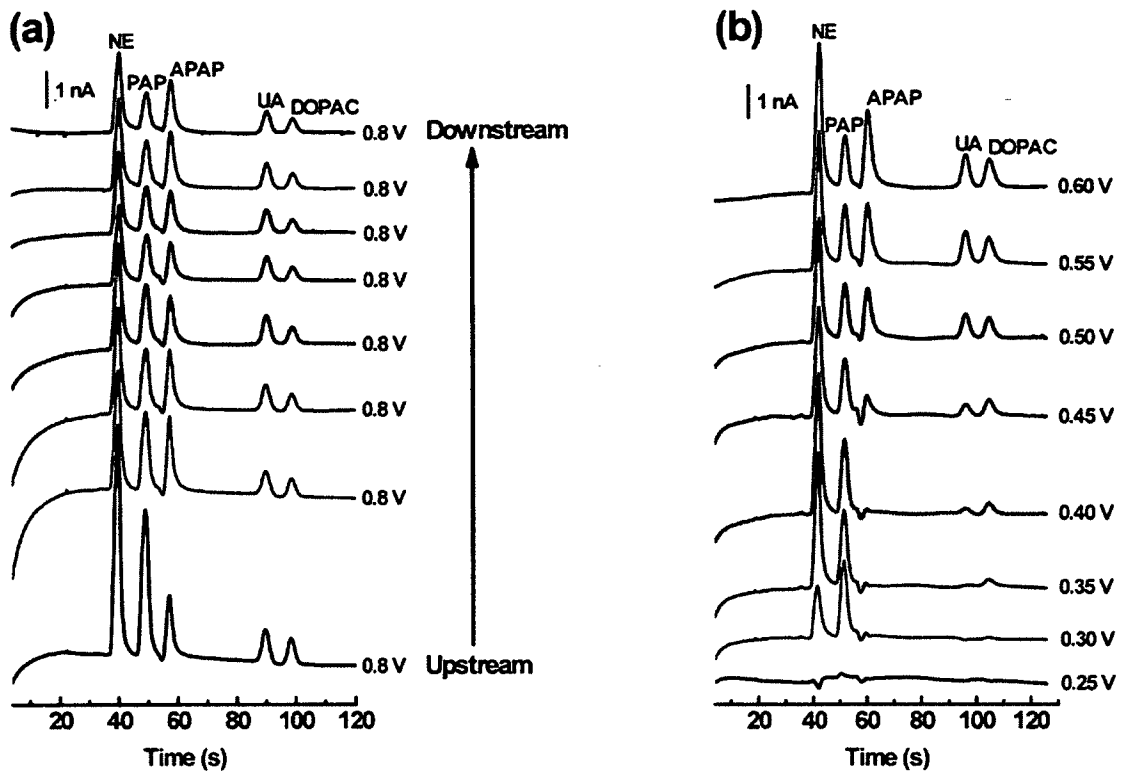

Figure 3. (a) Electropherograms showing separation and simultaneous ECD of 200 μM NE, PAP, APAP, UA, and, DOPAC at eight array electrodes biased to +0.8 V. (b) Potential step detection of the same analytes with electrodes biased from 0.25-0.60 V in 0.05 V steps. All other conditions the same as listed in Figure 2.

electrodes. To determine whether this was the case response of PAP, APAP, UA, and DOPAC relative to NE was analyzed at each array electrode. Peak areas for PAP, APAP, UA, and DOPAC were normalized to NE at each electrode to account for differences in response arising from oxidative depletion of analytes between electrodes. It should be noted depletion is more pronounced for certain analytes (i.e., NE and PAP) relative to others in the electropherograms shown in Figure 3(a), and is speculated to be the result of differences in electrode reaction rates for these compounds. RSD values for response of PAP, APAP, UA, and DOPAC relative to NE were calculated to be 11.8%, 7.7%, 8.9%, and 3.4% (n = 3) respectively for all electrodes in the array indicating relative response was consistent across the array.

Figure 3(b) shows detection at the same array electrodes biased from +0.25-0.60 V in 0.05 V steps from upstream to downstream, respectively. The potential step analysis shown in Figure 3(b) gives the dynamic response of NE, PAP, APAP, UA, and DOPAC in this potential window. The maximum response for NE, APAP, UA, and DOPAC was obtained at +0.60 V while that of PAP was obtained at +0.30 V. A decrease in response was seen for PAP at subsequent electrodes in the array due to analyte depletion arising from oxidation at the preceding electrodes in the array. Detector response decreased for APAP, UA, and DOPAC in the potential window of +0.60-0.40 V; APAP was no longer detected at +0.40 V and the response of UA and DOPAC was substantially reduced. Peak areas for UA and DOPAC at +0.40 V were 22.3 ± 3.4% and 46.3 ± 5.5% (n = 3) of that measured at +0.60 V, respectively. UA was no longer detected at +0.30 V and the response of NE relative to PAP decreased markedly. Peak areas for NE and DOPAC at +0.30 V were 53.4 ± 13.4% and 16.4 ± 12.2% (n =3) of that measured at +0.60 V,

respectively. At +0.25 V only a small response was seen for PAP and no response was seen for the remaining analytes in the mixture. The peak area of PAP at +0.25 V was 16.9 ± 7.4% (n = 3) of its maximum value at +0.30 V. The response profiles shown in Figure 3(b) demonstrate the utility of incorporating multiple working electrodes in a MCE device for improving the selectivity of an analysis. Applying multiple detection potentials at the various working electrodes allows for a more selective detection as analyte response at each electrode is dictated by their respective redox chemistries. With the analytes given in Figure 3(b), NE, PAP, and DOPAC can be preferentially detected at lower oxidation potentials while all the analytes can be detected at higher oxidation potentials.

Differences in electroactivity can further be exploited to improve the selectivity and resolution of an analysis in the event of co-migration or co-elution. Utilization of array detection in separation systems is beneficial as unresolved species can be resolved based upon differences in redox potential removing the need to change separation conditions to resolve the individual components. An example of selective detection of co-migrating species is shown in Figure 4. Electropherograms for each individually addressable array electrode have been offset for clarity. Figure 4 shows potential step detection of a mixture of NE, PAP, APAP, UA, and DOPAC with the addition of 3,4-dihydroxy-L-phenylalanine (L-DOPA). L-DOPA co-migrates with APAP under the given separation conditions; however, the two can be resolved based upon differences in their oxidation potentials. In comparison with Figure 3(b), Figure 4 shows the electrochemical resolution of L-DOPA from APAP at detection potentials less than or equal to +0.40 V (indicated by circled region) while both are detected at potentials greater than +0.40 V. This ability

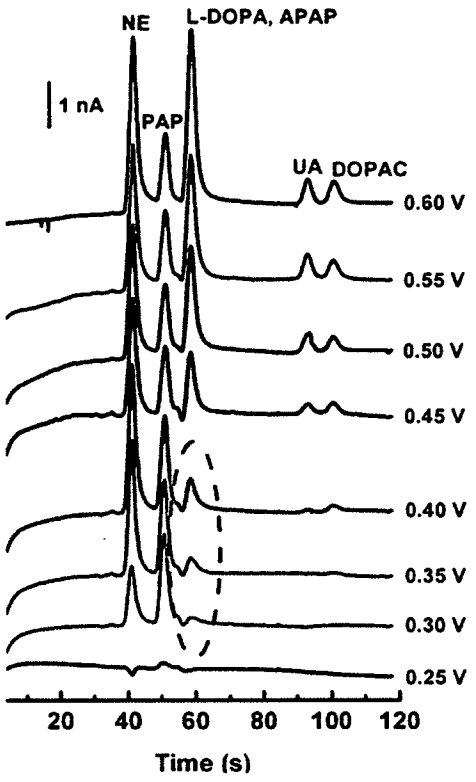

Figure 4. Potential step analysis of 200 μM NE, PAP, APAP, L-DOPA, UA, and DOPAC at eight array electrodes biased from +0.25-0.60 V in 0.05 V steps; L-DOPA co-migrates with APAP. The circled region depicts the potential window in which L-DOPA is selectively detected for in the presence of APAP as compared to the results shown in Figure 3(b). All other conditions the same as listed in Figure 2.

to electrochemically resolve components is advantageous for analysis of complex samples with numerous amounts of electrochemically active compounds as invariably some will co-migrate or co-elute, especially on separation systems having lower peak capacities. Use of array detection allows for an increase in resolution and ultimately an increase in the total number of compounds which can be analyzed on these systems. The ability to selectively detect for certain analytes or analyte classes and resolve co-migrating and co-eluting species using array detection has applications over a broad spectrum of complex chemical analyses (e.g., metabolomics) including point-of-care applications.

4.3.4 Urine Analysis

A human urine sample was analyzed with potential step detection to demonstrate the feasibility of using this device for analysis of complex samples. In this study, array electrodes were biased from +0.25-0.60 V in 0.05 V steps and electrochemically active species in the urine sample oxidized according to their corresponding oxidation potentials. The result of this analysis is shown in Figure 5. Electropherograms for each individually addressable array electrode have been offset for clarity. Multiple peaks are evident in the electropherograms shown in Figure 5 with the slowest peak at the most downstream electrode being ascribable to UA. As expected, response for UA decreases with decreasing detection potential in a manner similar to that seen in Figure 3(b). The peak adjacent to UA shows a similar response as well while earlier migrating analytes show a response at all applied potentials. Successful application of the device for analysis of a complex sample such as this is shows promise for future metabolic fingerprinting studies involving urine or some other biomatrix. For these analyses, sample pre-

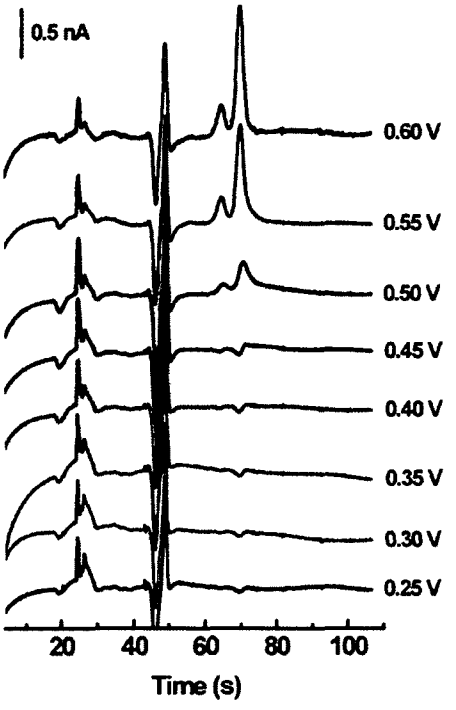

Figure 5. Potential step analysis of a human urine sample. Electrodes were biased from +0.25-0.60 V in 0.05 V steps. All other conditions the same as listed in Figure 2.

concentration in the form of solid phase extraction or on-chip, electrokinetic sample stacking would most likely be employed.

4.4 Conclusions

Use of electrode arrays for selective detection of small molecules has been largely unexplored in the fields of both conventional CE and MCE. This chapter described the successful fabrication and use of an eight electrode MCE-ECD array device for this purpose. Detection of biologically relevant compounds and xenobiotics was conducted using potential step analysis at eight working electrodes incorporated in series into a PDMS capillary electrophoresis microchip, showing improved detection selectivity relative to single electrode detectors. Applicability of this device for complex sample analysis was demonstrated by analyzing a human urine sample with potential step detection. The improvements in selectivity and resolution provided by this detection system could lead to future applications in multi-analyte profiling and point-of-care instrumentation.

4.5 References

(1) Holcomb, R. E.; Kraly, J. R.; Henry, C. S. *Analyst* **2009**, *134*, 486-492.

(2) Matson, W. R.; Langlais, P.; Volicer, L.; Gamache, P. H.; Bird, E.; Mark, K. A. *Clin. Chem.* **1984**, *30*, 1477-1488.

(3) Gamache, P.; Ryan, E.; Svendsen, C.; Murayama, K.; Acworth, I. N. *J. Chromatogr.* **1993**, *614*, 213-220.

(4) Devanesan, P.; Todorovic, R.; Zhao, J.; Gross, M. L.; Rogan, E. G.; Cavalieri, E. L. *Carcinogenesis* **2001**, *22*, 489-497.

(5) Todorovic, R.; Devanesan, P.; Higginbotham, S.; Zhao, J.; Gross, M. L.; Rogan, E. G.; Cavalieri, E. L. *Carcinogenesis* **2001**, *22*, 905-911.

(6) Vigneau-Callahan, K. E.; Shestopalov, A. I.; Milbury, P. E.; Matson, W. R.; Kristal, B. S. *J. Nutr.* **2001**, *131*, 924S-932.

(7) Gamache, P. H.; Meyer, D. F.; Granger, M. C.; Acworth, I. N. *J. Am. Soc. Mass Spectrom.* **2004**, *15*, 1717-1726.

(8) Katz, E. *Handbook of HPLC*; M. Dekker: New York, 1998.

(9) Schwarz, M. A.; Hauser, P. C. *Lab Chip* **2001**, *1*, 1-6.

(10) Johnson, M. E.; Landers, J. P. *Electrophoresis* **2004**, *25*, 3513-3527.

(11) Nyholm, L. *Analyst* **2005**, *130*, 599-605.

(12) Vandaveer, W. R.; Pasas-Farmer, S. A.; Fischer, D. J.; Frankenfeld, C. N.; Lunte, S. M. *Electrophoresis* **2004**, *25*, 3528-3549.

(13) Garcia, C. D.; Henry, C. S. *Electroanalysis* **2005**, *17*, 1125-1131.

(14) Woolley, A. T.; Lao, K. Q.; Glazer, A. N.; Mathies, R. A. *Anal. Chem.* **1998**, *70*, 684-688.

(15) Chen, R. S.; Cheng, H.; Wu, W. Z.; Ai, X. O.; Huang, W. H.; Wang, Z. L.; Cheng, J. K. *Electrophoresis* **2007**, *28*, 3347-3361.

(16) Gawron, A. J.; Martin, R. S.; Lunte, S. M. *Electrophoresis* **2001**, *22*, 242-248.

(17) Lai, C. C. J.; Chen, C. H.; Ko, F. H. *J. Chromatogr., A* **2004**, *1023*, 143-150.

(18) Castano-Alvarez, M.; Fernandez-Abedul, M. T.; Costa-Garcia, A. *J. Chromatogr., A* **2006**, *1109*, 291-299.

(19) Mecker, L. C.; Martin, R. S. *Electrophoresis* **2006**, *27*, 5032-5042.

(20) Martin, R. S.; Gawron, A. J.; Lunte, S. M.; Henry, C. S. *Anal. Chem.* **2000**, *72*, 3196-3202.

(21) Keynton, R. S.; Roussel, T. J.; Crain, M. M.; Jackson, D. J.; Franco, D. B.; Naber, J. F.; Walsh, K. M.; Baldwin, R. P. *Anal. Chim. Acta* **2004**, *507*, 95-105.

(22) Lee, K. J.; Tosser, K. A.; Nuzzo, R. G. *Adv. Funct. Mater.* **2005**, *15*, 557-566.

(23) Ordeig, O.; Godino, N.; del Campo, J.; Munoz, F. X.; Nikolajeff, F.; Nyholm, L. *Anal. Chem.* **2008**, *80*, 3622-3632.

(24) Kok, W. T.; Sahin, Y. *Anal. Chem.* **1993**, *65*, 2497-2501.

(25) Chen, D. C.; Hsu, F. L.; Zhan, D. Z.; Chen, C. H. *Anal. Chem.* **2001**, *73*, 758-762.

(26) Lacher, N. A.; Lunte, S. M.; Martin, R. S. *Anal. Chem.* **2004**, *76*, 2482-2491.

(27) Vickers, J. A.; Henry, C. S. *Electrophoresis* **2005**, *26*, 4641-4647.

(28) McDonald, J. C.; Duffy, D. C.; Anderson, J. R.; Chiu, D. T.; Wu, H. K.; Schueller, O. J. A.; Whitesides, G. M. *Electrophoresis* **2000**, *21*, 27-40.

(29) Lee, J. N.; Park, C.; Whitesides, G. M. *Anal. Chem.* **2003**, *75*, 6544-6554.

(30) Vickers, J. A.; Caulum, M. M.; Henry, C. S. *Anal. Chem.* **2006**, *78*, 7446-7452.

(31) Liu, Y.; Vickers, J. A.; Henry, C. S. *Anal. Chem.* **2004**, *76*, 1513-1517.

(32) Garcia, C. D.; Liu, Y.; Anderson, P.; Henry, C. S. *Lab Chip* **2003**, *3*, 324-328.

(33) Jacobson, S. C.; Hergenroder, R.; Koutny, L. B.; Warmack, R. J.; Ramsey, J. M. *Anal. Chem.* **1994**, *66*, 1107-1113.

(34) Effenhauser, C. S.; Manz, A.; Widmer, H. M. *Anal. Chem.* **1993**, *65*, 2637-2642.

(35) Koutny, L. B.; Schmalzing, D.; Taylor, T. A.; Fuchs, M. *Anal. Chem.* **1996**, *68*, 18-22.

(36) Shultz-Lockyear, L. L.; Colyer, C. L.; Fan, Z. H.; Roy, K. I.; Harrison, D. J. *Electrophoresis* **1999**, *20*, 529-538.

(37) Ocvirk, G.; Munroe, M.; Tang, T.; Oleschuk, R.; Westra, K.; Harrison, D. J. *Electrophoresis* **2000**, *21*, 107-115.

(38) Badal, M. Y.; Wong, M.; Chiem, N.; Salimi-Moosavi, H.; Harrison, D. J. *J. Chromatogr., A* **2002**, *947*, 277-286.

(39) Wallingford, R. A.; Ewing, A. G. *Anal. Chem.* **1987**, *59*, 1762-1766.

(40) Roston, D. A.; Kissinger, P. T. *Anal. Chem.* **1982**, *54*, 429-434.

Chapter 5. *Investigation of Stress-Induced Lipid Accumulation in Microalgae Using a Microfluidic Device*

5.1 Introduction

At this point in the dissertation, the focus shifts from metabolic analysis using electrophoretic techniques to the application of microfluidics for microalgal based, biofuels research. Recently, there has been a great deal of interest in using microalgae as a lipid feedstock for the production of biodiesel and "green" diesel. Historically, these biofuels have been produced from lipid feedstocks derived from oilseed crops, but lately attention has turned to utilizing microalgae for these purposes.[1-2] This interest stems largely from the high lipid yields and small production footprint that may be attainable using microalgae as a feedstock material.[1-2] Additionally, microalgae are seen as a more pragmatic choice for biodiesel and green diesel production as they can be cultivated in environments not typically suited for food or oilseed crops.[1-2]

Realization of microalgal diesel production will likely rely on the use of a limited number of species capable of high levels of lipid accumulation. Since lipid accumulation in many microalgal species depends on environmental and/or culturing conditions,[1,3] it is essential that these conditions are optimized to maximize yields. Currently, this is done using conventional bench-top culturing and lipid analysis techniques. While effective, this approach is not always efficient, and thus the process could benefit from a more streamlined, integrated approach. Microfluidics offers a way to accomplish this goal. With microfluidics, multiple functionalities can be integrated onto a single device, as has been demonstrated with micro-total analysis (μTAS)[4] and lab-on-a-chip (LOC) systems.[5]

This approach would be well suited for microalgal lipid screening as culturing and analysis functionalities could be integrated onto a single platform. Additionally, the ability to multiplex analyses in a high density format using microfluidics would make it possible to simultaneously conduct high throughput screening of multiple microalgal species and culturing conditions.

Here, we present data to establish the feasibility of using microfluidics to culture and screen for lipid accumulation in microalgae. The first step was to develop a microfluidic system having both culturing and analysis capabilities, and for this hybrid PDMS/glass microfluidic systems were found to work well. A valving system compatible with these materials was developed using the torque-actuated design first described by Weibel et al.,[6] but modified to improve device longevity and decrease fabrication time. Once a suitable device had been developed, microalgal compatibility and device performance were evaluated using a model culture of *Tetraselmis chuii*. While microfluidic devices have been widely used for culturing bacterial,[7-11] mammalian,[7-11] and some protozoan cells,[12] no previous examples of algae cell culture have been demonstrated. Additional culturing experiments were also conducted to determine the suitability of the device for growing and maintaining microalgal cultures for extended periods of time (3 wk). Finally, experiments focused on assessing the suitability of the microfluidic device for stimulating and analyzing microalgal lipid accumulation. Here, microfluidic cultures of *Neochloris oleabundans* were stressed under nitrogen (in the form of nitrate) deprivation conditions and then analyzed for lipid accumulation using fluorescence microscopy. Additionally, *Tetraselmis chuii* cultures were temperature stressed and imaged for lipid accumulation in an analogous manner. The development and utilization of this device for

culturing and investigating lipid accumulation in microalgae represents the first step in realizing a fully integrated device for high-throughput microalgal screening applications.

5.2 Materials and Methods

5.2.1 Chemicals and Materials

BODIPY 493/503 (4,4-difluoro-4-bora-3a,4a-diaza-s-indacene) was purchased from Molecular Probes, Inc. (Eugene, OR). Fluorescein diacetate was purchased from Sigma-Aldrich (St. Louis, MO). Absolute ethanol and reagent grade acetone were purchased from Pharmco-Aaper (Brookfield, CT) and Mallinckrodt Baker, Inc. (Phillipsburg, NJ), respectively. Silicon wafers (4 in) were purchased from University Wafer (South Boston, MA). SU-8 3025 negative photoresist was purchased from MicroChem Corp. (Newton, MA). Sylgard 184 elastomer and curing agent (PDMS) were purchased from Dow Corning (Midland, MI). Solid core copper wire (18 gauge) was purchased from Radio Shack (Fort Collins, CO). Glass microscope slides having dimensions of 25.4 mm × 76.2 mm, 1.2 mm thick were purchased from VWR International (West Chester, PA). Poly(methylmethacrylate) (PMMA) sheets (18 in × 24 in, 0.093 in thick) were purchased from Plaskolite, Inc. (Columbus, OH). KOA 300 UV curing epoxy was purchased from Kemxert Corp. (York, PA). Knurled thumbscrews (4-40 × 1 in) were obtained from McMaster-Carr (Aurora, OH). Small machine screws (2-26 × 0.5 in) and their corresponding nuts were obtained in-house. All chemicals were used as received without further purification.

5.2.2 Solution Preparation

A stock solution of BODIPY 493/503 was prepared at 1 mg/mL in absolute ethanol for

use as a fluorescent lipid stain. Fluorescein diacetate was employed as a fluorescent mortality stain, and stock solutions were prepared at 1% (w/w) in acetone. Both dye solutions were stored at -20 °C and shielded from ambient light when not in use. F/2 and Bristol's culturing media were prepared as described by Guillard et al.[13] and Bold,[14] respectively.

5.2.3 Stock Microalgae Cultures

Two different microalgae were used for the following experiments: the marine species *Tetraselmis chuii* (LB 232, UTEX; Austin, TX) and the freshwater species *Neochloris oleabundans* (UTEX 1185, UTEX; Austin, TX). *T. chuii* was used for biocompatibility, culturing, and lipid accumulation experiments while *N. oleabundans* was used only for lipid accumulation experiments. Stock cultures of *T. chuii* were grown in F/2 medium and kept at constant temperature (~25 °C) and light intensity levels (~70 μmol photons/m^2·s) before inoculation in the microfluidic device. Stock cultures of *N. oleabundans* were grown in Bristol's medium and maintained under the same temperature and irradiance conditions as described above for *T. chuii* prior to microfluidic inoculation.

5.2.4 Device Fabrication

A schematic of the microfluidic system used in the following experiments is shown in Figure 1(a); pertinent microfluidic and valving features are labeled for reference. The device consisted of a hybrid PDMS/glass microchip housed in a PMMA holder containing actuating screws for a torque-actuated valving system. Photographs of these

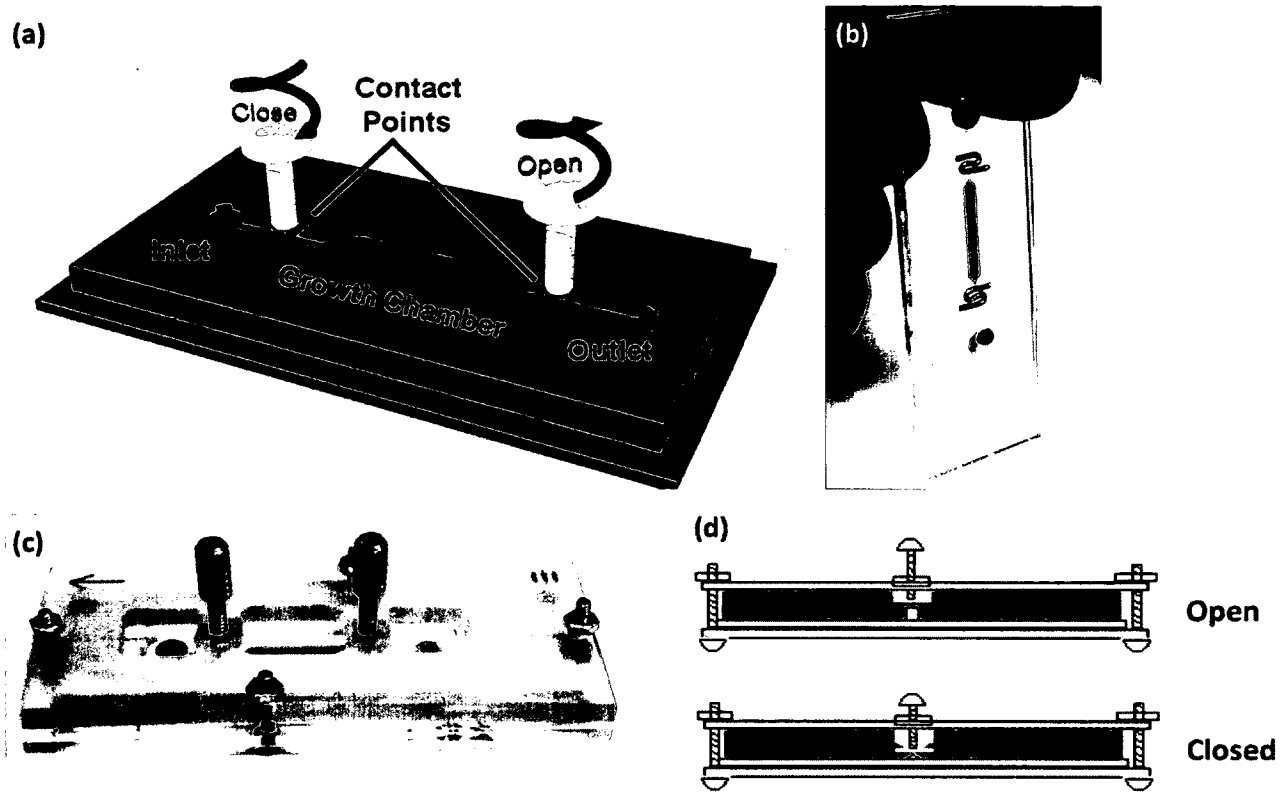

Figure 1. (a) Schematic of the microfluidic system used in microalgal culturing and environmental stress studies. (b) Photograph of the microchip showing microfluidic features and imbedded copper wire contact points. (c) Photograph of the microchip in the PMMA construct containing actuating screws (Note: markings on PMMA are non-consequential). (d) Schematic showing valve operation for the assembled device.

components are shown in Figures 1(b) and 1(c), respectively. All microfluidic features were molded into the PDMS portion of the microchip. These features consisted of a stretched hexagonal growth chamber connected to an inlet and outlet reservoir via two microfluidic channels. Diameters for the inlet and outlet reservoirs were 5 mm and 1 mm, respectively. A larger diameter inlet was used to accommodate adequate solution volumes for microalgal inoculation and on-chip assays, while a smaller diameter outlet was used to allow for leak-free connection to an external syringe pump. Both microfluidic connecting channels were 8.7 mm in length and 350 μm in width. All microfluidic feature heights were 59.3 ± 0.1 μm (n = 3) as determined by profilometry measurements of the master mold. The growth chamber was 17.5 mm in length and 2.5 mm in width at the center (2.4 μL). Final dimensions of the assembled PDMS/glass microchip were 24.4 mm × 76.2 mm, 2.8 mm thick.

Standard soft lithographic techniques were used to fabricate the PDMS portion of the microchip.[15] The following multi-step process was used for microchip fabrication. First, a master mold was prepared by photopolymerizing SU-8 3025 negative photoresist on a silicon wafer according to the manufacturer's recommendations (MicroChem Corp.; Newton, MA); microfluidic mold features were defined using a digitally produced photomask (Printing Services, Colorado State University). Once prepared, a 10:1 mixture of degassed PDMS elastomer and curing agent was spun onto the master mold at 400 rpm for 30 s to cover the mold features and the PDMS subsequently cured at 70 °C for 1 h. Contact points made from copper wire were then placed on the cured PDMS over the inlet and outlet channels (~247 μm above channel ceiling) at alignment marks located on the master mold. These contact points were made from 18-gauge solid core Cu wire (~3.4

mm × 7.0 mm) bent into an "S" shape to act as compression aids for the actuating screws. After adding the contact points, additional PDMS elastomer and curing agent was poured onto the mold to cover the copper wire contact points (~13 g PDMS) and thermally cured (~3 h). The PDMS portion was subsequently removed from the mold and the inlet and outlet reservoirs formed by cutting the PDMS with biopsy punches (Robbins Instruments; Chatham, NJ) at the end of the connecting channels. The PDMS/glass microchip was then assembled in either a reversible or irreversible fashion. For irreversible sealing, the PDMS piece was oxidized alongside a glass microscope slide in an air plasma (Harrick Plasma Cleaner/Sterilizer PDC-32G) at 18 W for 45 s, and the microchip assembled by bringing the two pieces into conformal contact.

A PMMA construct was fabricated to hold the PDMS/glass microchip using an automated Micromill 2000 computer numeric control instrument (MicroProto Systems; Chandler, AZ). Initially, blanks for the upper and lower pieces of the construct were cut from a larger sheet of PMMA. Both blanks had length and width dimensions of 82.6 mm and 34.9 mm, respectively. The upper blank was 4.7 mm thick while the lower blank was 2.36 mm thick. Once the blanks had been cut, a negative relief was milled into the lower blank to hold the microchip in place. The negative relief was 0.89 mm deep and had width and length dimensions slightly larger than that of the glass portion of the microchip (25.4 mm × 76.2 mm). Following this step, PMMA was removed from the upper piece at the inlet and outlet reservoirs to allow access to these reservoirs. PMMA was also removed over the entire length of the growth chamber in both the upper and lower pieces to make it compatible with microscopy. Thumbscrews for valve actuation were then incorporated into the upper PMMA piece using one of two methods: (1) setting a screw

in UV glue or (2) incorporation of the corresponding nut into the PMMA. In the first method, holes having a diameter larger than the valving screws were drilled into the upper piece and the screws then set in UV curable epoxy. The epoxy was cured under a long wavelength, Model UVGL-58 handheld UV lamp (UVP, Inc.; Upland, CA), the screws removed, and excess epoxy milled away. An analogous method was used to secure the nuts for method (2). Following this step, holes were precision drilled at the same point on all four sides of the upper and lower PMMA pieces to accommodate machine screws and their corresponding nuts to hold the entire assembly together. The device was assembled by placing the microchip into the recessed portion of the lower piece, adding the upper piece, and securing the two PMMA pieces together via the machine screws. Since the construct was precision machined, the actuating screws were reproducibly aligned over the copper wire contact points with every device assembly. Figure 1(c) shows a photograph of the assembled device containing a microchip filled with blue dye for visualization, while Figure 1(d) shows a cross-sectional schematic of the assembly depicting screw alignment and valve operation.

5.2.5 Microalgal Inoculation and Culturing

Microalgae were inoculated in the microfluidic device via the following steps. First, the growth chamber was flushed with either F/2 or Bristol's medium, depending on the experiment to be conducted. This was done by applying positive pressure to an aliquot of medium in the inlet reservoir with a 5 mL syringe (Becton-Dickinson; Franklin Lakes, NJ) while the microchip was removed from the PMMA construct. Following medium introduction, the microchip was secured in the PMMA construct and a 50-μL aliquot of microalgae suspension added to the inlet reservoir. Both inlet and outlet valves were then

opened and microalgae drawn through the growth chamber using a NE-1000 syringe pump (New Era Pump Systems, Inc.; Farmingdale, NY) operating in withdraw mode. The syringe pump was connected to the outlet port of the microfluidic device via 0.062 in o.d. (0.030 in i.d.) fluorinated ethylene propylene tubing (Upchurch Scientific, Inc.; Oak Harbor, WA) inserted into the smaller diameter outlet port. Flow rates for microalgal inoculation varied between 2-8 μL/min. During inoculation, microalgae could be concentrated in the growth chamber by partially closing the exit valve, which permitted fluid flow through the device but trapped most microalgae in the growth chamber due to size constraints. After the growth chamber had been inoculated, the syringe pump was turned off and both inlet and outlet valves were completely closed.

Following inoculation, microalgae were incubated and cultured on-chip without medium exchange for times ranging from 3 to 27 d. Biocompatibility and microalgal growth experiments were conducted using stationary- (non-replicating) and growth-phase (replicating) *T. chuii* cultures, respectively. Lipid accumulation experiments were conducted using growth-phase *N. oleabundans* and stationary-phase *T. chuii* cultures. For all culturing experiments, microfluidic devices were kept in a sealed polycarbonate container that had a transparent lid (Nalgene, Fisher Scientific; Pittsburgh, PA). An open vial of ultra-pure, 18.2 MΩ water (Milli-Q, Millipore Corp.; Billerica, MA) was stored in the container to maintain a 100% relative humidity environment; failure to maintain high humidity conditions resulted in solution evaporation from the growth chamber as well as formation of air pockets in the microchip. The container was incubated in an environmental chamber (Percival Scientific, Inc.; Perry, IA) that was maintained at a temperature of ~25 °C and light intensity of ~40 μmol photon/m^2·s. Differences in

illumination of the stock microalgal cultures and the microfluidic cultures arose from the different spatial orientation of these cultures inside the environmental chamber (i.e., middle vs. side). The transparent lid on the container allowed for 95.6 ± 0.3% of incident light to be transmitted to the microfluidic device. Light intensity was measured using a handheld LI-250A Light Meter (LI-COR Biosciences; Lincoln, NE).

5.2.6 Microscopy

Microscopy was used to obtain microfluidic cell concentrations as well as to conduct fluorescence mortality and fluorescence lipid staining experiments. All imaging experiments were conducted using a Nikon Eclipse TE2000-U epifluorescent microscope (Nikon, Inc. (USA); Melville, NY) interfaced with a Photometrics HQ^2 CCD camera (Roper Scientific; Tucson, AZ). The CCD camera was controlled externally using a personal computer and Metamorph imaging software (Molecular Devices; Sunnyvale, CA). The microscope was operated in bright-field mode for determining cell concentrations. Fluorescence experiments were conducted using a Hg halide arc lamp excitation source (X-Cite 120, EXFO Photonics Solutions Inc.; Mississauga, Ontario) and a filter set consisting of a 472 nm excitation filter and a 520 nm collection filter (Model # GFP-3035B-NTE, Semrock; Rochester, NY).

5.2.7 Microfluidic Cell Concentrations

Cell concentrations were calculated for both stationary- and growth-phase *T. chuii* cultures employed for biocompatibility and growth experiments, respectively. For the stationary-phase culture, bright-field images were obtained every 24 h and cell concentrations calculated using the cell counts obtained from these images. To calculate

concentration, cells were counted manually at four regions in images obtained under 100X magnification, 2 × 2 binning, and a 30 ms exposure time. The four regions consisted of 215 × 215 pixel squares drawn on the image using the box tool in Metamorph. The area of these square regions were converted from pixels^2 to cm^2 using a predetermined conversion factor, and the volume (cm^3) then calculated using the height dimension (59.3 ± 0.1 μm) of the growth chamber. Finally, cell concentration for each box region was calculated by dividing the cell count by the box volume, and average cell concentration calculated by averaging the concentrations of all four box regions. An analogous method was used to obtain cell concentrations for the growth-phase *T. chuii* culture. Cells were counted manually at four regions in images taken under 40X magnification, 2 × 2 binning, and a 30 ms exposure time. Cell concentrations were then calculated as described previously.

5.2.8 Mortality Assay

A fluorescein diacetate mortality assay[16-18] was employed to assess the viability of the microfluidic, stationary-phase *T. chuii* culture. This assay was carried out on-chip by filling the inlet reservoir with 0.01% (w/w) fluorescein diacetate in F/2 medium, opening the inlet valve, partially opening the exit valve, and perfusing fluorescein diacetate solution through the growth chamber via vacuum applied to the waste reservoir by a syringe pump (2 μL/min). The corresponding flask culture was also analyzed by adding 1% (w/w) fluorescein diacetate solution at a final concentration of 0.01% (w/w). Fluorescence microscopy was then used to assess the percent mortality for both cultures by counting the number of non-viable (non-fluorescent) and viable (fluorescent) cells in the image.

5.2.9 Environmental Stressing and Lipid Analysis

The effect of nitrate deprivation and temperature on microalgal lipid accumulation was investigated for microfluidic cultures of *N. oleabundans* and *T. chuii*, respectively. For *N. oleabundans*, a growth-phase culture was inoculated in nitrate-depleted Bristol's medium and cultured in the microfluidic device for 3 d. Following culturing, the microalgae were stained with BODIPY 493/503 and imaged using fluorescence microscopy. To stain the cells, a solution of 10 μg/mL BODIPY 493/503 in Bristol's medium was perfused through the growth chamber using a syringe pump and allowed to incubate with the cells for 15 min prior to imaging. Since the microalgae adhered strongly to the glass bottom piece of the microchip, both valves could be fully opened during the perfusion step with minimal loss of cells to the outlet reservoir. The same protocol cannot be used for mobile microalgae such as *T. chuii*, as they do not adhere would be lost to the outlet reservoir. After incubation with the dye, the following steps were taken to image the microalgae: (1) the microchip was removed from the PMMA construct, (2) the reversibly sealed PDMS piece was removed from the glass bottom piece, (3) a 10 μL aliquot of Bristol's medium was added to the immobilized microalgae on the glass bottom piece, (4) a glass coverslip was added on top of the microalgae, and (5) the microalgae imaged using fluorescence microscopy. Direct, on-chip imaging could not be conducted due to strong absorption of the BODIPY 493/503 dye into the PDMS portion of the microchip (see Results and Discussion section). The original culture used to inoculate the microchip (nitrate-replete culture) was also stained with 10 μg/ml BODIPY 493/503 and imaged as a control. Average fluorescence intensity for both cultures was compared by measuring the intensity of representative cells in multiple images using the region measurements

tool in Metamorph. This tool allowed the fluorescence of individual cells to be obtained by simply defining the region (i.e., the cell) to be measured. Intensities obtained in this manner were corrected for background fluorescence (blank subtraction) and then averaged for multiple cells (n = 24) in both cultures.

For *T. chuii,* a temperature stressor was applied by placing the microfluidic device on an ice bath for 4 h. After application of the stress, the culture was removed from the device for lipid imaging. As mentioned above, cells were analyzed off-chip due to dye absorption into the PDMS. To obtain the microfluidic cell culture, the growth chamber of the microchip was evacuated by applying positive pressure to the outlet reservoir with a 5 mL disposable syringe. The growth chamber was then rinsed with an additional 45 μL of F/2 medium and the cells collected from the inlet reservoir for lipid analysis. Lipid staining was conducted by adding an aliquot of 1 mg/mL BODIPY 493/503 stock solution to the cells at a final concentration of 10 μg/mL. The cells were allowed to incubate with dye for 15 min and subsequently imaged using fluorescence microscopy. The non-stressed, flask culture was analyzed in an analogous manner. Average fluorescence intensity for both cultures was then determined using the same procedure described above for *N. oleabundans* (n > 64 for each culture).

5.3 Results and Discussion

5.3.1 Microfluidic Device

This study focused on determining whether microfluidics could be used as a tool for culturing and investigating lipid accumulation in microalgae. The end goal required an integrated microfluidic device containing both culturing and analysis functionalities,

including a valving system to isolate microalgae in a growth chamber and to facilitate on-chip assays. In addition, compatibility with bright-field and fluorescence microscopy was needed as these techniques were used to assess microalgal viability and lipid accumulation. It was found that hybrid PDMS/glass microchips were well suited for these tasks as the optical transparency and low background fluorescence of PDMS[15] allowed both bright-field and live/dead fluorescence microscopy measurements to be conducted on-chip. Furthermore, both materials are compatible with standard microfluidic valving schemes including pneumatic-[19-20] and torque-actuated valves.[6]

For our devices, we utilized a variation of the torque-actuated valves first described by Weibel et al.[6] These valves operate on the principle that micro-channels formed in an elastomeric material such as PDMS can be opened or closed by compression with a screw. This valving scheme was well suited for the present experiments due to its operational simplicity, portability, and power-free mode of operation. These were all beneficial qualities as microfluidic culturing experiments were conducted inside an environmental chamber, which required use of a compact, self-contained valving system. Other microfluidic valving systems[19-20] were not practical for this purpose as they were either too complex or required ancillary equipment which limited their compatibility with the culturing constraints. Besides congruency with culturing studies, these valves were also well suited for fluid manipulation needed to conduct assays on-chip. The non-digital nature of the valves allowed for partial opening or closing of the micro-channels, thus permitting cell trapping during the inoculation step as well as cell retention while imaging reagents were perfused through the growth chamber.

While the valve design described by Weibel et al.[6] would have been suitable for the present experiments, we found it advantageous to modify this design to decrease fabrication times and improve device longevity. The first major modification employed in our design was incorporation of contact points in the PDMS microchip between the micro-channel ceilings and the actuating screws. The purpose of these contact points was to improve device longevity by preventing tearing of the PDMS micro-channels upon valve actuation. Tearing tended to occur with repeated actuations and was largely eliminated by using these contact points. In the present design, contact points consisted of copper wires bent into an S shape to inhibit torsional movement in the PDMS upon valve actuation. A picture of these contact points imbedded inside a PDMS microchip is shown in Figure 1(b). Using this design, leak-free valve operation was achieved with nearly every device used for culturing and lipid accumulation experiments.

The second modification employed in our design involved integrating the actuating screws in a reusable PMMA construct that housed the microfluidic portion of the device. In the original torque valve design,[6] actuating screws were imbedded into the microchip itself. While effective, microchip fabrication is slower and more tedious due to the multi-step process required for setting the screws in the device. Conversely, fabrication times using our design were minimal as the actuating screws were set into the reusable PMMA construct, as can be seen in Figure 1(c). Actual hands-on fabrication of the PDMS/glass portion of the device usually took 30 min or less; the majority of fabrication time involved the actual physical curing of PDMS (~3 h). Because of the simple, rapid, and inexpensive nature of the microchip fabrication, this approach lends itself towards a truly disposable microfluidic platform. The PMMA construct and valving hardware can be re-

used indefinitely, so the only fabrication required to conduct new culturing experiments is that of the inexpensive, disposable microchip.

5.3.2 Microalgal Compatibility and Culturing Studies

After developing a prototype device, focus shifted toward determining the suitability of the system for microalgal culturing. To date, cell culturing using microfluidics has been demonstrated for mammalian,[7-11] prokaryotic,[7-11] and some protozoan systems,[12] but has been largely unexplored for algae and plant cells. Therefore, preliminary studies focused on determining whether microalgae could be cultured in a microfluidic device for extended periods of time, since stress conditions must often be maintained for days to achieve lipid accumulation. Initially, this involved inoculating and monitoring the viability of a stationary-phase (non-replicating) culture of *T. chuii*. These microalgae were utilized because they are relatively large (~20 μm) and mobile, making them easy to image and analyze for cell viability. Experiments were conducted over a period of 5 d, during which the valve performance and culture viability were monitored every 24 h. Valve performance was assessed by examining the cell concentration in the culturing chamber over the 5 d period. A constant culture concentration confirmed leak-free valve performance (Figure 2). Figure 2(a) shows cell concentrations for each 24 hr time point (n = 4), and it is seen that cell concentrations remained statistically equivalent during the duration of the experiment. These results are encouraging as they imply that microalgae can be successfully isolated in the culturing chamber for extended periods of time, something that will be necessary for conducting long-term lipid accumulation studies. The viability of this culture was ascertained by visually inspecting the mobility and morphology of the cells using bright-field microscopy. Based on these examinations,

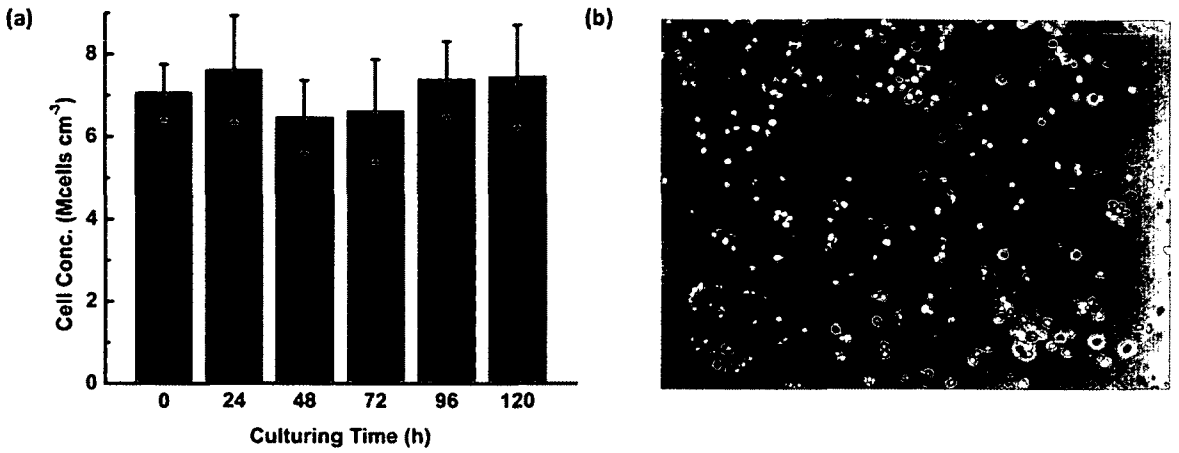

Figure 2. (a) Cell concentrations for stationary-phase *T. chuii* cultured in microfluidic device. Cells were cultured in the device over a period of 120 h. (b) 100X image of *T. chuii* cells stained with fluorescein diacetate at 120 h inside a microfluidic growth chamber.

there was no indication of significant cell mortality over this time period indicating compatibility of the device for cultivation of *T. chuii*. As expected, the optical transparency and gas permeability of PDMS[21] allowed for the light transmission and CO_2/O_2 gas exchange necessary for successful microalgal photosynthesis and overall culture viability.

In addition to visually inspecting the microalgal culture for viability, a quantitative fluorescein diacetate mortality assay[16-18] was conducted to separately confirm these results. Fluorescein diacetate is a non-fluorescent molecule that is converted to the highly fluorescent fluorescein by esterase enzymes inside living cells.[16] This reaction was used to obtain a quantitative measure of cell mortality by simply counting the number of fluorescent (live) vs. non-fluorescent cells (dead) in a culture, as shown in Figure. 2(b). The assay was conducted on-chip to demonstrate the possibility of integrating both culturing and analysis functionalities within a single microfluidic platform. Mortality was calculated for both the microfluidic culture as well as the original flask culture used to inoculate the device. It was found that mortality of the microfluidic culture ($31.9 \pm 7.8\%$) was statistically equivalent to that of the corresponding flask culture ($29.7 \pm 6.3\%$).

While it was possible to conduct this mortality assay on-chip, there were two problems associated with it. First, there was a sizeable loss of cells (*T. Chuii*) to the outlet reservoir that occurred when initially opening the valves to perfuse fluorescein diacetate through the growth chamber. This resulted in a reduced population of cells in which to conduct mortality counts (note: no preferential loss of live vs. dead cells was seen). Secondly, the fluorescein diacetate solution did not distribute evenly throughout the growth chamber,

and was more concentrated at the center of the device than at the sides. Therefore, microalgae used for calculating mortality were chosen from the center of the device. Presently, several methods are being investigated to improve cell retention and dye dispersion in the growth chamber. One method which can prevent cell loss during the perfusion step is employing a bead pack or particle bed in front of the exit valve. This can be accomplished by partially closing the exit valve and allowing particles to pack in front as they are being drawn through the device. The packed bed will still allow for solution flow through the device, but will retain the microalgae (~20 μm) as they are larger than the interstitial spacing of the particles. A weir system could be used in analogous manner.[22] An alternate and perhaps simpler way to quantify microalgal mortality would be to measure the auto-fluorescence of chlorophyll.[18] Using this method, viable cells should fluoresce and non-viable cells should not due to chlorophyll degradation. Conducting the assay in this manner would be ideal as fluorescence measurements could be performed without having to perfuse any fluorescent dye through the system.

Following initial biocompatibility experiments using the stationary-phase culture, a second culturing experiment was performed to determine the feasibility of growing microalgae in the microfluidic device. For this experiment, a stationary-phase culture of *T. chuii* was diluted 10× with F/2 medium and loaded into the microfluidic device. Dilution of the original stationary-phase culture was necessary in order to stimulate cellular division in the inoculated culture. Once inoculated, the microalgal culture showed a statistical difference in population after 3 d in the device. The resulting growth curve for the culture is shown in Figure 3. Inspection of this growth curve reveals two prominent features, a linear growth phase (0-16 d) followed by a stationary-phase. Both

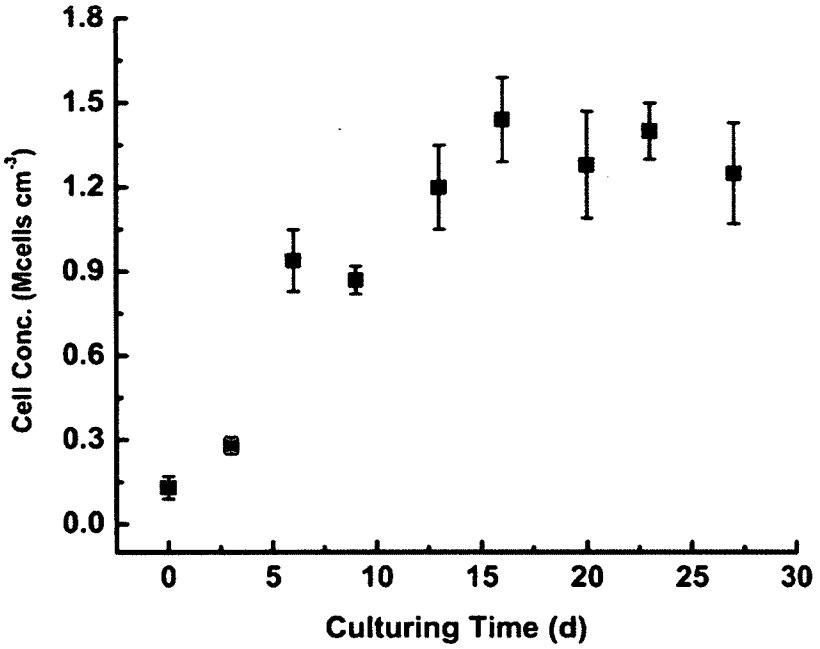

Figure 3. Growth curve for *T. chuii* cultured for 27 days in the microfluidic device.

trends are characteristic of *T. chuii* cultured at the macroscale. Population measurements were taken for 27 d, after which it was noticed that the culture was beginning to die. Evaluation of cell mortality was established by analyzing both cell motility and morphology using bright-field microscopy. Cell death was likely attributable to depletion of nutrients (e.g., nitrate) required for proper cell functioning as well as accumulation of toxic metabolic by-products. Nevertheless, this experiment demonstrated the possibility of growing microalgae at the microscale and reflects positively on the use of microfluidics as a screening tool for various microalgal culturing conditions.

5.3.3 Microalgal Lipid Analysis

It is known that certain species of microalgae accumulate lipids when exposed to specific environmental stimuli.[1,23-24] Determination of these stimuli is important for biofuels production as it allows for lipid accumulation to be maximized for a given species of microalgae by simply controlling culturing conditions. The small scale of microfluidic devices is well suited for the rapid screening of the conditions responsible for lipid accumulation. Since microalgal lipid accumulation has not been investigated in microfluidic environments, the following analysis focused on feasibility.

N. oleabundans microalgae were used for these experiments as they are known to accumulate substantial amounts of lipid when cultured under nitrate-deficient conditions.[24] To determine whether they would exhibit similar behavior in a microfluidic environment, a growth-phase culture of *N. oleabundans* was resuspended in nitrate-depleted medium, inoculated in the microfluidic device, and cultured for a period of 3 d. At the conclusion of the culturing period, microalgae were stained with the fluorescent

dye BODIPY 493/503 for lipid imaging. This particular dye was used as it is highly specific for the nonpolar, cytosolic lipid bodies[25] formed in stressed microalgae. These lipid bodies consist almost entirely of nonpolar triacylglycerols (TAGs),[1] and are easily visualized when stained with a lipophilic fluorophore like BODIPY 493/503. However, use of this dye was initially problematic as it readily absorbed into the PDMS, thus rendering fluorescence lipid imaging impossible. Several attempts were made to block the PDMS surface to prevent this dye absorption including use of polyelectrolyte multi-layers[26] and bovine serum albumin; however, neither method proved effective in preventing dye absorption. This was most likely due to dye diffusion through the blocking agents as the result of the long, quiescent incubation time (15 min) of the dye with the microalgae. Nevertheless, imaging could still be conducted in a relatively straightforward manner by simply removing the PDMS portion of microchip. This worked quite well for this particular microalga species as it is non-motile, which caused cells to settle and stick to the glass portion of the microchip. While this worked for *N. oleabundans,* it is not a permanent solution, and we are currently looking at additional methods and device designs to circumvent this problem.

Despite the inability to perform lipid analysis directly on-chip, fluorescent imaging of the microfluidic *N. oleabundans* culture revealed substantial lipid accumulation for these microalgae (Figure 4). Cytosolic lipid bodies are clearly seen in the stressed microalgal culture (Figure 4(b)) while they are absent from the non-stressed culture (Figure 4(a)). In Figure 4(b), these cytosolic lipid bodies appear as the higher intensity fluorescent regions within the cells. White circles have been drawn around a few of the cells in this figure to help aid in visualization of the cell boundary. This boundary tends to become obscured in

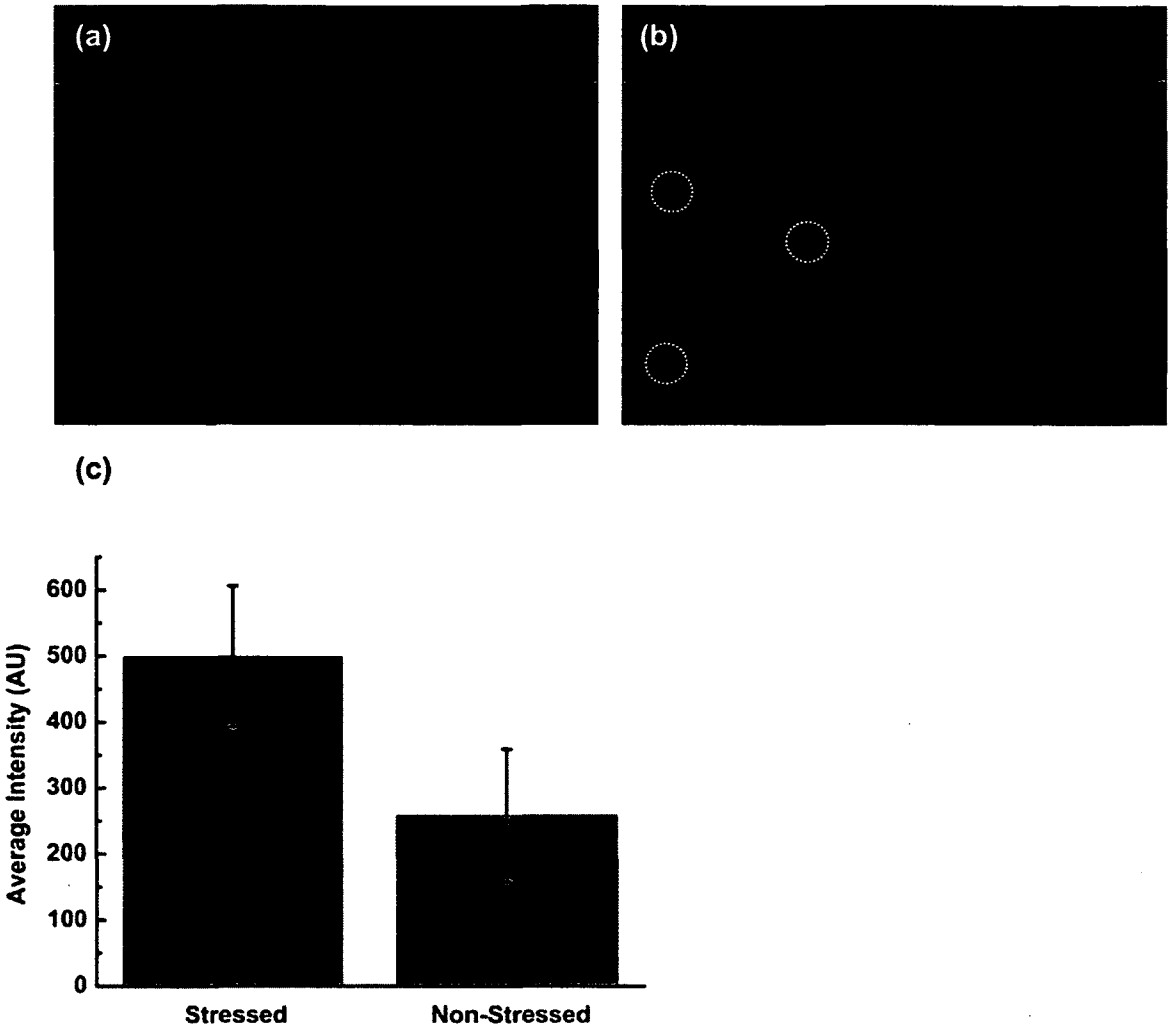

Figure 4. (a) 600X image of non-stressed *N. oleabundans* microalgae cultured in nitrate-replete medium. Microalgae were lipid stained with the fluorescent dye BODIPY 493/503. (b) 600X image of a stressed, microfluidic culture of *N. oleabundans* microalgae cultured in nitrate-depleted medium and stained with BODIPY 493/503. Cytosolic lipid bodies are clearly evident as the higher intensity fluorescent regions inside the cells. Dashed white circles are drawn around selected cells as an aid to help discern cell boundaries. (c) Comparison of average fluorescence intensity for stressed (nitrate deprivation) and non-stressed *N. oleabundans*.

the image due to the higher fluorescence intensity of the cytosolic lipid bodies as opposed to the cell membrane. Measured fluorescence intensities for representative cells (n = 24 cells) in both cultures are shown in Figure 4(c). The nitrate-depleted culture had an average fluorescence intensity of 499 ± 107 AU while the nitrate-replete culture had an average intensity of 258 ± 101 AU. The higher fluorescence intensity for the stressed cells indicates higher cellular lipid content, which is consistent with the visual evidence shown for cytosolic lipid accumulation in Figure 4(b). Together, these results suggest lipid accumulation can be stimulated for microfluidic cultures of microalgae, making high throughput screening using this technology readily attainable.

In addition to stressing *N. oleabundans*, a second lipid accumulation experiment was conducted using *T. chuii* to determine how this microalga responded to temperature stress. Shifts in ambient temperature have been shown to stimulate lipid accumulation in microalgae,[3,27] and was investigated here for *T. chuii* as preliminary data (not shown) suggested this microalga accumulated lipids under temperature duress. Temperature stressing *T. chuii* was accomplished by placing the microfluidic culture in an ice bath for several hours (4 h), and then recovering the cells off-chip to analyze for lipid accumulation. A fluorescent image of temperature stressed *T. chuii* cells is shown in Figure 5(a). Comparison of average fluorescence intensity (n > 64 cells) between the stressed and non-stressed cultures is shown in Figure 5(b). As evident from this figure, there was no statistical difference in the fluorescence intensity between these two cultures, although the stressed culture did have higher absolute fluorescence intensity. These results indicate the microalga *T. chuii* does not rapidly internalize lipid to significant extents when exposed to a temperature stressor. Despite this, some visual

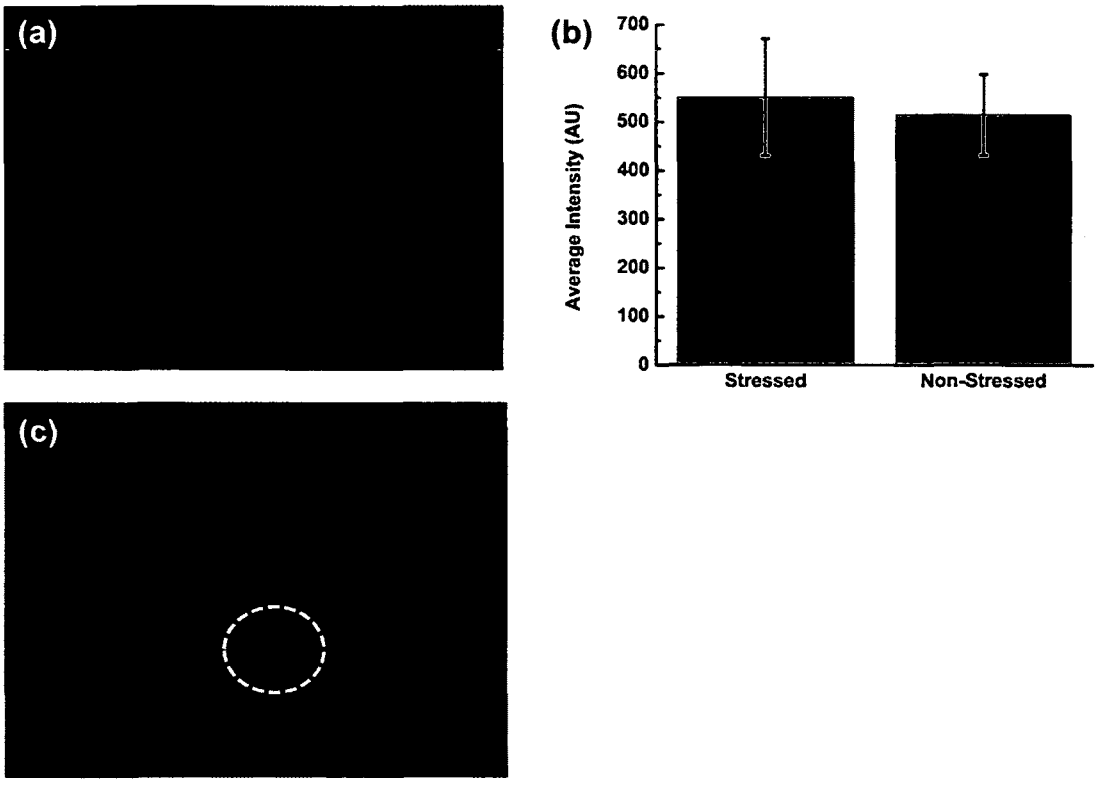

Figure 5. (a) 400X image of temperature stressed *T. chuii* lipid stained with BODIPY 493/503. Microalgae were removed from the microfluidic device, stained, and then imaged for lipid accumulation. (b) Comparison of average fluorescence intensity for stressed (temperature) and non-stressed *T. chuii*. (c) Magnified image of a *T. chuii* cell showing cytosolic lipid bodies. The dashed circular region (white) depicts the location of several of these lipid bodies.

evidence of lipid accumulation was seen in the form of cytosolic lipid bodies in a few cells. Figure 5(c) shows a magnified cell image in which internalized lipid bodies are clearly visible in the cell cytosol; the white circle drawn on the cell highlights the location of several of these lipid bodies. However, since these lipid bodies were seen in only a limited number of cells, an absolute affirmation as to whether these resulted from the temperature stress could not be determined.

5.4 Conclusions

This chapter describes the development and implementation of a microfluidic device for culturing and screening lipid accumulation in microalgae. The device consisted of a PDMS/glass microchip with integrated valving for conducting prolonged culturing studies and on-chip imaging assays. A unique adaptation of an existing valving technique[6] was used in our device to allow for rapid fabrication of microfluidic culturing systems. The successful application of this device for both microalgal culturing and stress testing represents the first step in developing a completely integrated microfluidic platform for high throughput microalgal lipid screening.

5.5 Acknowledgements

First, I would like to thank Lucas J. Mason for his invaluable contributions to this work which involved developing the valving system, fabricating the PMMA constructs, and helping conduct initial microalgal culturing and stress experiments. Also, I would like to thank our collaborator Dr. Kenneth F. Reardon and his graduate student Tara D. Schumacher for providing microalgae samples and relevant information regarding microalgal culturing. Additionally, I thank James T. Palmer for his rendering of Figure

1(a). Finally, I would like to thank Joshua M. Stillahn for his assistance in conducting profilometry measurements.

5.6 References

(1) Hu, Q.; Sommerfeld, M.; Jarvis, E.; Ghirardi, M.; Posewitz, M.; Seibert, M.; Darzins, A. *Plant J.* **2008**, *54*, 621-639.

(2) Greenwell, H. C.; Laurens, L. M.; Shields, R. J.; Lovitt, R. W.; Flynn, K. J. *J. R. Soc. Interface* **2010**, *7*, 703-726.

(3) Guschina, I. A.; Harwood, J. L. *Prog. Lipid Res.* **2006**, *45*, 160-186.

(4) West, J.; Becker, M.; Tombrink, S.; Manz, A. *Anal. Chem.* **2008**, *80*, 4403-4419.

(5) Erickson, D.; Li, D. Q. *Anal. Chim. Acta* **2004**, *507*, 11-26.

(6) Weibel, D. B.; Kruithof, M.; Potenta, S.; Sia, S. K.; Lee, A.; Whitesides, G. M. *Anal. Chem.* **2005**, *77*, 4726-4733.

(7) Sia, S. K.; Whitesides, G. M. *Electrophoresis* **2003**, *24*, 3563-3576.

(8) Khademhosseini, A.; Langer, R.; Borenstein, J.; Vacanti, J. P. *Proc. Natl. Acad. Sci. U. S. A.* **2006**, *103*, 2480-2487.

(9) Weibel, D. B.; Whitesides, G. M. *Curr. Opin. Chem. Biol.* **2006**, *10*, 584-591.

(10) Yi, C. Q.; Li, C. W.; Ji, S. L.; Yang, M. S. *Anal. Chim. Acta* **2006**, *560*, 1-23.

(11) Tanaka, Y.; Sato, K.; Shimizu, T.; Yamato, M.; Okano, T.; Kitamori, T. *Biosens. Bioelectron.* **2007**, *23*, 449-458.

(12) Nagai, M.; Ryu, S.; Thorsen, T.; Matsudaira, P.; Fujita, H. *Lab Chip* **2010**, *10*, 1574-1578.

(13) Guillard, R. R.; Ryther, J. H. *Can. J. Microbiol.* **1962**, *8*, 229-239.

(14) Bold, H. C. *B. Torrey Bot. Club* **1949**, *76*, 101-108.

(15) McDonald, J. C.; Duffy, D. C.; Anderson, J. R.; Chiu, D. T.; Wu, H. K.; Schueller, O. J. A.; Whitesides, G. M. *Electrophoresis* **2000**, *21*, 27-40.

(16) Heslop-Harrison, J.; Heslop-Harrison, Y. *Stain Technol.* **1970**, *45*, 115-120.

(17) Heslop-Harrison, J.; Heslop-Harrison, Y.; Shivanna, K. R. *Theor. Appl. Genet.* **1984**, *67*, 367-375.

(18) Sakamoto, M.; Tada, Y.; Nakayashiki, H.; Tosa, Y.; Mayama, S. *J. Gen. Plant Pathol.* **2005**, *71*, 387-394.

(19) Unger, M. A.; Chou, H. P.; Thorsen, T.; Scherer, A.; Quake, S. R. *Science* **2000**, *288*, 113-116.

(20) Thorsen, T.; Maerkl, S. J.; Quake, S. R. *Science* **2002**, *298*, 580-584.

(21) Merkel, T. C.; Bondar, V. I.; Nagai, K.; Freeman, B. D.; Pinnau, I. *J. Polym. Sci. Pt. B-Polym. Phys.* **2000**, *38*, 415-434.

(22) Zhu, L.; Zhang, Q.; Feng, H. H.; Ang, S.; Chauc, F. S.; Liu, W. T. *Lab Chip* **2004**, *4*, 337-341.

(23) Roessler, P. G. *J. Phycol.* **1990**, *26*, 393-399.

(24) Gouveia, L.; Marques, A. E.; da Silva, T. L.; Reis, A. *J. Ind. Microbiol. Biotechnol.* **2009**, *36*, 821-826.

(25) Gocze, P. M.; Freeman, D. A. *Cytometry* **1994**, *17*, 151-158.

(26) Ro, K. W.; Chan, W. J.; Kim, H.; Koo, Y. M.; Hahn, J. H. *Electrophoresis* **2003**, *24*, 3253-3259.

(27) Arts, M. T.; Brett, M. T.; Kainz, M. J. *Lipids in aquatic ecosystems*; Springer: Dordrecht, 2009.

CHAPTER 6. *Microalgal Lipid Profiling*

6.1 Introduction

This chapter of the dissertation describes initial progress towards a comprehensive lipid profiling study of microalgal triacylglycerols (TAGs) and associated TAG intermediates. As mentioned in Chapter 1, knowledge of these lipid components can be used along with proteomics data to determine TAG biosynthesis pathways. Currently, knowledge of these pathways is incomplete, even for the most studied systems.[1] Determination of these pathways would be beneficial for microalgal biofuels production as it would allow for manipulation of factors responsible for lipid accumulation in microalgae. This could include development of genetically engineered species capable of producing a desired type of TAG under a given set of environmental conditions.

Lipid profiling methods for microalgae are well established, and generally consist of GC analysis of fatty acid methyl esters (FAMEs).[2-6] Since TAGs are non-volatile, they are first converted to a volatile species such as FAMEs before analysis with GC. Direct analysis of TAGs is less common, but has been accomplished using thin layer chromatography systems coupled with flame ionization detectors (FID),[7-8] and to a lesser extent using MS.[9-10] Fatty acids can be analyzed in a similar manner by converting to FAMEs prior to GC analysis,[4-6,8] or analyzed using MS methods.[11] Analysis of charged lipid intermediates can be achieved using LC-MS techniques.[11]

This chapter discusses the development of GC methods for analyzing TAGs in several different microalgal species. Two different methods were employed including GC-FID

and GC-MS. For both methods, TAGs were extracted from microalgal cells and converted to FAMEs for GC analysis. Initial separation conditions were developed for standard solutions of FAMEs before analyzing microalgal samples. Lipid composition for a nitrate deprived *Pavlova lutheri* culture was analyzed using GC-FID. In a similar manner, the lipid composition of a stationary phase *Dunaliella tertiolecta* culture was determined using GC-MS.

6.2 Materials and Methods

6.2.1 Chemicals and Materials

Boron trifluoride (14%) methanol solution, a 37 component FAME mixture (C4-C24), a C14-C22 FAME mixture, and anhydrous magnesium sulfate ($MgSO_4$) were purchased from Sigma-Aldrich (St. Louis, MO). Chloroform (reagent grade), hexane (reagent grade), and Pasteur pipettes were purchased from Fisher Scientific (Pittsburgh, PA). Methanol (MeOH) was purchased from Mallinckrodt Baker, Inc. (Phillipsburg, NJ). All chemicals were used as received without further purification.

6.2.2 Microalgal Samples

Profiling experiments were conducted using *Dunaliella tertiolecta* and *Pavlova lutheri* microalgae. The *D. tertiolecta* culture was a stationary phase culture which showed evidence of lipid accumulation when imaged with fluorescence microscopy (see Chapter 5). *P. lutheri* used for nitrate stressing experiments were grown in nitrate replete medium and then stressed by placing in nitrate deplete medium. Time point samples for nitrate deprivation were obtained at 0 h and 3 h, respectively. All microalgae were cultured in the research laboratory of Dr. Kenneth F. Reardon.

6.2.3 Extraction of TAGs

Microalgal TAGs were extracted according to the method of Bligh and Dyer.[12] Prior to lipid extraction, 10 mL of cell culture was placed in a 15 mL conical tube and pelleted via centrifugation (1,000 rpm, 10 min). Being careful not to disturb the pellet, 9.5 mL of the supernatant was removed and the cells resuspended in the remaining 0.5 mL. The resuspended cells were transferred to a 4 mL dram vial with a Teflon lined lid and 1 mL of 2:1 $CHCl_3$:MeOH added. This caused the cells to rupture and the nonpolar TAGs to fractionate into the $CHCl_3$ layer. This layer was removed from the aqueous/MeOH layer, and evaporated to near dryness under a N_2 (g) stream for the subsequent transesterification reaction.

6.2.4 Transesterification of TAGs

TAGs were transesterified to FAMEs using the method described by Morrison et al.[13] which utilizes a BF_3 catalyst for TAG conversion. The complete reaction is shown below in Equation 6.1.

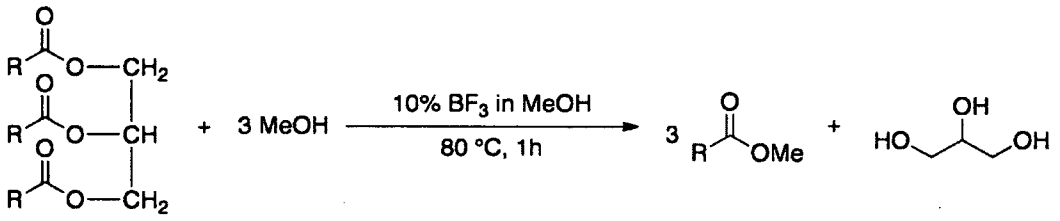

(6.1)

The first step of this process involved adding hexane (0.5 mL) and 10% BF_3 in MeOH (1 mL) to the TAG fraction (in dram vial). Following this, the mixture was shaken and then covered with N_2 (g) using a vented septa. The dram vial was capped tightly, placed in an 80-85 °C oil bath, and allowed to react for 1 h. The reaction mixture was then allowed to cool to room temperature and washed sequentially (in dram vial) with 0.5 mL ultra-pure

18.2 MΩ water (Milli-Q, Millipore Corp.; Billerica, MA) and 2 mL of hexane. The hexane layer containing FAMEs (top layer) was allowed to phase separate, removed with a Pasteur pipette, and dried by adding $MgSO_4$ (s) (forms hydrate). The majority of this hexane volume was then carefully removed from the hydrated $MgSO_4$ (s), and the remaining volume filtered through a Pasteur pipette containing a cotton plug. Finally, the hexane/FAME fraction was concentrated by evaporating off the hexane under a N_2 (g) stream; ~200 μL of hexane/FAME solution remained for GC analysis.

6.2.5 GC Analysis of FAMEs

Both GC-FID and GC-MS methods were developed for analysis of FAMEs. The GC-FID method was adapted from a previous report by Budge et al.[14] which utilized a poly(ethylene) glycol (PEG) wall coated open tubular (WCOT) capillary column for separation of FAMEs. Using this method, FAMEs generated from *P. lutheri* TAG extracts were analyzed. The column (FAMEWAX, Restek Corp.; Bellefonte, PA) used for these experiments had a total length of 30 m, an inner diameter of 0.25 mm, and a stationary phase thickness of 0.25 μm. He (g) was used as the carrier gas and maintained at a constant flow rate of 2 mL/min (linear velocity = 51.9 cm/s) for all experiments. Constant pressure programming was also employed to prevent changes in flow rate which would otherwise occur with temperature ramping. Samples were injected manually (1 μL) into a split injector held at 250 °C. Split ratios of 88:1 and 2.5:1 were used for the 37 component FAME mixture and the microalgal FAME samples, respectively. Separations were conducted using the following temperature ramp: 65 °C for 30 s, ramp to 195 °C at 40 °C/min and hold for 8 min, ramp to 225 °C at 6 °C/min and hold for 13 min. For detection, the FID was held at 250 °C with gas flow rates of 35 mL/min for the H_2 (g)

fuel, 350 mL/min for the air (oxidant), and 20-25 mL/min for the N_2 (g) makeup gas. All GC-FID experiments were conducted using a Hewlett Packard 5890 Series II GC (Agilent Technologies, Inc.; Santa Clara, CA).

Following development of a GC-FID method, a complementary GC-MS method was developed for the analysis of *D. tertiolecta* FAME samples. GC-MS experiments were conducted using an Agilent 5890 Series GC system interfaced with an Agilent 5973 Network Mass Selective Detector (Agilent Technologies, Inc.; Santa Clara, CA). A 5% phenyl/methyl WCOT capillary column (Supelco SPB1, Sigma-Aldrich; St. Louis, MO) having a length of 30 m, an inner diameter of 0.25 mm, and a stationary phase thickness of 0.25 μm was employed for these experiments. He (g) was used as the carrier gas at a flow rate of 1 mL/min (linear velocity = 37 cm/s). Again, a constant pressure program was utilized to maintain this flow rate throughout the duration of the run. Samples were injected (1 μL) with an autosampler into a split injector having a split ratio of 50:1. Separations were conducted using a temperature ramp consisting of the following: 100 °C for 2 min, ramp to 180 °C at 30 °C/min, ramp to 240 °C at 5 °C/min, ramp to 290 °C at 10 °C/min and hold for 2 min. FAMEs in the standard and microalgal sample were detected using the accompanying MS detector and identified with a mass spectral library.

6.3 Results and Discussion

6.3.1 Lipid Profiling with GC-FID

Separation conditions for GC-FID were initially developed using a 37 component FAME mixture (C4-C24). This mixture was used as it contained many of the same FAMEs present in the transesterified microalgal samples. Thus, separation conditions could be

developed without using the microalgal FAMEs which were available in limited quantity. It was found these components could be resolved using a polar, PEG WCOT capillary column in combination with an appropriate temperature ramp (see section 6.2.4). A chromatogram showing the resolution of all 37 components in this mixture is shown in Figure 1. It should be noted some of these components were not completely baseline resolved (e.g., peaks at $t_R \sim 12.5$ min); however, this was not a problem for the present analysis as these components were absent in the microalgal samples analyzed.

Following development of suitable separation conditions, the lipid profile for nitrate deprived *P. lutheri* cultures was analyzed. Chromatograms of the lipid profile for both the initial time point sample and 3 h time point sample are shown in Figure 2(a) and Figure 2(b), respectively. The circled region in Figure 2(a) depicts FAME species (and correspondingly the TAGs) present in these microalgae before stressing. These FAMEs most likely correspond to C16:0 (palmitic acid methyl ester) and C16:1 (palmitoleic acid methyl ester), and were identified by comparing their adjusted retention times to the corresponding components in the standard mixture. Adjusted retention times were determined by subtracting the actual retention time of the peak by that of the hexane (i.e., the solvent) peak which was common to both samples. Analysis of Figure 2(b) shows additional peaks in this chromatogram (red circle) which most likely correspond to unsaturated C20 containing FAME species. Unsaturated C20 lipid species are known to be present in *P. lutheri*,[5,8] and their appearance in this chromatogram suggests they are being produced and accumulated under nitrate depleted conditions. This was confirmed with a separate fluorimetry measurement which showed increased lipid content in the stressed microalgae over this timeframe (data obtained by collaborators).

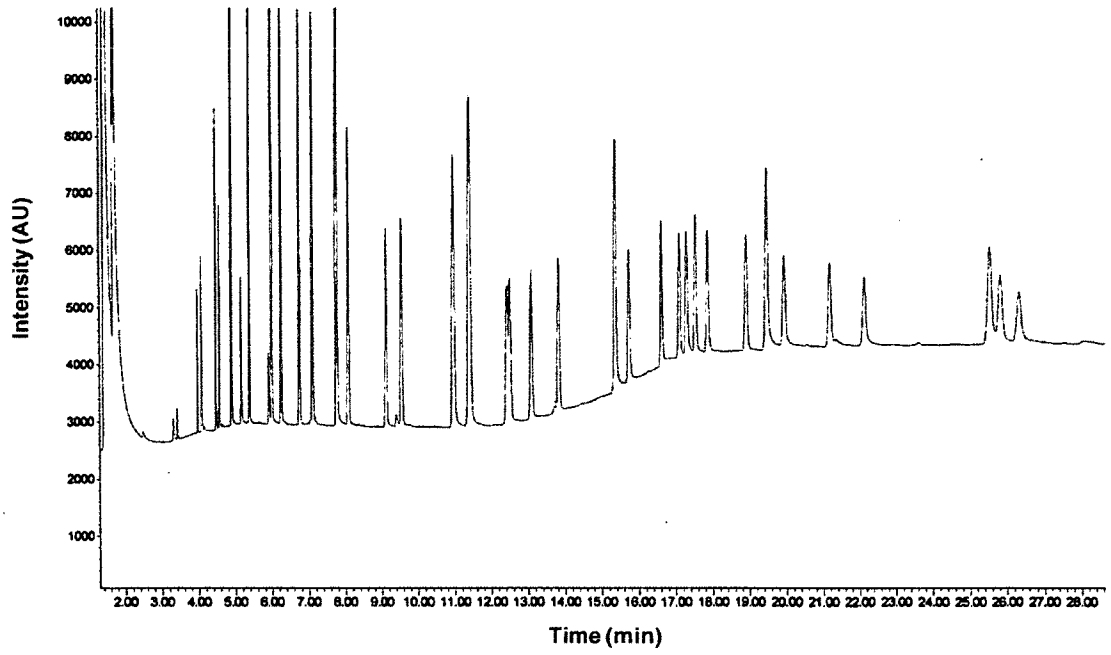

Figure 1. Chromatogram showing separation of a 37 component FAME mixture (C4-C24) obtained using GC-FID. Separation was achieved using a PEG WCOT column, He (g) carrier gas at a flow rate of 1 mL/min, and the following temperature ramp: 65 °C for 30 s, ramp to 195 °C at 40 °C/min and hold for 8 min, ramp to 225 °C at 6 °C/min and hold for 13 min.

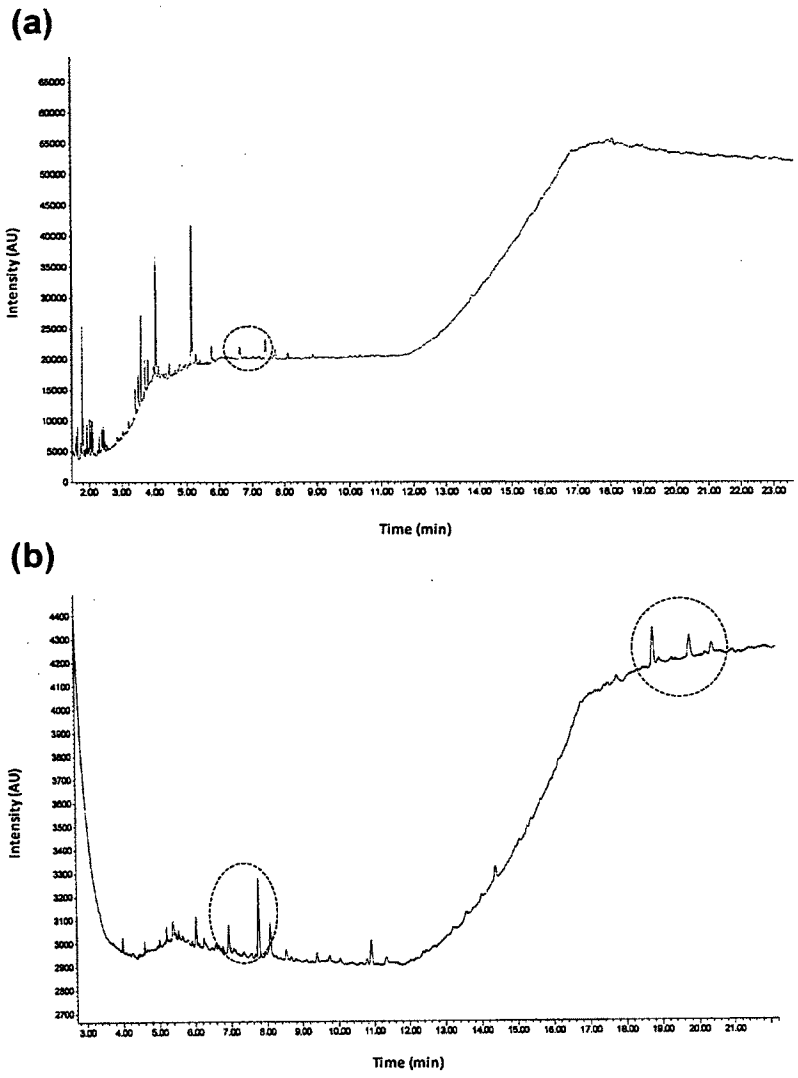

Figure 2. (a) Chromatogram showing FAME components of a transesterified TAG sample obtained from *P. lutheri* prior to nitrate deprivation. Circled peaks (black) most likely correspond to C16:0 and C16:1 FAMEs. (b) Chromatogram showing FAME components of a transesterified TAG sample obtained from *P. lutheri* 3 h after nitrate deprivation. The peaks circled in black most likely correspond to C16:0 and C16:1 FAMEs while the peaks circled in red likely consist of unsaturated C20 FAMEs. Separation conditions for both figures are the same as those given in Figure 1.

While this method was effective in resolving FAME components in these samples, additional work needs to be conducted to quantify percent lipid composition and to confirm lipid identity. For quantitative determination of lipid content, an internal standard which is baseline resolved from the other FAME components will need to be employed. A good candidate is C20:0 (arachidic acid methyl ester) as the corresponding lipid is not produced in most microalgae including *P. lutheri*.[5,8] Lipid composition can be determined using peak areas and response factors for both the microalgal FAME components and internal standard. Additionally, identity of FAME components in the microalgal samples can be obtained by comparing against the adjusted retention times of corresponding standards, or alternatively using a retention index system.

6.3.2 Lipid Profiling with GC-MS

The lipid profile for a stationary phase culture of *D. tertiolecta* was determined using GC-MS. Similar to the previous analysis, separation conditions were initially developed using a standard solution of C14-C22 FAMEs. A 5% phenyl/methyl WCOT column was used in lieu of the PEG, WCOT column used previously as the latter tends to bleed at high temperature, and thus is not suitable for MS detection. A chromatogram showing FAME components of the *D. tertiolecta* sample is shown in Figure 3. Labeled peaks in this chromatogram were determined by matching fragmentation spectra with those in a MS library. These peaks consisted of the following FAMEs: (1) hexadecadienoic acid methyl ester (16:2n4), (2) palmitoleic acid methyl ester (16:1), (3) palmitic acid methyl ester (C16:0), (4) γ-linolenic acid methyl ester (C18:3n6), (5) 11, 14-octadecadienoic acid methyl ester (18:2n4), (6) linolenic acid methyl ester (C18:3n3), and (7) stearic acid methyl ester (C18:0). The lipid profile seen here is typical of *D. tertiolecta* as this micro-

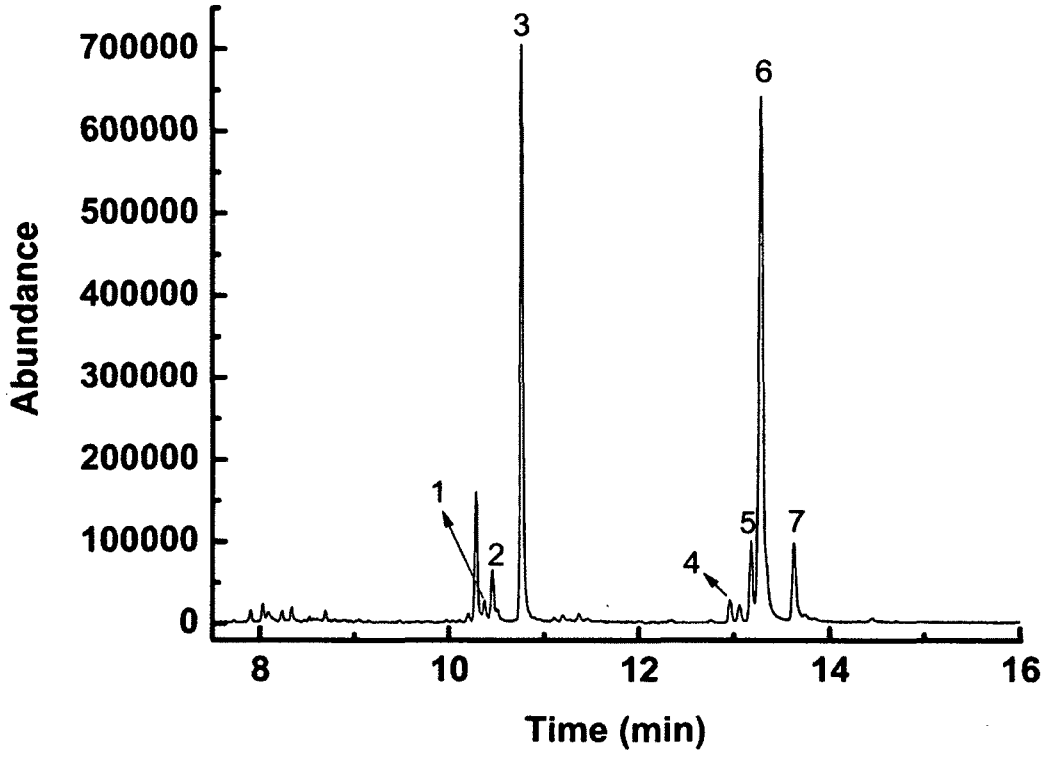

Figure 3. Chromatogram (GC-MS) showing FAME components of a transesterified TAG sample obtained from a stationary phase culture of *D. tertiolecta*. Labeled peaks correspond to the following FAMEs: hexadecadienoic acid methyl ester (16:2n4), (2) palmitoleic acid methyl ester (16:1), (3) palmitic acid methyl ester (C16:0), (4) γ-linolenic acid methyl ester (C18:3n6), (5) 11, 14-octadecadienoic acid methyl ester (18:2n4), (6) linolenic acid methyl ester (C18:3n3), (7) stearic acid methyl ester (C18:0). FAMEs were identified via comparison of fragmentation patterns with a mass spectral library. Separation was achieved using a 5% phenyl/methyl WCOT column, He (g) carrier gas at a flow rate of 1 mL/min, and the following temperature ramp: 100 °C for 2 min, ramp to 180 °C at 30 °C/min, ramp to 240 °C at 5 °C/min, ramp to 290 °C at 10 °C/min and hold for 2 min.

alga is known to produce multiple C16 and C18 lipid species.[15] An internal standard will be needed for quantitative determination of lipid composition, and for this C20:0 (arachidic acid methyl ester) is the most attractive candidate, as described previously.

6.4 Conclusions

This chapter described the development of GC-FID and GC-MS methods for profiling TAGs in microalgae. Lipid profiles for both a nitrate deprived *P. lutheri* culture and stationary phase *D. tertiolecta* culture were analyzed. Developing these methods represents the first step in conducting a comprehensive lipid profiling study of TAGs and TAG intermediates. A more in depth description of proposed experiments for this profiling study is given in the following chapter.

6.5 Acknowledgements

I would like to thank Dr. Luciania P. Pereyra for culturing and extracting TAGs from the *D. tertiolecta* and *P. lutheri* cultures. Also, I would like to thank Donald L. Dick for his help in developing GC-MS separation conditions.

6.6 References

(1) Hu, Q.; Sommerfeld, M.; Jarvis, E.; Ghirardi, M.; Posewitz, M.; Seibert, M.; Darzins, A. *Plant J.* **2008**, *54*, 621-639.

(2) Berge, J. P.; Gouygou, J. P.; Dubacq, J. P.; Durand, P. *Phytochemistry* **1995**, *39*, 1017-1021.

(3) Brown, M. R.; Dunstan, G. A.; Norwood, S. J.; Miller, K. A. *J. Phycol.* **1996**, *32*, 64-73.

(4) Budge, S. M.; Parrish, C. C. *Lipids* **2003**, *38*, 781-791.

(5) Guiheneuf, F.; Mimouni, V.; Ulmann, L.; Tremblin, G. *J. Exp. Mar. Biol. Ecol.* **2009**, *369*, 136-143.

(6) Paik, M. J.; Kim, H.; Lee, J.; Brand, J.; Kim, K. R. *J. Chromatogr., A* **2009**, *1216*, 5917-5923.

(7) Volkman, J. K.; Everitt, D. A.; Allen, D. I. *J. Chromatogr.* **1986**, *356*, 147-162.

(8) Volkman, J. K.; Dunstan, G. A.; Jeffrey, S. W.; Kearney, P. S. *Phytochemistry* **1991**, *30*, 1855-1859.

(9) Han, X.; Gross, R. W. *Anal. Biochem.* **2001**, *295*, 88-100.

(10) Ham, B. M.; Jacob, J. T.; Keese, M. M.; Cole, R. B. *J. Mass Spectrom.* **2004**, *39*, 1321-1336.

(11) Roberts, L. D.; McCombie, G.; Titman, C. M.; Griffin, J. L. *J. Chromatogr., B* **2008**, *871*, 174-181.

(12) Bligh, E. G.; Dyer, W. J. *Can. J. Biochem. Phys.* **1959**, *37*, 911-917.

(13) Morrison, W. R.; Smith, L. M. *J. Lipid Res.* **1964**, *5*, 600-&.

(14) Budge, S. M.; Parrish, C. C.; Mckenzie, C. H. *Mar. Chem.* **2001**, *76*, 285-303.

(15) Siron, R.; Giusti, G.; Berland, B. *Mar. Ecol. Prog. Ser.* **1989**, *55*, 95-100.

CHAPTER 7. *Dissertation Summary and Future Directions*

7.1 Introduction

The final chapter of this doctoral dissertation summarizes research presented in Chapters 2-6 as well as perceived future directions for these projects. Research endeavors discussed in these chapters were varied, but generally focused on applications of capillary electrophoresis (CE), microchip capillary electrophoresis (MCE), and microfluidics for metabolomics and microalgal based, biofuels research. Preliminary chapters focused on metabolomics applications using CE and MCE while later chapters focused on microalgal screening applications and lipid analysis using microfluidics and GC, respectively. Synopses of this work as well as insight into the immediate and long term directions of this research are given in the following text.

7.2 Summary and Proposed Research

Successful implementation of a microfluidic device for biomarker determination would represent an important first step in developing a fully integrated device for point-of-care disease diagnosis and monitoring. Chapter 2 described initial progress towards this goal with the development of a MCE device for the targeted metabolic profiling of total homocysteine (tHcys) in blood serum. Determination of serum tHcys was of interest due to its utility as a biomarker for cardiovascular disease.[1-3] For this analysis, MCE was integrated with pulsed amperometric detection (PAD) for the direct determination of tHcys. PAD was used as it incorporates an electrode cleaning step in situ to prevent electrode fouling, a problem frequently encountered when making electrochemical measurements in biological samples. Separation conditions were developed to resolve

tHcys from other electrochemically active species in serum. Using these conditions, tHcys could be quantified at levels above the "normal" clinical range (~5-15 μM),[4] which could be useful for a "yes/no" diagnostic decision; however, concentrations within the normal clinical range could not be detected as they were below the limit-of-detection (LOD) of the device.

Since the detector was operating at maximum performance, future methods to measure serum tHcys will likely rely on sample preconcentration techniques to bring the target analyte into the dynamic range of the system. Initial work will focus on developing suitable sample preconcentration methods using solid phase extraction (SPE) columns or cartridges. Sorbents and extraction protocols discovered in this step can then be integrated on-chip. Similar systems have been reported,[5] and these could be used as an initial starting point for our microfluidic design. It is envisioned a system like this would have applications not only for tHcys analysis, but also for other biologically significant thiols (e.g., glutathione).

Chapter 3 described a metabolic fingerprinting study of dogs undergoing chemotherapy for diffuse large B cell lymphoma using conventional CE with UV detection. The goal of this study was to compare levels of small molecule components in dog urine as a means to monitor the effectiveness of chemotherapy over time. Urine was analyzed for this study as it negates the need for invasive sample collection techniques like those required for serum or plasma analyses and to date has not been investigated extensively for cancer fingerprinting studies.[6] A CE method was developed which maximized separation efficiency and analyte resolution while at the same time kept analysis times to a

minimum. Fingerprinting analyses of dog urine collected pre-chemotherapy, during-chemotherapy, post-chemotherapy, and after cancer reoccurrence was conducted to determine whether statistical differences in the metabolite fingerprint existed over this time period, and also whether specific metabolic markers were indicative of observed clinical change. Fingerprints of healthy dogs were used as a control and compared to those of diseased dogs to determine whether there was a statistical difference in the urine metabolites present in these two populations. Analysis of these fingerprints using principle component analysis (PCA) showed no statistical difference in metabolite make-up between dogs while z-scores showed little difference in individual metabolite concentrations in these populations.

Differences in these fingerprints could manifest themselves if the number of metabolites measured in the urine samples were increased. Methods to increase the number of measured urine metabolites will again rely on preconcentration techniques to bring low concentration analytes into the dynamic range of the system. For this, multiple SPE protocols will need to be developed to isolate the multiple classes of compounds present in urine. In the long run, it would be beneficial to use MS detection for CE fingerprinting analyses to aid in the identification of disease biomarkers.

Chapter 4 described the development of a MCE device with an integrated electrochemical array detector to conduct rapid metabolic profiling or fingerprinting analyses like those discussed in Chapter 3. Biomatrices encountered in these studies make analyses difficult using MCE due to limited selectivity in many of these systems. One way to improve resolution and selectivity for MCE devices is to increase the total number of individually

addressable detection elements in the system. This was successfully demonstrated with the integration of an eight working electrode array detector into a MCE device. Selective detection and electrochemical resolution of biologically significant analytes was demonstrated using multi-potential detection at the eight working electrode array. The ability to electrochemically resolve co-migrating species is particularly promising for analysis of biofluids as co-migration inevitably occurs due to the large number of compounds present in these samples.

The next logical step for this project will be to utilize the device for metabolic profiling and fingerprinting studies. Again, these studies would require sample preconcentration with SPE for determination of low concentration analytes. Metabolites of interest for profiling experiments include those associated with cancer as well as others which can be profiled in blood or urine (e.g., xenobiotics, phenylalanine, etc.).[7-8] Long term, the possibility of using this system as a second dimension separation technique following HPLC may be explored. It is likely these systems could be interfaced using coupling technologies currently being developed in our laboratories.

The final two chapters of this dissertation (Chapters 5-6) described microalgal biofuels related research. Chapter 5 dealt with the use of microfluidics as a tool to rapidly screen for lipid accumulation in microalgae while Chapter 6 discussed lipid profiling using GC. For the microfluidics work, a device was developed as a screening tool to determine culturing and stress conditions which result in lipid accumulation in microalgae. The microfluidic device contained integrated valves for isolating microalgae in a growth chamber. Additionally, these valves could be used for manipulating fluid flow to conduct

on-chip imaging assays. Using this device, microalgae were successfully grown and stressed to accumulate lipids on-chip. This work represents the first example of microalgal culturing in a microfluidic device and signifies an important expansion of microfluidics into the domain of biofuels research.

While microalgae could be successfully stressed on-chip, direct fluorescence imaging of the resulting lipid accumulation could not due to absorbance of the fluorescent dye into the microchip substrate (poly(dimethylsiloxane)). Therefore, future work will involve discovering ways to circumvent this problem. One possible way of doing this is to block or chemically modify the PDMS surface to prevent dye absorption, or alternatively design a microchip in which microalgae are stained in one location and then imaged downstream in a dye free region. Additionally, impedance cytometry could be used in lieu of fluorescence for measuring microalgal lipid accumulation on-chip.[9] Once these problems have been solved, the long term goal of the project is to multiplex the system for simultaneous analysis of multiple stress conditions and microalgal species. Initial prototypes containing up to three separate microfluidic chambers have been developed; however, higher density systems (growth chambers) which operate in a more autonomous fashion are desired.

In addition to screening for microalgal lipid accumulation, the types of lipids (triacylglycerols or TAGs) being produced by microalgae under stress conditions were also of interest. Knowledge of these lipids and lipid intermediates can be used in a synergistic manner with proteomics data to elucidate lipid biosynthetic pathways. Chapter 6 described initial progress towards this goal with the development of GC

methods for profiling microalgal TAGs. Two different GC methods were employed including GC-MS and GC with flame ionization detection (FID).

Future work on this project will involve global lipid profiling using both GC-MS and HPLC-MS. GC-MS will be used for profiling TAGs, while fatty acid intermediates, including enzyme complexes (i.e., CoA and ACP species), will be profiled using LC-MS. The latter will be conducted using lipid profiling methods developed by Donald L. Dick in the Central Instrument Facility at Colorado State University. These methods were initially developed for profiling lipids in bacterial cells, but should be applicable to microalgal cells as well. For these analyses, lipids can be extracted as described previously and directly analyzed using reverse phase LC-MS with electrospray ionization. Lipid profiles generated in this manner can then be analyzed with comprehensive MS libraries which Mr. Dick is currently working to compile. Data obtained from these lipid profiling studies will be used with the proteomics data obtained by our collaborators (Dr. Kenneth F. Reardon) for determination of TAG biosynthetic pathways.

7.3 References

(1) Jacobsen, D. W. *Clin. Chem.* **1998**, *44*, 1833-1843.

(2) Nappo, F.; De Rosa, N.; Marfella, R.; De Lucia, D.; Ingrosso, D.; Perna, A. F.; Farzati, B.; Giugliano, D. *JAMA* **1999**, *281*, 2113-2118.

(3) Anderson, J. L.; Muhlestein, J. B.; Horne, B. D.; Carlquist, J. F.; Bair, T. L.; Madsen, T. E.; Pearson, R. R. *Circulation* **2000**, *102*, 1227-1232.

(4) Kang, S. S.; Wong, P. W.; Cook, H. Y.; Norusis, M.; Messer, J. V. *J. Clin. Invest.* **1986**, *77*, 1482-1486.

(5) Marchiarullo, D. J.; Lim, J. Y.; Vaksman, Z.; Ferrance, J. P.; Putcha, L.; Landers, J. P. *J. Chromatogr., A* **2008**, *1200*, 198-203.

(6) Szymanska, E.; Markuszewski, M. J.; Capron, X.; van Nederkassel, A. M.; Vander Heyden, Y.; Markuszewski, M.; Krajka, K.; Kaliszan, R. *J. Pharm. Biomed. Anal.* **2007**, *43*, 413-420.

(7) Mrochek, J. E.; Dinsmore, S. R.; Ohrt, D. W. *Clin. Chem.* **1973**, *19*, 927-936.

(8) Huang, Y.; Jiang, X.; Wang, W.; Duan, J.; Chen, G. *Talanta* **2006**, *70*, 1157-1163.

(9) Benazzi, G.; Holmes, D.; Sun, T.; Mowlem, M. C.; Morgan, H. *IET Nanobiotechnol.* **2007**, *1*, 94-101.

APPENDIX 1: *List of Abbreviations*

APAP- acetaminophen

ASP- Aquatic Species Program

BCD- β-cyclodextrin

BGE- background electrolyte

BODIPY 493/503- 4,4-difluoro-4-bora-3a,4a-diaza-s-indacene

CD- cyclodextrin

CE- capillary electrophoresis

CMC- critical micelle concentration

CME- chemically modified electrode

CVD- cardiovascular disease

CZE- capillary zone electrophoresis

DA- dopamine

L-DOPA- 3,4-dihydroxy-L-phenylalanine

DOPAC- 3,4-dihydroxyphenylacetic acid

ECD- electrochemical detection

EOF- electroosmotic flow

FAME- fatty acid methyl ester

FID- flame ionization detector

Hcys- homocysteine

tHcys- total homocysteine

LIF- laser induced fluorescence

LOC- lab-on-a-chip

LOD- limit of detection

MCE- microchip capillary electrophoresis

MEKC- micellar electrokinetic chromatography

MES- 2-(4-morpholino)ethanesulfonic acid

NE- norepinephrine

PAD- pulsed amperometric detection

iPAD- integrated pulsed amperometric detection

PAP- 4-aminophenol

PCA- principle component analysis

PDMS- poly(dimethylsiloxane)

PED- pulsed electrochemical detection

PEG- poly(ethylene) glycol

PMMA- poly(methylmethacrylate)

POC- point-of-care

RSD- relative standard deviation

SDS- sodium dodecyl sulfate

S/N- signal-to-noise

TAG- triacylglycerol

μTAS- micro-total analysis system

TCEP- tris(2-carboxyethyl)phosphine

UA- uric acid

WCOT- wall coated open tubular

APPENDIX 2: *Research Proposal*

Rapid Determination of Ischemic or Hemorrhagic Stroke Using an Aptameric Biosensor

Ryan E. Holcomb, Department of Chemistry, Colorado State University, Fort Collins, CO 80523

Abstract/Specific Aims

Stroke is a disease affecting nearly 795,000 Americans each year, and is currently the third leading cause of death in the United States behind heart disease and cancer.[1] The condition is characterized by rapid loss of brain function resulting from disruption of blood supply to the brain. Generally, stroke occurs when a blood vessel leading to the brain is blocked by a clot (ischemic stroke), or when hemorrhaging occurs within the brain (hemorrhagic stroke). Depending on the type of stroke, blood thinners or coagulants need to be administered in a rapid, time sensitive manner to exact life saving treatment. There is a limited time frame in which these treatments are effective;[2] therefore, it is crucial diagnosis be as rapid as possible to ensure the best possible outcome for the stroke victim. Current methodologies used for diagnosing stroke consist mainly of imaging techniques,[1,3] but electrical impulse and blood flow tests are also employed.[1,3] While these techniques are effective, they are slow and their use is limited to a hospital setting. Thus, the ability to diagnose stroke in a pre-hospital setting would be extremely beneficial as it would expedite administration of cause specific stroke treatments and hence improve patient prognosis.

To date, no measurement technologies exist for the accurate diagnosis of stroke in a pre-hospital setting. One way of achieving this goal is through the utilization of point-of-care (POC) measurement devices.[4-8] As the name suggests, POC involves use of analysis systems which can be used in a variety of settings outside of a clinical diagnostics laboratory. These systems consist of handheld or self contained, benchtop devices which can be operated by a broad spectrum of medical personnel in a rapid, straightforward manner.[6] Towards this end, we propose the development of a simple microfluidic biosensor for the cause specific diagnosis of stroke. The proposed biosensor would consist of aptamer based, electrochemical sensors capable of capturing and measuring specific protein biomarkers of stroke in blood serum. We hypothesize the measurement of biomarkers specific to both ischemic and hemorrhagic stroke on a single analysis platform will allow for the rapid elucidation of stroke type. Additionally, we hypothesize increasing the total number of aptamer sensors, and thus biomarkers measured in this device, will improve the overall accuracy of the diagnosis.

Specific Aim 1. Develop a microfluidic biosensor device capable of rapid (several minutes), multiplexed analysis of protein biomarkers in blood serum. Specifically, this will involve fabrication of a microfluidic system capable of passively transporting serum to integrated sensing electrodes.

Specific Aim 2. Develop aptamers for selected protein biomarkers of both ischemic and hemorrhagic stroke. Subsequently, optimize the sensor system for the specific aptamers to be employed in the device.

Specific Aim 3. Test the diagnostic utility of the finalized device by measuring biomarkers in serum samples obtained from ischemic and hemorrhagic stroke patients. Additionally, determine the number of biomarkers needed for an accurate diagnosis.

If successful, this would represent the first time a blood based sensor has been used in the diagnosis of stroke. The overall simplicity of the sensor design should allow for easy integration into a standalone, portable POC device capable of use in a pre-hospital setting. Furthermore, the ability of the sensing platform to be adapted to analysis of biomarkers other than those of stroke makes the device relevant to additional applications in blood based diagnostics.

Background and Significance

Currently, there is increasing interest in developing POC measurement technologies for medical diagnostics.[4-8] This interest is driven largely by the opportunity to obtain near real-time diagnostic information without having to send patient samples to an off-site testing facility. Obtaining diagnostic information in this manner would help to streamline medical care as diagnosis and treatment could be conducted in a single visit to the doctor. This not only improves efficiency, but also drives down medical costs as a direct result. Besides these obvious benefits, one key advantage of POC technology is its ability to be used outside of the clinical domain. This would be extremely advantageous for time sensitive cases where diagnosis in a pre-hospital setting would improve patient care.

One such instance where this would be extremely useful is in the diagnosis of stroke. As mentioned previously, the effectiveness of treatment for ischemic and hemorrhagic stroke relies on how quickly a diagnosis can be procured.[2] Thus, the ability to rapidly diagnose stroke in a pre-hospital setting would vastly improve the cause specific treatment of the disease. Current methodologies for diagnosing stroke rely mostly on imaging techniques such as CT or MRI scans,[1,3] although Doppler ultrasound, electrical impulse, and arteriography are also sometimes used.[1,3] While these techniques are effective in accurately diagnosing stroke type, they are slow and there implementation outside a clinical setting is not readily feasible. Therefore, a simple POC technology capable of rapidly and accurately diagnosing stroke in these cases would be highly valuable.

One of the most direct ways of achieving this type of diagnosis is through the analysis of protein biomarkers in blood serum. Within the past decade, multiple protein biomarkers specific to ischemic[9-12] or hemorrhagic stroke[11-15] have been identified. These proteins are up-regulated in body during stroke, and as a result there is a concomitant concentration increase in the blood stream.[10-12] Thus, it is possible to measure these biomarkers using an appropriate blood based measurement technology. Currently, enzyme-linked immunosorbent assays (ELISA)[9,16-18] and mass spectrometry[13,19-20] are most often employed. However, these techniques are not readily amenable to POC due to their long analysis times and instrumental complexity. Conversely, the simplicity and rapid analysis times inherent to miniaturized biosensors make them ideal candidates for use within a POC framework.

Multiple biosensor systems have been reported capable of measuring analytes in complex matrices such as blood serum.[21-26] Sensor systems incorporating mass,[22,26] electrochemical,[24,27] and optical detection[21,23,26] techniques have all been employed to

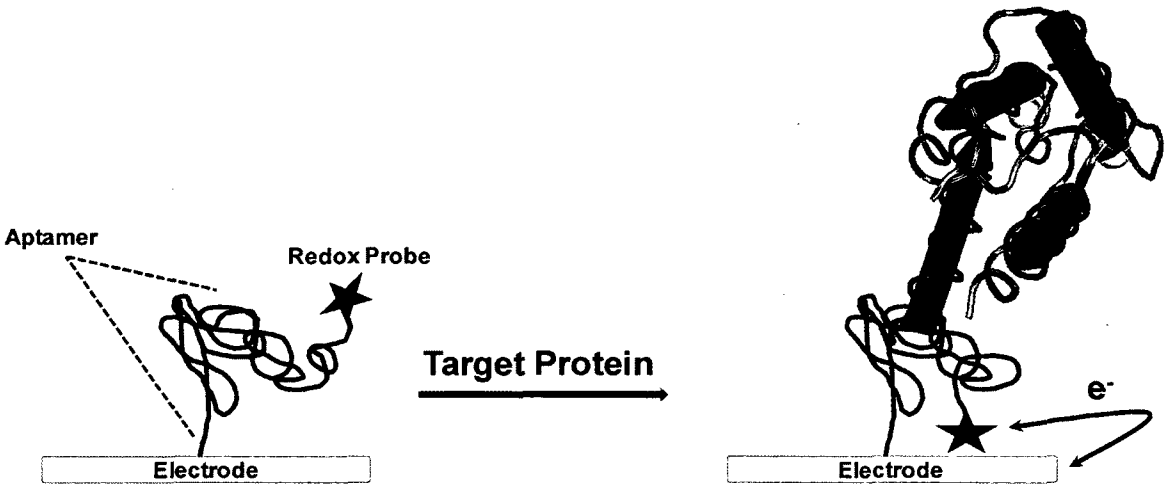

Figure 1. Schematic showing general operational principle of the aptameric, electrochemical biosensor. Here, a conformational changing aptamer is conjugated at one terminus to a gold sensing electrode and at the other terminus to an electrochemically active redox probe (star). In the absence of target, the redox probe is farther from the electrode surface resulting in limited current flow. Target binding induces a conformational change in the aptamer which brings the redox probe closer to the electrode surface, thus facilitating an increased rate of electron transfer (current) which is distinguishable from background. Schematic concept adapted from Lai et al.[28]

measure a broad range of analytes ranging from small molecules to proteins. While all these techniques are valid, some suffer more than others from false positives in detection arising from non-specific adsorption of proteins. In particular, quartz-crystal microbalance[22,26] and surface plasmon resonance[21,26] sensors are the most susceptible to these false positives due to the non-specific nature of the detection techniques. To eliminate many of the problems associated with non-specific adsorption, antibodies[29] or aptamers[24,30-31] (oligionucleotide ligands) can be employed to selectively isolate target analytes. In these systems, signal is theoretically generated only for target analytes bound to the antibody or aptamer, thus improving detection selectivity.

Of these selective systems, aptameric sensors show particular promise for use in POC devices. Aptamers are generally more robust than antibodies and can also be used in reagentless, reusable, and non-ELISA based formats.[32] This makes them especially attractive for protein based, POC applications. For these reasons, we propose utilizing an aptameric biosensor for selectivity quantifying protein biomarkers of stroke. Specifically, we will use an aptameric based, electrochemical sensing platform developed by the Heeger and Plaxco groups[28,33-35] which relies on conformational changing aptamers to capture analyte and generate signal. A schematic demonstrating this general sensing approach is shown in Figure 1. In this design, conformational changing aptamers are functionalized with a redox probe (i.e. methylene blue) and immobilized to an electrochemical sensing electrode. Upon binding of the target protein, the aptamer/protein ensemble changes conformation resulting in a change in the spatial orientation of the

conjugated redox probe relative to the sensing electrode. This in turn affects efficiency of electron transfer from the sensing electrode to the redox probe resulting in an increase or decrease in signal. In the schematic shown in Figure 1, binding of target brings the redox probe closer to the sensing electrode increasing current flow and thus total signal for the system.

Similar approaches have been explored using fluorescently labeled aptamers.[31,36-38] Like the previous approach, binding of the target induces a conformational change in the aptamer/protein ensemble which can be quantified.[31,36-38] Although this is a viable alternative to the proposed electrochemical sensor system, its implementation for POC is a bit more challenging as it requires an optical detection system which is generally more complex and expensive. Furthermore, fluorophores are prone to photobleaching and thus are generally not as robust as electrochemical systems for POC purposes. Additional aptamer systems have been reported for protein sensing applications, but again these include functionalized quartz-crystal microbalance[39-40] and surface plasmon resonance[41-42] sensors which suffer from nonspecific protein adsorption to the transducer surface. Thus, the proposed electrochemical system represents the most pragmatic aptameric approach to realize a selective POC sensing technology for stroke biomarkers.

Multiplexed detection of stroke biomarkers with the proposed sensor platform should be possible by integrating multiple sensors in parallel on a planar, microfluidic device.[43] Microfluidics will allow for simple manipulation of fluid flow which will be required for electrode functionalization and serum handling. Additionally, fabrication costs will be minimal using a microfluidic format thus lending itself to a disposable platform. The finalized device should be capable of rapid detection of stroke biomarkers in a straightforward, reagentless fashion. This is important in the present context as it readily lends itself to further development into a standalone POC device. Currently, no such technology exits, so the successful development of this sensor would represent a major step forward in the cause specific management of stroke.

Research and Design Methods

Specific Aim 1. In *Specific Aim 1* we seek to develop a microfluidic biosensor capable of multiplexed analysis of protein biomarkers in serum. A schematic of the proposed design is shown in Figure 2. This design incorporates parallel microfluidic channels for serum transport to individual sensing electrodes in a planar, microfluidic device (~ 2 cm × 4 cm). The device shown in Figure 2 is capable of measuring three specific biomarkers of stroke; however, the number of channels and corresponding sensing electrodes can be increased depending on the number of biomarkers one wishes to measure. For biomarker analysis, serum is placed in the inlet wells and transported through the microfluidic channels to the parallel sensing electrodes via passive pumping.[44] This mode of bulk fluid transport has been successfully demonstrated previously for serum in microfluidic channels,[44-46] and thus we anticipate minimal problems implementing it in this system. A passive mode of sample transport (i.e. no pumps) is ideal for this device as it is not only simpler, but also makes it more amenable to POC. Although a multiplexed sensor could be fabricated without the use of microfluidics, in the present case it is the simplest option for individually functionalizing each electrode with specific aptamers. Here, the

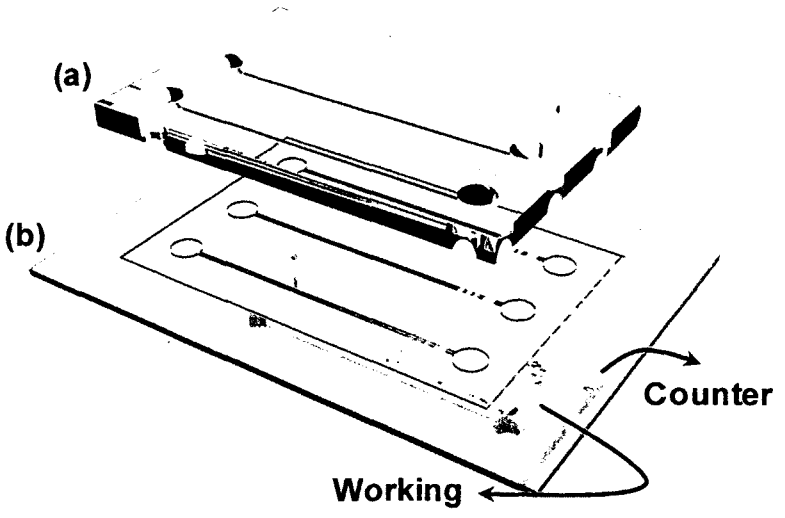

Figure 2. Schematic showing expanded view of the micro-fluidic biosensor. The PDMS top piece (a) contains parallel flow channels and inlet/outlet wells (left and right sides, respectively) for solution containment. The glass bottom piece (b) contains parallel electrochemical cells for each associated flow channel. Three, series, gold working electrodes precede a larger counter electrode in each electrochemical cell. The assembled device will be able to fit into the palm of a hand.

microfluidic channels isolate each parallel electrochemical cell, thus allowing individual aptamer coupling schemes to be conducted with relative ease.

The microfluidic portion of the biosensor will be fabricated from poly(dimethylsiloxane) (PDMS) using well established soft lithographic techniques.[47-48] PDMS is advantageous as a substrate material as it allows for rapid prototyping and optimization of the microfluidic features in a simple, cost effective manner. Additionally, PDMS soft lithography does not require the use of clean room facilities, thus allowing for in-house fabrication of our devices. This will not only be more cost effective, but also increase the throughput in which new designs can be tested. Similarly, glass will be used as a complementary substrate material as electrode pattering on glass can be conducted in-house in a relatively straightforward fashion. Also, it is compatible with PDMS and can be easily bonded to this material in either a reversible or irreversible fashion.[48] For electrode fabrication, we will employ standard photolithographic lift-off techniques[49] using gold as an electrode material. Multiple materials can be used for patterning electrodes, but gold is suitable for these devices as our capture aptamers are easily conjugated to this metal.[28,34] Besides compatibility with glass, lift-off is desirable in the present case as it utilizes the same equipment employed in PDMS soft lithography. The only additional piece of equipment required is a thermal evaporation chamber for metal deposition, which is generally accessible in most research settings.

The heart of the microfluidic device is comprised of the parallel, electrochemical sensors. Each electrochemical sensor shown in Figure 2 consists of a two electrode cell: three series, working electrodes (electrode 1) and one larger counter electrode (electrode 2). Electrical connections to these electrodes are made outside the assembled device at the circular "pads" shown in Figure 2. A traditional three electrode cell including reference is not required in the present case as micron sized, working electrodes are employed. It is

well known microelectrodes do not require use of reference electrodes due to the limited electrode polarization and potential drop in these systems.[50-51] The currents passed by microelectrodes are typically in the nanoamp to picoamp regime, thus largely eliminating these aforementioned phenomena.[50-51] Here, use of a two electrode cell is desirable as it simplifies the overall operation of the device making it more desirable from a POC standpoint.

In the present design, we will use three sensing (working) electrodes for each individual electrochemical cell as this allows for replicate measurements to be obtained simultaneously.[35] Additionally, the multiple sensing electrodes can be used as single working electrode to improve limits of detection (LOD) via current summation techniques if needed. The proposed electrode array format will require use of a multi-potentiostat, and these can be readily acquired from a large number of commercial sources (CH Instruments, BAS, etc.) or, alternatively, built in-house.

Specific Aim 2. *Specific Aim 2* is comprised of two objectives, the first being synthesis of aptamers for known protein biomarkers of stroke, and the second incorporation and characterization of the resulting aptamers in the biosensor device. Table 1 lists protein biomarkers which we are interested in developing aptamers for. Initially, we propose to synthesize aptamers for six protein biomarkers of stroke: 2 indicative of hemorrhagic and 4 indicative of ischemic stroke. These include glial fibrillary acidic protein (GFAP), S100B, fibrinogen, matrix metalloproteinaise-9 (MMP-9), B-neurotrophic growth factor (B-NGF), and activated protein C - protein C inhibitor complex (APC-PCI). We are interested in measuring these particular proteins as preliminary studies suggest them to be the most effective in discriminating stroke type. [9,12,52-53] Additionally, they have shown suitability for early diagnosis due to their rapid concentration increase in the bloodstream following onset of stroke symptoms.[9,12,52-53] Ideally, we would like to include more biomarkers of hemorrhagic stroke, but currently are limited to the few known listed in Table 1 (GFAP and S100B). Also, we will synthesize an aptamer specific to glyceraldehyde-3-phosphate dehydrogenase (GAPDH) as this protein will be used an internal standard for data normalization. GAPDH is the protein product of a housekeeping gene, and thus has a relatively constant concentration in blood serum.[54] Normalization of biomarkers to this protein will allow us to account for differences in concentrations arising from the hydration state of the patient. For all these studies, we anticipate obtaining the target proteins from commercial or collaborative sources. However, if this is not a viable option gene sequences for target proteins will be cloned into plasmid vectors and obtained in high purity from a bacterial source.[55]

Theoretically, aptamers can be synthesized for all the proteins listed in Table 1 using a process known as systematic evolution of ligands by exponential enrichment, or SELEX.[32,56-58] Using SELEX, aptamers selective for a given target are initially discovered by incubating the target with a large library of oligionucleotide structures ($\sim 10^{15}$).[32] Aptamers showing selectivity for the target are then amplified and isolated in a series of subsequent enrichment steps.[32] Multiple SELEX approaches have been reported for developing conformational changing aptamers,[31,37,59] and we propose using these as a starting point for our aptamer development. If limited conformational changing aptamers are developed using these methods, we propose splicing small oligionucleotide sequences

showing specificity for our targets into larger sequences known to undergo spatial reconfiguration upon target binding.[59-60] Suitable aptamers discovered in the previous steps will then be synthesized in bulk for incorporation into the biosensor device. These aptamers will be conjugated to a thiol at one terminus (e.g. 3' or 5') and methylene blue at the opposite terminus for electrode immobilization and electroactivity, respectively.[28,34-35] For the present studies, we will use DNA aptamers in lieu of RNA aptamers as they are less susceptible to nuclease degradation,[24,32] and thus lend themselves to a more robust, stable biosensor platform.

Table 1. Protein Biomarkers for Diagnosing Stroke

Stroke Type	Protein Name	Description	Reference
Hemorrhagic	Glial fibrillary acidic protein	Brain specific astrocytic intermediate filament protein	14,53,61
Ischemic/ Hemorrhagic	S100B	Calcium binding protein produced in glial cells	9,11,52,62-63
Ischemic	D-Dimer	Breakdown product of fibrin mesh	3,10,12
Ischemic	Fibrinogen	Plasma glycoprotein which produces fibrin	12
Ischemic	Myelin basic protein	Myelin membrane proteolipid	16
Ischemic	Serum free hemoglobin	Hemoglobin not associated with erythrocytes	20
Ischemic	Matrix metalloproteinase-9	Collagenase associated with endothelial damage	3,9-10,19,52
Ischemic	SCUBE1	Platelet-endothelial secreted protein	18
Ischemic	Neuron specific enolase	Dimeric isoenzyme of the glycolytic enzyme enolase	16,53
Ischemic	APC-PCI	Activated protein C - protein C inhibitor complex	53
Ischemic	von Willebrand factor	Blood glycoprotein involved in hemostasis	9,11,52
Ischemic	B-type neurotrophic growth factor	Growth factor for the nervous system	9
Ischemic	Monocyte chemotactic protein-1	Small cytokine protein	9
Ischemic	Visinin-like protein 1	Neuronal calcium sensor protein expressed in the brain	17
Ischemic	Apolipoprotein C1	Plasma protein found in LDL and VLDL	10,13
Ischemic	Apolipoprotein C3	Component of VLDL, HDL, and LDL produced in the liver	10,13

Aptamers developed in the previous steps will be immobilized onto the gold sensing electrodes using well characterized gold-thiol, monolayer chemistries.[28,34] For this step, optimal coupling densities will be determined for each individual aptamer sensor

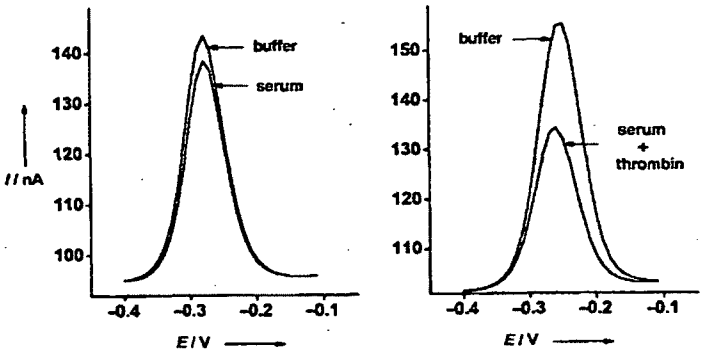

Figure 3. Differential pulse voltammograms showing the electrochemical response of an aptamer conjugated, methylene blue redox probe. Here, a reduction peak is observed for the probe centered at ~ -0.26 V. In the absence of target little change in signal is observed (left trace). In the presence of target signal decreases due to conformational change of the aptamer (right trace). Figure obtained from Xiao et al.[34]

employed in the device. This is a critical step as sensor performance (sensitivity, LOD, etc.) is dependent on electrode surface coverage of the aptamer.[28,34] Coupling densities will be quantified using differential pulse voltammetry as has been described in previous reports.[28,33-35]

After determination of optimal surface coverage, the performance of each parallel, aptameric sensor will be assessed. For each biomarker of interest, dose response curves will be generated to determine its dynamic range and LOD. Association and dissociation constants for each aptamer/biomarker ensemble will then be extrapolated from these curves to quantify binding specificity.[45] Additionally, we'll analyze specificity of binding and susceptibility towards non-specific protein binding by measuring sensor response in blank serum samples. These measurements will be compared against those obtained from sensors with non-specific aptamer sequences as a control. Sensors will be regenerated between measurements by removing aptamer bound protein with sodium dodecyl sulfate or concentrated salt solutions.[28,34] The ability to regenerate the sensors in this manner is beneficial as they can be used multiple times, which is not the case for most antibody based sensors.

All the aforementioned measurements will be conducted using differential pulse voltammetry (DPV). DPV will be used as it gives lower LODs than similar cyclic voltammetric techniques, and has shown previous compatibility with redox labeled aptamer systems.[28,34-35] Additionally, response times are rapid (usually a few minutes) and data analysis relatively straightforward due to simplistic nature of the electrochemical signal.[28,34] Example DPV measurements for an aptameric system specific to thrombin are shown in Figure 3.[34] As seen in this figure, the electrochemical signal consists of a single reduction peak of the methylene blue redox probe. Current change resulting from target binding to the redox labeled aptamer is seen as a reduction in peak current, which is easily quantified by subtracting it from the background current. This technique gives LODs in the picomolar range (ng mL^{-1})[28] which should be sufficient to detect most of our biomarkers of interest.[10] For biomarkers having serum concentrations below the LOD of the sensor, current summation techniques can be employed to improve

the LOD (see *Specific Aim 1*). Additionally, simple sample pretreatment methods such as microcentrifugation with molecular weight cut-off filters can be employed to bring proteins within the dynamic range of the system if needed.

Specific Aim 3. The final aim of this work involves determining the utility of the biosensor device for real life diagnosis of stroke. Ultimately, this will entail measuring a panel of serum biomarkers obtained from patients who have suffered an ischemic or hemorrhagic stroke. Samples from a population of non-stroke patients will be measured as a control. This portion of the study will be conducted in collaboration with a teaching hospital allowing us access to multiple time-point serum samples. Ideally, we want to measure early time-point samples (i.e. upon admittance to the hospital) as biomarker concentrations in these samples will be most like those encountered in a POC setting. As stated above, we initially intend to conduct these studies using the following biomarkers: GFAP, S100B, fibrinogen, MMP-9, B-NGF, and APC-PCI. These biomarkers will serve as a primary starting point, but eventually we would like to examine additional biomarkers to determine the exact number and type needed for a definitive diagnosis.

To obtain a diagnosis using the selected biomarker panel, we will first measure their serum concentrations using the multiplexed sensor device. As mentioned in *Specific Aim 2*, these concentrations will be normalized to GAPDH and then analyzed using an appropriate univariate logistic regression to establish a diagnosis.[3,9,52] This type of analysis should allow for elucidation of stroke type based solely on the differences in biomarker concentrations between both stroke and control samples. To assess the accuracy of our diagnosis, we will compare against clinical results obtained using MRI or an equivalent diagnostic technique. Additionally, we will utilize a multivariate logistic regression to evaluate the sensitivity of our biomarker panel in discriminating stroke type.[3,9,52] The multivariate analysis will include biomarker concentrations as well as additional clinical data to help assess diagnostic sensitivity.[3,9,52] This approach should allow for determination of both the number and specific biomarker identities which yield the most sensitive diagnosis. In the end, this will allow us to determine whether measuring a mixed panel of biomarkers specific to both ischemic and hemorrhagic stroke will be sufficient to exact an accurate diagnosis.

Summary

Miniaturized analysis systems show particular promise for applications in the emerging field of POC diagnostics. Proposed here is a novel microfluidic biosensor for the rapid diagnosis of stroke. The heart of the proposed system consists of aptamer based, electrochemical sensors which selectively bind and detect protein biomarkers of stroke. The immediate impact of this work will be the development of a device capable of diagnosing stroke in pre-hospital setting using a simple blood based measurement. To date this has not been possible, and the successful demonstration of this device would be a major step forward in the cause specific management of the disease. Ultimately, the simplistic operational features, rapid analysis times, and near universality of the protein sensing technology will have a broader impact in the field of clinical diagnostics as the platform can be adapted to multiple blood based protein analyses with relative ease.

References

(1) American Stroke Association Home Page. http://www.strokeassociation.org (accessed Apr 2010).

(2) Furlan, A.; Higashida, R.; Wechsler, L.; Gent, M.; Rowley, H.; Kase, C.; Pessin, M.; Ahuja, A.; Callahan, F.; Clark, W. M.; Silver, F.; Rivera, F. *JAMA* **1999**, *282*, 2003-2011.

(3) Laskowitz, D. T.; Kasner, S. E.; Saver, J.; Remmel, K. S.; Jauch, E. C. *Stroke* **2009**, *40*, 77-85.

(4) Herr, A. E.; Hatch, A. V.; Throckmorton, D. J.; Tran, H. M.; Brennan, J. S.; Giannobile, W. V.; Singh, A. K. *Proc. Natl. Acad. Sci. U.S.A.* **2007**, *104*, 5268-5273.

(5) Sia, S. K.; Kricka, L. J. *Lab Chip* **2008**, *8*, 1982-1983.

(6) Ouellette, A. L.; Li, J. J.; Cooper, D. E.; Ricco, A. J.; Kovacs, G. T. A. *Anal. Chem.* **2009**, *81*, 3216-3221.

(7) Fang, X.; Liu, Y.; Kong, J.; Jiang, X. *Anal. Chem.* **2010**, *82*, 3002-3006.

(8) Jokerst, J. V.; Jacobson, J. W.; Bhagwandin, B. D.; Floriano, P. N.; Christodoulides, N.; McDevitt, J. T. *Anal. Chem.* **2010**, *82*, 1571-1579.

(9) Reynolds, M. A.; Kirchick, H. J.; Dahlen, J. R.; Anderberg, J. M.; McPherson, P. H.; Nakamura, K. K.; Laskowitz, D. T.; Valkirs, G. E.; Buechler, K. F. *Clin. Chem.* **2003**, *49*, 1733-1739.

(10) Whiteley, W.; Tseng, M. C.; Sandercock, P. *Stroke* **2008**, *39*, 2902-2909.

(11) Dassan, P.; Keir, G.; Brown, M. M. *Cerebrovasc. Dis.* **2009**, *27*, 295-302.

(12) Maas, M. B.; Furie, K. L. *Biomark. Med.* **2009**, *3*, 363-383.

(13) Allard, L.; Lescuyer, P.; Burgess, J.; Leung, K. Y.; Ward, M.; Walter, N.; Burkhard, P. R.; Corthals, G.; Hochstrasser, D. F.; Sanchez, J. C. *Proteomics* **2004**, *4*, 2242-2251.

(14) Foerch, C.; Curdt, I.; Yan, B.; Dvorak, F.; Hermans, M.; Berkefeld, J.; Raabe, A.; Neumann-Haefelin, T.; Steinmetz, H.; Sitzer, M. *J. Neurol. Neurosurg. PS* **2006**, *77*, 181-184.

(15) Delgado, P. *Stroke* **2007**, *38*, 1117-1117.

(16) Jauch, E. C.; Lindsell, C.; Broderick, J.; Fagan, S. C.; Tilley, B. C.; Levine, S. R.; Grp, N. r.-P. S. S. *Stroke* **2006**, *37*, 2508-2513.

(17) Laterza, O. F.; Modur, V. R.; Crimmins, D. L.; Olander, J. V.; Landt, Y.; Lee, J. M.; Ladenson, J. H. *Clin. Chem.* **2006**, *52*, 1713-1721.

(18) Dai, D. F.; Thajeb, P.; Tu, C. F.; Chiang, F. T.; Chen, C. H.; Yang, R. B.; Chen, J. J. *J. Am. Coll. Cardiol.* **2008**, *51*, 2173-2180.

(19) Kelly, P. J.; Morrow, J. D.; Ning, M. M.; Koroshetz, W.; Lo, E. H.; Terry, E.; Milne, G. L.; Hubbard, J.; Lee, H.; Stevenson, E.; Lederer, M.; Furie, K. L. *Stroke* **2008**, *39*, 100-104.

(20) Huang, P. Y.; Lo, L. H.; Chen, Y. C.; Lin, R. T.; Shiea, J.; Liu, C. K. *J. Neurol.* **2009**, *256*, 625-631.

(21) Homola, J.; Yee, S. S.; Gauglitz, G. *Sens. Actuators, B* **1999**, *54*, 3-15.

(22) Janshoff, A.; Galla, H. J.; Steinem, C. *Angew. Chem., Int. Ed. Engl.* **2000**, *39*, 4004-4032.

(23) Tombelli, S.; Minunni, M.; Mascini, M. *Biosens. Bioelectron.* **2005**, *20*, 2424-2434.

(24) Tombelli, S.; Minunni, M.; Mascini, M. *Biomol. Eng.* **2007**, *24*, 191-200.
(25) Arruda, D. L.; Wilson, W. C.; Nguyen, C.; Yao, Q. W.; Caiazzo, R. J.; Talpasanu, I.; Dow, D. E.; Liu, B. C. S. *Expt. Rev. Mol. Diagn.* **2009**, *9*, 749-755.
(26) Qavi, A. J.; Washburn, A. L.; Byeon, J. Y.; Bailey, R. C. *Anal. Bioanal. Chem.* **2009**, *394*, 121-135.
(27) Pohanka, M.; Skladai, P. *J. Appl. Biomed.* **2008**, *6*, 57-64.
(28) Lai, R. Y.; Plaxco, K. W.; Heeger, A. J. *Anal. Chem.* **2006**, *79*, 229-233.
(29) Marquette, C. A.; Blum, L. J. *Biosens. Bioelectron.* **2006**, *21*, 1424-1433.
(30) Cho, E. J.; Lee, J. W.; Ellington, A. D. *Annu. Rev. Anal. Chem.* **2009**, *2*, 241-264.
(31) Sefah, K.; Phillips, J. A.; Xiong, X. L.; Meng, L.; Van Simaeys, D.; Chen, H.; Martin, J.; Tan, W. H. *Analyst* **2009**, *134*, 1765-1775.
(32) Jayasena, S. D. *Clin. Chem.* **1999**, *45*, 1628-1650.
(33) Fan, C.; Plaxco, K. W.; Heeger, A. J. *Proc. Natl. Acad. Sci. U.S.A.* **2003**, *100*, 9134-9137.
(34) Xiao, Y.; Lubin, A. A.; Heeger, A. J.; Plaxco, K. W. *Angew. Chem., Int. Ed. Engl.* **2005**, *44*, 5456-5459.
(35) Swensen, J. S.; Xiao, Y.; Ferguson, B. S.; Lubin, A. A.; Lai, R. Y.; Heeger, A. J.; Plaxco, K. W.; Soh, H. T. *J. Am. Chem. Soc.* **2009**, *131*, 4262-4266.
(36) Fang, X.; Cao, Z.; Beck, T.; Tan, W. *Anal. Chem.* **2001**, *73*, 5752-5757.
(37) Hamaguchi, N.; Ellington, A.; Stanton, M. *Anal. Biochem.* **2001**, *294*, 126-131.
(38) Fang, X.; Sen, A.; Vicens, M.; Tan, W. *ChemBioChem* **2003**, *4*, 829-834.
(39) Liss, M.; Petersen, B.; Wolf, H.; Prohaska, E. *Anal. Chem.* **2002**, *74*, 4488-4495.
(40) Minunni, M.; Tombelli, S.; Gullotto, A.; Luzi, E.; Mascini, M. *Biosens. Bioelectron.* **2004**, *20*, 1149-1156.
(41) Tombelli, S.; Minunni, M.; Mascini, M. *Anal. Lett.* **2002**, *35*, 599-613.
(42) Verhelst, S. H.; Michiels, P. J.; van der Marel, G. A.; van Boeckel, C. A.; van Boom, J. H. *ChemBioChem* **2004**, *5*, 937-942.
(43) Mark, D.; Haeberle, S.; Roth, G.; von Stetten, F.; Zengerle, R. *Chem. Soc. Rev.* **2010**, *39*, 1153-1182.
(44) Lynn, N. S.; Dandy, D. S. *Lab Chip* **2009**, *9*, 3422-3429.
(45) Murphy, B. M.; He, X. Y.; Dandy, D.; Henry, C. S. *Anal. Chem.* **2008**, *80*, 444-450.
(46) Murphy, B. M.; Dandy, D. S.; Henry, C. S. *Anal. Chim. Acta* **2009**, *640*, 1-6.
(47) Duffy, D. C.; McDonald, J. C.; Schueller, O. J. A.; Whitesides, G. M. *Anal. Chem.* **1998**, *70*, 4974-4984.
(48) McDonald, J. C.; Duffy, D. C.; Anderson, J. R.; Chiu, D. T.; Wu, H. K.; Schueller, O. J. A.; Whitesides, G. M. *Electrophoresis* **2000**, *21*, 27-40.
(49) Park, B. Y.; Zaouk, R.; Madou, M. J. Fabrication of Microelectrodes Using the Lift-Off Technique. In *Methods in Molecular Biology*; Minteer, S. D., Eds.; Humana Press Inc.: Totowa, NJ, 2005; Vol. 321, pp 23.
(50) Ching, S.; Dudek, R.; Tabet, E. *J. Chem. Educ.* **1994**, *71*, 602-605.
(51) Forster, R. J. *Chem. Soc. Rev.* **1994**, *23*, 289-297.
(52) Lynch, J. R.; Blessing, R.; White, W. D.; Grocott, H. P.; Newman, M. F.; Laskowitz, D. T. *Stroke* **2004**, *35*, 57-63.

(53) Unden, J.; Strandberg, K.; Malm, J.; Campbell, E.; Rosengren, L.; Stenflo, J.; Norrving, B.; Romner, B.; Lindgren, A.; Andsberg, G. *J. Neurol.* **2009**, *256*, 72-77.
(54) Thellin, O.; Zorzi, W.; Lakaye, B.; De Borman, B.; Coumans, B.; Hennen, G.; Grisar, T.; Igout, A.; Heinen, E. *J. Biotechnol.* **1999**, *75*, 291-295.
(55) Ninfa, A. J.; Ballou, D. P. Recombinant DNA Techniques. In *Fundamental Laboratory Approaches for Biochemistry and Biotechnology*; Fitzgerald Science Press: Bethesda, Md., 1998; pp 277-310.
(56) Ellington, A. D.; Szostak, J. W. *Nature* **1990**, *346*, 818-822.
(57) Tuerk, C.; Gold, L. *Science* **1990**, *249*, 505-510.
(58) Ellington, A. D.; Szostak, J. W. *Nature* **1992**, *355*, 850-852.
(59) Nutiu, R.; Li, Y. F. *Angew. Chem., Int. Ed. Engl.* **2005**, *44*, 1061-1065.
(60) Green, L. S.; Jellinek, D.; Jenison, R.; Ostman, A.; Heldin, C.-H.; Janjic, N. *Biochemistry* **1996**, *35*, 14413-14424.
(61) Dvorak, F.; Haberer, I.; Sitzer, M.; Foerch, C. *Cerebrovasc. Dis.* **2009**, *27*, 37-41.
(62) Foerch, C.; Wunderlich, M. T.; Dvorak, F.; Humpich, M.; Kahles, T.; Goertler, M.; Alvarez-Sabin, J.; Wallesch, C. W.; Molina, C. A.; Steinmetz, H.; Sitzer, M.; Montaner, J. *Stroke* **2007**, *38*, 2491-2495.
(63) Delgado, P.; Sabin, J. A.; Santmarina, E.; Molina, C. A.; Quintana, M.; Rosell, A.; Montaner, J. *Stroke* **2006**, *37*, 2837-2839.